University of Alberta

A Semi-Analytical Algorithm for Indentation Test of Viscoelastic Materials

by

Tadayoshi Yamanaka

A thesis submitted to the Faculty of Graduate Studies and Research
in partial fulfillment of the requirements for the degree of *Master of Science*

Department of Mechanical Engineering

Edmonton, Alberta
Fall 2006

Your file Votre référence
ISBN: 978-0-494-22412-0
Our file Notre référence
ISBN: 978-0-494-22412-0

Abstract

A semi-analytical algorithm was developed to simulate the load response of viscoelastic materials when subjected to indentation by using a spherical indenter. The algorithm uses the elastic boundary value problem to determine the contact load. With the assumption that the response of a viscoelastic material can be approximated by an elastic solution when the time scale is sufficiently short, the algorithm successfully generates the unloading response of viscoelastic material in the displacement-controlled indentation test. A modification factor obtained through the correction of the surface displacement in the stress relaxation test is proven to be very effective. The computation time required when using the algorithm is 2 orders of magnitude faster than that required when using finite element modeling, and the same precision is achieved. The study also proposes a strategy for selecting the computational parameters to ensure the results' accuracy.

Acknowledgements

I would like to express my gratitude to my supervisor, Dr. Ben Jar, for his supervision and support. I would like to thank Dr. T. Kuboki for his valuable discussions with me.

My thanks go to the members of the Durable Materials Research Lab -- Mr. Chengye Fan, Mr. Lei Ji, Mr. Hyock-Ju Kwon, Mr. Yemi Setiadi, and Ms. Tik Dick-- for their friendship and discussions.

I would also like to express my gratitude to my parents, Takao and Etsuko, and my sisters, Fumi Yoshida and Mitsuko, for their love and support. I am particularly grateful to my parents for their understanding and financial support.

TABLE OF CONTENTS

LIST OF TABLES

LIST OF FIGURES

1. Introduction

Hertz [1] was the first to study contact mechanics for linear elastic material. The contact of two bodies was solved by using the mixed boundary value problem of linear elasticity. For the analysis of two bodies in contact with known profiles, the key issue is the contact pressure distribution. Obtaining it is the first step in tackling any contact problems. In the elastic regime, Hertz obtained the contact pressure distribution due to the contact between two elastic spheres by making geometric assumptions about the contact profile. He then proposed a contact law relating the contact load and indentation depth.

Lee and Radok [2] obtained the solution of the linear viscoelastic boundary value problem by using the corresponding linear elastic boundary value problem and the correspondence principle. The correspondence principle allows the solution of a linear viscoelastic boundary value problem to be found by taking the following three steps:

1. applying the Laplace transforms to the corresponding linear elastic boundary value problem.
2. replacing the elastic constants by the corresponding Laplace transformed viscoelastic material properties.
3. applying the inverse Laplace transforms

Because of the violation of the traction-free boundary condition outside the contact area, the correspondence principle is not applicable to the viscoelastic contact problem in the contact-area-decreasing phase. Therefore, viscoelastic contact problems are often solved by using numerical techniques such as finite element methods. The solution of

even a very simple contact problem, such as contact between a rigid sphere and a semi-infinite viscoelastic body, requires numerical techniques. An example of a contact problem requiring the use of numerical techniques in its solution is the simulation of indentation tests.

1.1 Scope of the Study

In this study, a semi-analytical algorithm for a quasi-static contact between an axisymmetric rigid indenter and a semi-infinite viscoelastic body was developed. The algorithm was developed for the indentation test that possesses a single maximum contact area, i.e., indentation test with a single phase of monotonic loading and a single phase of monotonic unloading. The indentation problem has a closed form solution when the contact load is prescribed for both the contact-area-increasing and decreasing phases. The solution for the load-controlled indentation can be obtained by using the correspondence principle because with the known contact load, the problem is the same as that with the traction boundary condition prescribed throughout the contact-area-increasing and decreasing phases. However, for the displacement-controlled indentation tests, a closed form solution cannot be obtained because the contact pressure in the contact-area-decreasing phase cannot be obtained as a function of the indentation depth by using the correspondence principle.

The semi-analytical algorithm is developed for the contact between a rigid spherical indenter and a semi-infinite viscoelastic body. The algorithm is based on the solution of

an axisymmetric linear elastic contact problem that was proposed by Sneddon [3]. The solutions are expressed in terms of the contact profile, defined as the initial gap between two bodies in contact. The algorithm uses the idea that the stress obtained by the linear viscoelastic boundary value problem can be obtained by using the linear elastic boundary value problem. The problem is named hereafter the "equivalent linear elastic boundary value problem." Using the equivalent linear elastic boundary value problem and the characteristics of the viscoelastic materials, which can be approximated as elastic materials provided that the time scale is very short, the viscosity contribution can be negligible in determining the contact area and the contact load in the next time step. The viscosity contribution is taken into account before proceeding to the next time step by correcting the surface displacement of the semi-infinite body used to obtain the contact profile of the equivalent elastic boundary value problem.

The results of the semi-analytical algorithm were compared with the FEM solution, and the analytical solution for the indentation relaxation test. For the indentation test, the result was compared with FEM solution.

The semi-analytical algorithm for the indentation test of viscoelastic materials has the advantage of high efficiency in computation. A strategy for selecting the parameters for the algorithm is proposed based on a parametric study.

2. Contact Mechanics Review

Contact mechanics for elastic materials, mainly rigid-elastic contact, is reviewed in sections 2.1 to 2.2 and is based on Johnson [4]. First, a brief history of contact mechanics is provided. The derivation of the contact law relating the indentation depth and contact load via the corresponding contact stiffness, including the solution of a three-dimensional linear elastic problem, known as Boussinesq's problem, is discussed. This contact law is restricted to rigid-elastic contact, as this contact is based on the condition that the indenters used have much higher stiffness than the tested materials. The full derivation of an elastic-elastic contact law can be found in Johnson [4]. The review also includes more generalized axisymmetric contact problems solved by using the dual integral equations, as given by Sneddon [3]. Also, the relationship between the surface displacement and contact pressure, with various contact profiles, is derived based on Sneddon's approach.

A brief review of linear viscoelastic boundary value problems, the correspondence principle, the viscoelastic contact problems, and the previous work which violates the restriction of the boundary condition imposed by the correspondence principle is presented in sections 2.3 to 2.5. The surface displacement of a semi-infinite viscoelastic body due to an arbitrary normal pressure distribution on a circular area is presented in section 2.3. This solution is used to obtain the contact load-indentation depth relationship in section 2.4. This solution will be used in Chapter 3. The previous work that violates the restriction is pointed out in section 2.5.

2.1 Hertz Theory for Indentation

In 1882, Hertz [1] first studied contact mechanics by using the solution of Boussinesq's problem, i.e., a concentrated force at a point on the surface of a semi-infinite elastic body. He investigated the contact of two glass lenses, i.e., two spherical bodies, assuming the contact area was very small compared to the dimensions of two bodies in contact, so that the two lenses could be treated as semi-infinite elastic bodies. He further assumed that the contact profile of the two lenses (with spherical contours) could be approximated by using a parabolic function, $f(x,y) = Ax^2 + By^2$, where A and B are constants. This approximation gives a closed-form expression of the pressure distribution in terms of parabolic surface displacements, in the framework of a linear elasticity. Knowing the contact pressure and the corresponding surface displacements, Hertz obtained the relationship between the indentation (penetration) depth and the corresponding contact load, known as "the Hertz contact law". The coefficient relating the two parameters is known as "contact stiffness". The approximation of the contact profile is valid when the contact radius is much smaller than the radii of the two bodies. The simplification of the contact profile allowed the corresponding contact pressure to be expressed in terms of the displacement, in the form of $\delta - f(x,y)$, where δ is the indentation depth, and (x,y) is the point within the contact area of each body. The contact pressure was determined based on the solution of Boussinesq's problem with the following boundary conditions.

At the surface of two bodies, tangential stresses are ignored; i.e.,

$$\sigma_{xy} = \sigma_{yz} = 0. \tag{2.1.1}$$

Within the contact area, normal pressure exists, and the two bodies conform to each other as

$$\sigma_{zz} \neq 0 \quad \text{and } u_z = \delta - f(x,y), \tag{2.1.2}$$

where $f(x,y)$ is the contact profile defined as the initial gap between two bodies in contact within the radius of the contact area.

Outside the contact area, normal pressure is absent; i.e.,

$$\sigma_{zz} = 0. \tag{2.1.3}$$

To use Boussinesq's solution, Hertz stated the following assumption [1]:

"The particular form of the surface of the two bodies only occurs in the boundary condition, apart from which each of the bodies acts as if it were an infinitely extended body occupying all space on one side of the plane $z = 0$, *and as if only normal pressure acted on this plane."*

Consequently, the use of the Hertz theory for indentation has the following limitations:

1. approximation of the contact profile
2. geometric limitations due to the use of the solution for a semi-infinite elastic body
3. limitations due to the idealization of the absence of the tangential traction of the surface of a semi-infinite elastic body

The Hertz theory is used in the analysis of an indentation test. Since the indenter is much stiffer than the tested material, the deformation of the indenter can be ignored. Therefore, the indenter can be treated as a rigid body during the indentation test. Also, for

the sake of simplicity in the data analysis, the specimen is often assumed to initially have a flat surface. Even though an initially flat surface is preferred in all types of indentation tests, the indenter profile varies with the type of test. For example, the Vickers hardness test uses the form of a square pyramid, but the Brinell hardness test uses a spherical indenter. Conical and wedge indenters are also used in indentation tests. A spherical indenter is considered in deriving the contact law for an indentation test. The contact law for more generalized contact profiles was proposed by Ting [5] and Sneddon [3] for axisymmetric cases. The procedure proposed by Sneddon is discussed in section 2.2.

In accordance with the indentation test considered in this study, the Hertz theory is discussed only for a special case, i.e., an axisymmetric rigid indenter on a semi-infinite elastic body, as shown in Figure 2-1-1. According to the Hertz approximation, the contact profile defined as the initial gap between the sphere and the surface of a semi-infinite elastic body can be approximated in the axisymmetric case as

$$f(r) = (1/2R)r^2, \tag{2.1.4}$$

where R is the radius of the indenter. Eq. (2.1.4) approximates the contact profile of the problem depicted in Figure 2-1-1. The approximation of the spherical indenter for a parabolic contact profile was later removed by Ting [5] and Sneddon [3] in order to introduce more general solutions for linear elastic contact problems.

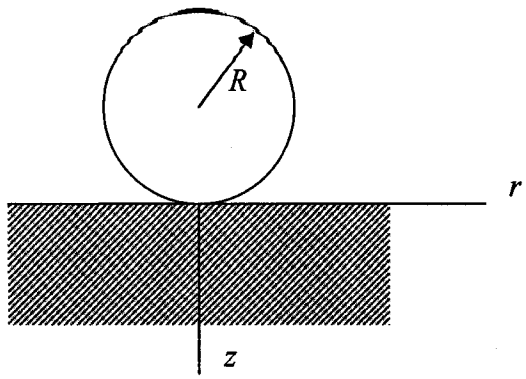

Figure 2-1-1. A spherical indenter on the surface of a semi-infinite body.

Since the spherical indenter is rigid, the normal surface displacement $u_z(r)$ on a semi-infinite elastic body should conform to the indenter profile; i.e.,

$$u_z(r) = \delta - f(r)$$

$$= \delta - \frac{1}{2R} r^2 \ . \tag{2.1.5}$$

This equation states the implicit restriction of the Hertz theory. A displacement component should have been present in the r direction; however, in the Hertz theory, the lateral displacement is assumed to be negligible.

For linear elastic problems, strains are defined as

$$\varepsilon_{ij} = \frac{1}{2}\left(u_{i,j} + u_{j,i}\right), \tag{2.1.6}$$

where ε_{ij} is the strain, and u is the displacement. The comma indicates the spatial derivative, i.e., $\partial u_i / \partial x_j = u_{i,j}$. For the indices i and j, the summation convention is implied when no specific explanation of their use is given. The normal contact pressure distribution due to the contact is determined by solving the mixed boundary condition problem, i.e., Eqs. (2.1.1), (2.1.3), (2.1.5) and the equilibrium equations:

$$p(r) = p_0 \left\{1 - (r/a)^2\right\}^{1/2}, \tag{2.1.7}$$

where p_0 is a function of the radius of the contact area, the material properties, and the radius of the indenter, and a is the radius of the contact area.

The normal surface displacement produced by pressure distribution over a circular surface area can be found by superposition by using the solutions of Boussinesq's problem. The normal surface displacement under a concentrated force, F, is given by Boussinesq's solution at $z = 0$ as

$$\begin{aligned} \bar{u}_z(r) &= \frac{F}{4\pi\mu}\left[\frac{2(1-\nu)}{r} + \frac{z^2}{r^3}\right]_{z=0} \\ &= \frac{(1-\nu)}{2\pi\mu\, r} F, \end{aligned} \tag{2.1.8}$$

where μ is the shear modulus, and ν is Poisson's ratio. The magnitude of the concentrated force can be given by Eq. (2.1.9) by using the polar coordinate system, originating at the observer point of the displacement, B_S, in Figure 2-1-2.

$$dF = p_{A_S}(s_c, \phi) s_c ds_c d\phi. \tag{2.1.9}$$

Substituting Eq. (2.1.9) into Eq. (2.1.8) gives the normal surface displacement due to the concentrated force applied at A_s:

$$\begin{aligned} d\bar{u}_z\left(r_{A_S/B_S}\right) &= \frac{(1-\nu)}{2\pi\mu\, r_{A_S/B_S}} dF \\ &= \frac{(1-\nu)}{2\pi\mu} p_{A_S}(s_c, \phi) ds_c d\phi, \end{aligned} \tag{2.1.10}$$

where r_{A_S/B_S} is the distance from the point where a concentrated force is applied to the point where displacement was observed; i.e., $r_{A_S/B_S} = A_S B_S = s_c$.

The normal surface displacement at point B_s due to the pressure distribution $p(s_c,\phi)$, over the surface, S, is obtained by replacing $p_{A_S}(s_c,\phi)$ by $p(s_c,\phi)$ and integrating Eq. (2.1.10) over the surface; i.e.,

$$\bar{u}_z(r)=\frac{(1-\nu)}{2\pi\mu}\iint_S p(s_c,\phi)ds_c d\phi. \tag{2.1.11}$$

The bar $\bar{u}_z$ distinguishes the surface displacement from the displacement within a semi-infinite elastic body. Throughout this thesis, this notation is used for displacements and pressures at the surface.

Here, a concentrated force is replaced by the corresponding distributed stress, so that the surface displacement due to an arbitrary normal pressure distribution may be expressed by superposition of surface displacements, Eq. (2.1.10).

The surface displacement at point B_S due to the given pressure distribution by Eq. (2.1.7) can be obtained by expressing the variable r in Eq. (2.1.7) by s_c and ϕ, substituting the pressure distribution into Eq. (2.1.10) and then integrating it over the surface area S. Point B_S could lie either within or outside the circular area S.

First, the normal surface displacement at point B_S inside the circular surface S is considered, as shown in Figure 2-1-3. The pressure distribution given by Eq. (2.1.7) in polar coordinates can be expressed in another polar coordinate system with its origin at point B_S so that the displacement at point B_S can be given by the superposition of the concentrated forces in terms of the pressure over the area, $s_c ds_c d\phi$.

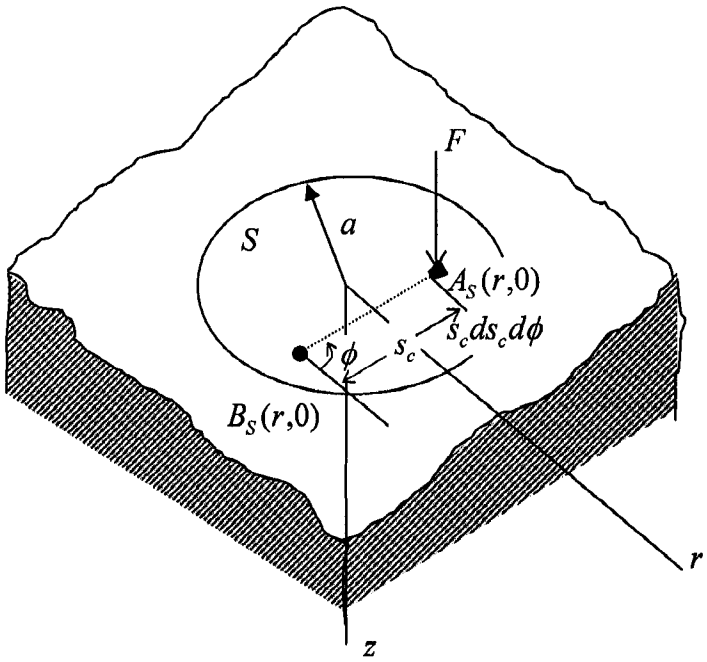

Figure 2-1-2. A concentrated force acting on point A_S in the surface S, from Johnson [4]

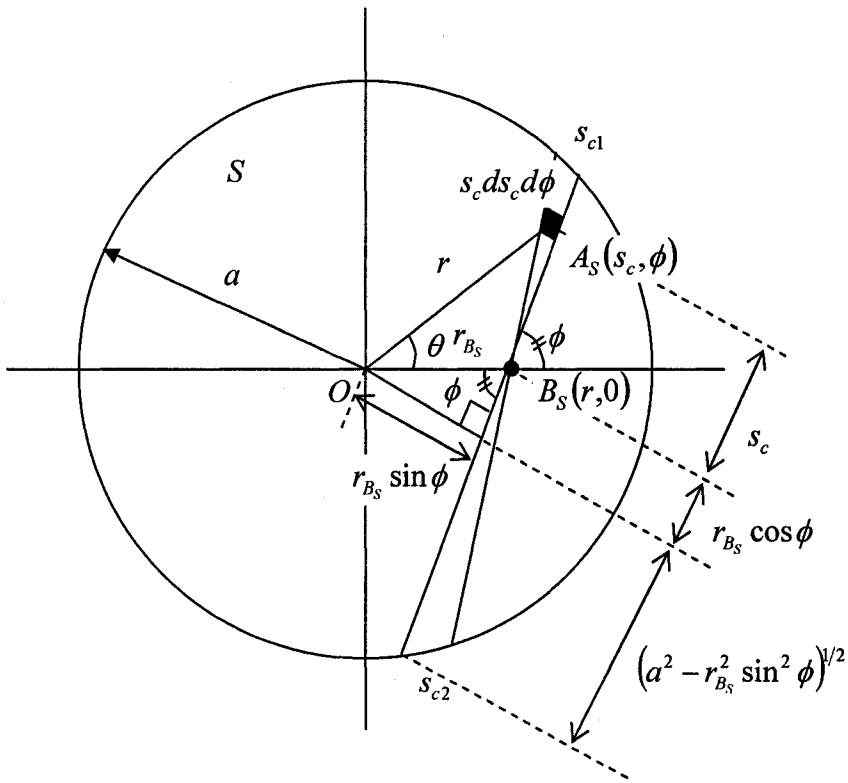

Figure 2-1-3. Pressure applied to circular surface S and the observer of displacement B_S lies inside the surface S, from Johnson [4]

From Figure 2-1-3, r^2 is expressed as

$$r^2 = \left(r_{B_S} \sin\phi\right)^2 + \left(s_c + r_{B_S} \cos\phi\right)^2$$

$$= r_{B_S}^2 + s_c^2 + 2r_{B_S} s_c \cos\phi \qquad (2.1.12)$$

Substituting Eq. (2.1.12) into Eq. (2.1.7) gives

$$p = \frac{p_0}{a}\left(\alpha^2 - 2\beta s_c - s_c^2\right)^{1/2} \qquad (2.1.13)$$

where $\alpha^2 = a^2 - r_{B_S}^2$ and $\beta = r_{B_S} \cos\phi$. From now on, the coordinate system of the pressure distribution is changed to the polar coordinate system, s_c and ϕ, introduced in Figure 2-1-3. From Figure 2-1-3, the limits of the integration of Eq.(2.1.11) are given by

$$s_{c1,2} = -r_{B_S} \cos\phi \pm \left\{r_{B_S}^2 \cos^2\phi + \left(a^2 - r_{B_S}^2\right)\right\}^{1/2} \qquad (2.1.14)$$

Considering that ϕ is integrated between the limits 0 and 2π, the limit on s_c required for the surface integration is only one of the limits. In this case, the limit which has a positive value, i.e., s_{c1}, is chosen for convenience. The limits can also be determined as the roots of $-\alpha^2 + 2\beta s_c + s_c^2 = 0$; i.e.,

$$s_{c1,2} = \frac{-2\beta \pm \sqrt{4\beta^2 + 4\alpha^2}}{2}$$

$$= -\beta \pm \left(\beta^2 + \alpha^2\right)^{1/2}$$

$$= -r_{B_S} \cos\phi \pm \left\{r_{B_S}^2 \cos^2\phi + \left(a^2 - r_{B_S}^2\right)\right\}^{1/2} \qquad (2.1.15)$$

Thus, by using α and β,

$$s_{c1} = -\beta + \left(\beta^2 + \alpha^2\right)^{1/2}. \qquad (2.1.16)$$

Then, the surface displacement within the loaded circular surface, by using Eq. (2.1.11), is

$$\bar{u}_z(r_{B_S}) = \frac{(1-\nu)}{\mu}\frac{p_0}{2\pi a}\int_0^{2\pi} d\phi \int_0^{s_{c1}} \left(\alpha^2 - 2\beta s_c - s_c^2\right)^{1/2} ds_c . \tag{2.1.17}$$

The above integral over s_c can be simplified as follows:

$$\int_0^{s_{c1}} \left(\alpha^2 - 2\beta s_c - s_c^2\right)^{1/2} ds_c = \int_{\beta}^{s_{c1}+\beta} \left\{\left(\alpha^2 + \beta^2\right) - x_d^2\right\}^{1/2} dx_d , \tag{2.1.18}$$

where $x_d = s_c + \beta$. The integration on the right hand side of Eq. (2.1.18) can be determined by using an integral table, Zwillinger [6]:

$$\int_0^{s_{c1}} \left\{\left(\alpha^2 + \beta^2\right) - x_d^2\right\}^{1/2} dx_d = \frac{1}{2}\left[x_d\sqrt{\left(\alpha^2 + \beta^2\right) - x_d^2} + \left(\alpha^2 + \beta^2\right)\sin^{-1}\left(\frac{x_d}{\left|\sqrt{\alpha^2 + \beta^2}\right|}\right)\right]_{\beta}^{s_{c1}+\beta}$$

$$= -\frac{1}{2}\alpha\beta + \frac{\pi}{4}\left(\alpha^2 + \beta^2\right). \tag{2.1.19}$$

The term $\alpha\beta$ vanishes in the above equation when integrated with respect to ϕ between 0 and 2π. Recalling $\alpha^2 = a^2 - r_{B_S}^2$ and $\beta = r_{B_S}\cos\phi$, we have

$$\bar{u}_z(r_{B_S}) = \frac{(1-\nu)}{\mu}\frac{p_0}{2\pi a}\int_0^{2\pi} \frac{\pi}{4}\left\{a^2 - r_{B_S}^2 + r_{B_S}^2\cos^2(\phi)\right\} d\phi$$

$$= \frac{(1-\nu)}{\mu}\left\{\frac{\pi p_0}{8a}\left(2a^2 - r_{B_S}^2\right)\right\} \tag{2.1.20}$$

The normal surface displacement at point B_S within the loaded circular surface is then given by Eq. (2.1.20). The terms related to material properties are excluded from the bracket. By replacing r_{B_S} by r, the normal surface displacement at any point within the loaded circular surface is given by

$$\bar{u}_z(r) = \frac{(1-\nu)}{\mu}\left\{\frac{\pi p_0}{8a}\left(2a^2 - r^2\right)\right\}. \tag{2.1.21}$$

The surface displacement outside the loaded circular surface should be treated differently due to the limits of the surface integration over the loaded circular surface S, as shown in Figure 2-1-4. Analogous to the case when point B_S lies within the loaded circular surface, the variable, r, in the expression of the pressure distribution can be expressed in terms of r_{B_S}, s_c and ϕ.

From Figure 2-1-4,

$$\begin{aligned} r^2 &= \left(r_{B_S} - s_c\cos\phi\right)^2 + \left(-s_c\sin\phi\right)^2 \\ &= s_c^2 + r_{B_S}^2 - 2r_{B_S}s_c\cos\phi \end{aligned} \tag{2.1.22}$$

By substituting Eq. (2.1.22) into Eq. (2.1.7), the pressure distribution can be expressed as

$$p = \frac{p_0}{a}\left(\alpha^2 + 2\beta s_c - s_c^2\right)^{1/2}. \tag{2.1.23}$$

Analogous to the previous case, the limits s_{c1} and s_{c2} are the roots of $\alpha^2 + 2\beta s_c - s_c^2 = 0$. From Figure 2-1-4, the limits are given by $\phi_1 = \sin^{-1}\left(a/r_{B_S}\right)$ and $\phi_2 = -\phi_1$. Then, by substituting Eq. (2.1.23) into Eq.(2.1.11), we have

$$\bar{u}_z\left(r_{B_S}\right) = \frac{(1-\nu)}{\mu}\frac{p_0}{2\pi a}\int_{\phi_2}^{\phi_1} d\phi \int_{s_{c1}}^{s_{c2}}\left(\alpha^2 + 2\beta s_c - s_c^2\right)^{1/2} ds_c \tag{2.1.24}$$

The integration over a circular surface S can be carried out in term of s_c and ϕ separately.

$$\int_{s_{c1}}^{s_{c2}}\left(\alpha^2 + 2\beta s_c - s_c^2\right)^{1/2} ds_c = \int_{s_{c1}-\beta}^{s_{c2}-\beta}\left\{\left(\alpha^2 + \beta^2\right) - x_d^2\right\}^{1/2} dx_d$$

$$= \frac{1}{2}\left[x_d \sqrt{(\alpha^2+\beta^2)-x_d^2} + (\alpha^2+\beta^2)\sin^{-1}\left(\frac{x_d}{\left|\sqrt{\alpha^2+\beta^2}\right|} \right) \right]_{s_{c1}-\beta}^{s_{c2}-\beta}$$

$$= \frac{1}{2}\pi(\alpha^2+\beta^2). \qquad (2.1.25)$$

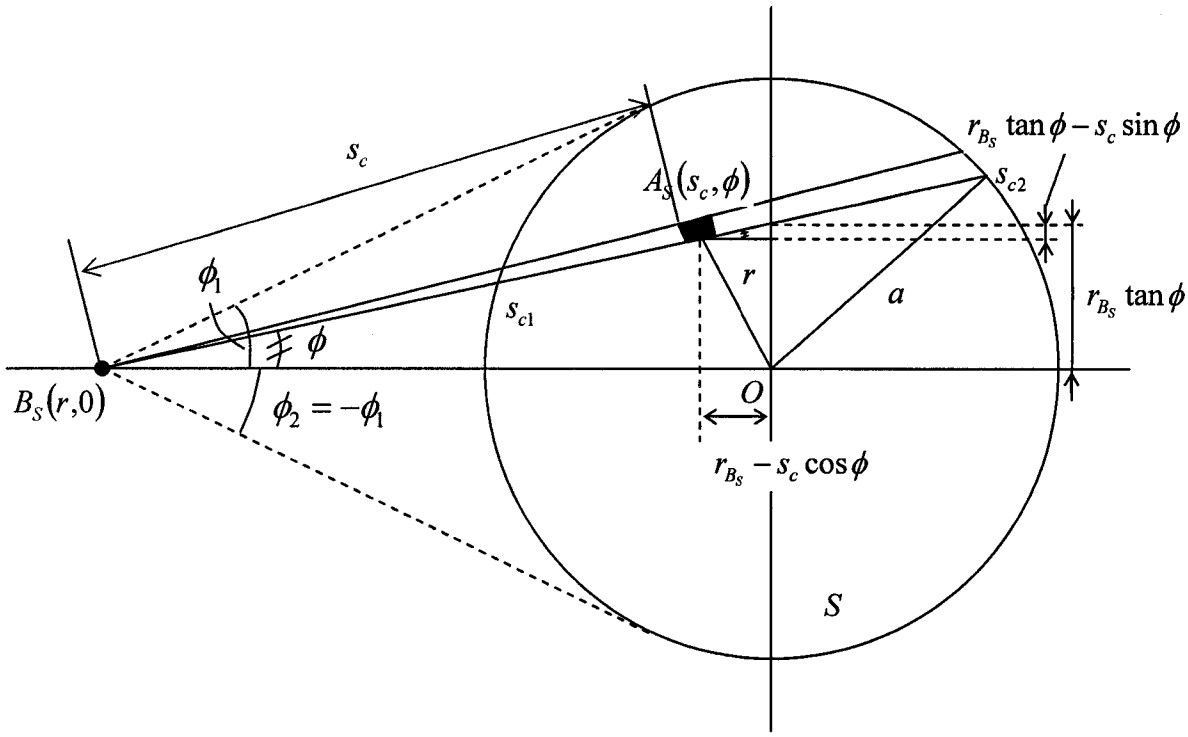

Figure 2-1-4. Pressure applied to circular surface S and the observer of the displacement B_S lies outside the circular surface S, from Johnson [4]

The integration of Eq. (2.1.24) gives the normal surface displacement at point B_S outside the loaded circular surface S, expressed as

$$\overline{u}_z(r_{B_S}) = \frac{(1-\nu)}{\mu}\frac{p_0}{2\pi a}\int_{\phi_2=-\phi_1}^{\phi_1}\frac{\pi}{2}\left(a^2 - r_{B_S}^2 + r_{B_S}^2\cos^2\phi\right)d\phi$$

$$= \frac{(1-\nu)}{\mu}\frac{p_0}{8a}\left\{\left(2a^2 - r_{B_S}^2\right)\phi + r_{B_S}^2\cos(\phi)\sin(\phi)\Big|_{-\phi_1}^{\phi_1}\right\}$$

$$= \frac{(1-\nu)}{\mu}\left[\frac{p_0}{4a}\left\{\left(2a^2 - r_{B_S}^2\right)\sin^{-1}\left(\frac{a}{r_{B_S}}\right) + r_{B_S}^2\left(\frac{a}{r_{B_S}}\right)\left(1-\frac{a^2}{r_{B_S}^2}\right)^{1/2}\right\}\right]. \qquad (2.1.26)$$

Replacing r_{B_S} by r, like the normal surface displacement within the loaded circular surface, the normal surface displacement at any point outside the loaded circular surface can be written as

$$\bar{u}_z(r) = \frac{(1-\nu)}{\mu}\left[\frac{p_0}{4a}\left\{\left(2a^2 - r^2\right)\sin^{-1}\left(\frac{a}{r}\right) + r^2\left(\frac{a}{r}\right)\left(1-\frac{a^2}{r^2}\right)^{1/2}\right\}\right] \qquad (2.1.27)$$

The Hertz theory takes advantage of the parabolic surface displacement of Eq. (2.1.21), due to the pressure distribution Eq.(2.1.7) and the approximate contact profile, Eq.(2.1.4). Both Eqs. (2.1.4) and (2.1.21) are parabolic functions of r. This result allows one to find the pressure distribution from the known contact area (indentation depth). For the approximation of the spherical indenter to conform to the surface, the normal surface displacement should meet the following conditions:

$$\bar{u}_z(r) = \delta - f(r)$$

$$\frac{(1-\nu)}{\mu}\left\{\frac{\pi p_0}{8a}\left(2a^2 - r^2\right)\right\} = \delta - \frac{1}{2R}r^2 \qquad (2.1.28)$$

For $r = 0$, at the center of the contact area, one can find the indentation depth as

$$\delta = \frac{(1-\nu)\pi p_0 a}{4\mu} \qquad (2.1.29)$$

Making use of Eq.(2.1.29) and substituting $r = a$ into Eq. (2.1.28), one can find the radius of the contact area, a, as

$$a = \frac{(1-\nu)\pi\, p_0 R}{4\mu} \tag{2.1.30}$$

Substituting Eq. (2.1.30) into Eq. (2.1.29) yields

$$\delta = \frac{a^2}{R} \tag{2.1.31}$$

In practice, the indentation depth and the corresponding total contact load are usually measured separately in the indentation test. Therefore, the contact load-indentation depth relationship in an analytical form that fits the experimental data is desired.

Recall the pressure distribution, Eq. (2.1.7),

$$p(r) = p_0 \left\{1 - (r/a)^2\right\}^{1/2}.$$

The contact load, F_c, corresponding to the pressure acting on the loaded circular surface, S, is given by the integration of the pressure over the loaded circular surface; i.e.,

$$F_c = \int_0^a p(r) 2\pi r dr = \frac{2}{3} p_0 \pi a^2. \tag{2.1.32}$$

By expressing p_0 in terms of the rest of Eq. (2.1.32) and substituting the expression into Eq. (2.1.30), the radius of the contact area is given by

$$a = \left(\frac{(1-\nu)3RF_c}{8\mu} \right)^{1/3}. \tag{2.1.33}$$

By substituting Eq.(2.1.33) into Eq.(2.1.31), the indentation depth is given by

$$\delta = \left(\frac{(1-\nu)^2 9F_c^2}{64R\mu^2} \right)^{1/3}. \tag{2.1.34}$$

By rearranging Eq. (2.1.30), the maximum contact pressure can be expressed as

$$p_0 = \frac{4\mu a}{\pi R(1-\nu)} \tag{2.1.35}$$

The contact load F_c as a function of the indentation depth is then determined by rearranging Eq. (2.1.34):

$$F_c = \frac{8\sqrt{R}\,\mu}{3(1-\nu)}\delta^{3/2} \tag{2.1.36}$$

This equation is known as "the Hertz contact law". The coefficient, $8\sqrt{R}\,\mu/\{3(1-\nu)\}$, which relates the indentation depth and the contact load is known as "the contact stiffness". This coefficient is a function of not only material properties, but also of the contact profile, i.e., the radius of the spherical indenter.

The relationship between the indentation depth and the corresponding contact load for a viscoelastic material can be obtained by using the correspondence principle based on the elastic solution, as will be discussed in section 2.3.

The restrictions on the Hertz theory when a rigid-indenter is applied are summarized here:

1) Values of a have to be much smaller than R.

2) An indented body can be considered as a semi-infinite elastic body.

3) The surfaces are frictionless.

Restriction (1) has to be verified by comparing the analytical solution with the experimental results; restriction (2) will be discussed in more details later; and restriction

(3) can be satisfied when negligible friction occurs between two bodies in contact. Restriction (2) is vague. Therefore, it requires some quantitative specifications. Meijers [7] validated the Hertz theory for the contact of an isotropic material layer with a rigid substrate. According to his results, the ratio of the thickness of the layer to the contact area should be larger than 10 for the Hertz theory to be valid. Swanson [8] proposed a stricter limitation. He studied the contact between a rigid body and an orthotropic material layer on a rigid substrate by applying the Fourier series expansion technique to partial differential equations. According to Swanson's results, the effect of the layer's finite geometry of the layer can be ignored when the layer's width/length, and thickness are at least 50 times the radius of the contact area. This implies that if the ratios of the width/length and thickness to the radius of the contact area are larger than 50, the layer can be considered as a semi-infinite body; thus, the Hertz theory is applicable.

2.2 Generalized Axisymmetric Contact Problem

As Johnson [4] reported, the Hertz contact theory can also be applied to problems having a circular/elliptical contact area. Sneddon [3] obtained the solution of more general contact problems for axisymmetric cases with rigid indenters in rigid-elastic contact. Sneddon used a pair of dual integral equations to obtain the contact pressure distribution with a known contact profile. Thus, this technique does not have the same limitation as that imposed on the Hertz theory, i.e., the parabolic approximation of a sphere indenter.

Considering the contact of a rigid indenter with a contour profile $g(\rho)$ and a semi-infinite elastic body, the contact profile is equivalent to $g(\rho)$; i.e.,

$$f(\rho)=g(\rho), \tag{2.2.1}$$

where $\rho=r/a$ and a is the contact area, provided that the origin of the coordinate system coincides with the first contact point, so that $f(0)=g(0)=0$. The boundary conditions are given by

$$\bar{\sigma}_{rz}(\rho)=0 \qquad \rho\geq 0 \tag{2.2.2}$$

$$\bar{u}_z(\rho)=\delta-f(\rho) \qquad 0\leq\rho\leq 1 \tag{2.2.3}$$

$$\bar{\sigma}_{zz}(\rho)=0 \qquad \rho>1 \tag{2.2.4}$$

Sneddon [3] solved the above mixed boundary value problem by using the Hankel transforms. See *Appendix A* for details of the derivation. By using the Hankel transform, the possible displacement field is given by

$$u_r(r,z)=\frac{-a}{2(1-\nu)}\mathcal{H}_1\left[\{(1-2\nu)-\xi z\}\xi^{-1}\psi(\xi a)e^{-\xi z};\ \xi\rightarrow r\right] \tag{2.2.5}$$

$$u_z(r,z)=\frac{a}{2(1-\nu)}\mathcal{H}_0\left[\{2(1-\nu)+\xi z\}\xi^{-1}\psi(\xi a)e^{-\xi z};\ \xi\to r\right] \tag{2.2.6}$$

where the Hankel transform is defined as

$$\mathcal{H}_\nu[f(\xi,z);\ \xi\to r]=\int_0^\infty \xi f(\xi,z)J_\nu(\xi r)d\xi \tag{2.2.7}$$

where J_ν is a Bessel function of the first kind and ν is a non-negative integer. By inserting the displacements into the following linear elastic stress-displacement relationship, i.e.,

$$\sigma_{rz}(r,z)=\mu\left(\frac{\partial u_r}{\partial z}+\frac{\partial u_z}{\partial r}\right) \tag{2.2.8}$$

$$\sigma_{zz}(r,z)=\lambda\left(\frac{\partial}{\partial r}+\frac{1}{r}\right)u_r+(\lambda+2\mu)\frac{\partial u_z}{\partial z}, \tag{2.2.9}$$

the stresses are expressed as

$$\sigma_{rz}(r,z)=-\frac{\mu a z}{1-\nu}\mathcal{H}_1\left[\xi\psi(\xi a)e^{-\xi z};\ \xi\to r\right] \tag{2.2.10}$$

$$\sigma_{zz}(r,z)=-\frac{\mu a}{1-\nu}\mathcal{H}_0\left[(1+\xi z)\psi(\xi a)e^{-\xi z};\ \xi\to r\right]. \tag{2.2.11}$$

The boundary values at $z=0$ can be expressed explicitly by using Eqs. (2.2.6), (2.2.10), and (2.2.11):

$$\bar{u}_z(r)=\mathcal{H}_0\left[\zeta^{-1}\psi(\zeta);\ \zeta\to\rho\right] \tag{2.2.12}$$

$$\bar{\sigma}_{zz}(r)=-\frac{\mu}{a(1-\nu)}\mathcal{H}_0[\psi(\zeta);\ \zeta\to\rho] \tag{2.2.13}$$

$$\bar{\sigma}_{rz}(r)=0, \tag{2.2.14}$$

where $\rho = r/a$, and a is the contact area. Thus, the boundary conditions (2.2.2), (2.2.3) and (2.2.4) are satisfied by solving

$$\mathcal{H}_0\left[\zeta^{-1}\psi(\zeta);\quad \zeta \to \rho\right] = \delta - f(\rho) \qquad 0 \le \rho < 1 \qquad (2.2.15)$$

$$\mathcal{H}_0[\psi(\zeta);\ \zeta \to \rho] = 0 \qquad 1 < \rho \qquad (2.2.16)$$

for $\psi(\zeta)$. The dual integral equations have the following solution:

$$\psi(\zeta) = \int_0^1 \chi(\vartheta)\cos(\zeta\vartheta)d\vartheta\,. \qquad (2.2.17)$$

This function automatically satisfies Eq. (2.2.16), by Sneddon [9]. Substituting Eq. (2.2.17) into Eq. (2.2.15) gives

$$\int_0^\rho \frac{\chi(\vartheta)}{\sqrt{\rho^2 - \vartheta^2}}d\vartheta = \delta - f(\rho). \qquad 0 \le \rho \le 1 \qquad (2.2.18)$$

This form of integration is called "the Abel integral equation," and its solution can be obtained from Zabreyko et al. [10]:

$$\chi(\vartheta) = \frac{2\delta}{\pi} - \frac{2}{\pi}\frac{d}{d\vartheta}\left[\int_0^\vartheta \frac{\rho f(\rho)}{\sqrt{\vartheta^2 - \rho^2}}d\rho\right]. \qquad (2.2.19)$$

Substituting Eq. (2.2.19) into Eq. (2.2.17) gives the solution for the mixed boundary value problem. The following parameters for contact problems are expressed in terms of the contact profile, $f(\rho)$.

For the indentation depth,

$$\delta = \int_0^1 \frac{f'(\rho)}{\sqrt{1-\rho^2}}d\rho\,. \qquad (2.2.20)$$

For the surface displacement within the contact area,

$$\bar{u}_z(r) = \int_0^{\rho} \frac{\chi(\vartheta)}{\sqrt{\rho^2 - \vartheta^2}} d\vartheta, \qquad 0 \le \rho \le 1 \qquad (2.2.21)$$

with $\chi(\vartheta)$ defined by Eq. (2.2.19).

For the surface displacement outside the contact area,

$$\bar{u}_z(r) = \int_0^{1} \frac{\chi(\vartheta)}{\sqrt{\rho^2 - \vartheta^2}} d\vartheta. \qquad 1 < \rho \qquad (2.2.22)$$

For the contact pressure distribution,

$$\bar{\sigma}_{zz}(r) = \frac{\mu}{a\rho(1-\nu)} \frac{d}{d\rho} \left[\int_{\rho}^{1} \frac{\vartheta \chi(\vartheta)}{\sqrt{\vartheta^2 - \rho^2}} d\vartheta \right]. \qquad (2.2.23)$$

For the contact load,

$$F_c = \frac{4\mu a}{(1-\nu)} \int_0^{1} \frac{\rho^2 f'(\rho)}{\sqrt{1-\rho^2}} d\rho, \qquad (2.2.24)$$

where $f(\rho)$ can be a function of real numbers which satisfies $f(0) = 0$, due to the solution of the Abel integration given by Eq. (2.2.19).

When the indenter profile is not given in any analytical form, an approximation of the indenter profile by using known functions will lead to the approximate solution of the contact problem. A commonly used approximation function is a polynomial function. When the contact profile is given by a polynomial function,

$$f(\rho) = \sum_{n=1}^{\infty} c_n a^n \rho^n \qquad (2.2.25)$$

$$\chi(\vartheta) = \frac{2}{\sqrt{\pi}} \sum_{n=1}^{\infty} \frac{\Gamma(\frac{1}{2}n + 1)}{\Gamma(\frac{1}{2}n + \frac{1}{2})} c_n a^n (1 - \vartheta^n), \qquad (2.2.26)$$

where Γ is a gamma function defined as $\Gamma(n) = (n-1)!$. The parameters given by Eqs. (2.2.20) to (2.2.24) are as follows.

For the indentation depth,

$$\delta = \sqrt{\pi}\sum_{n=1}^{\infty}\frac{\Gamma(\frac{1}{2}n+1)}{\Gamma(\frac{1}{2}n+\frac{1}{2})}c_n a^n . \tag{2.2.27}$$

For the surface displacement within the contact area,

$$\bar{u}_z(r) = \frac{2}{\sqrt{\pi}}\sum_{n=1}^{\infty}\frac{\Gamma(\frac{1}{2}n+1)}{\Gamma(\frac{1}{2}n+\frac{1}{2})}c_n a^n j_n(\rho), \qquad r \le a \tag{2.2.28}$$

where

$$j_n(\rho) = \int_0^{\rho}\frac{1-\vartheta^n}{\sqrt{\rho^2-\vartheta^2}}d\vartheta . \qquad n \ge 1 \tag{2.2.29}$$

For the surface displacement outside the contact area,

$$\bar{u}_z(r) = \frac{2}{\sqrt{\pi}}\sum_{n=1}^{\infty}\frac{\Gamma(\frac{1}{2}n+1)}{\Gamma(\frac{1}{2}n+\frac{1}{2})}c_n a^n\left[\sin^{-1}\left(\frac{1}{\rho}\right)-k_n(\rho)\right], \qquad r \ge a \tag{2.2.30}$$

where

$$k_n = \int_0^{1}\frac{\vartheta^n}{\sqrt{\rho^2-\vartheta^2}}d\vartheta . \tag{2.2.31}$$

For the contact pressure distribution,

$$\bar{\sigma}_{zz}(r) = -\frac{2\mu}{\sqrt{\pi}(1-\nu)a}\sum_{n=1}^{\infty}\frac{n\Gamma(\frac{1}{2}n+1)}{\Gamma(\frac{1}{2}n+\frac{1}{2})}c_n a^n i_n(\rho) , \qquad 0 \le \rho < 1 \tag{2.2.32}$$

where

$$i_n(\rho) = \int_{\rho}^{1}\frac{\vartheta^{n-1}}{\sqrt{\vartheta^2-\rho^2}}d\vartheta . \qquad \begin{matrix} 0 \le \rho < 1 \\ n \ge 1 \end{matrix} \tag{2.2.33}$$

For the contact load,

$$F_c = \frac{4\sqrt{\pi}\,\mu a}{1-\nu}\sum_{n=1}^{\infty}\frac{n\Gamma(\frac{1}{2}n+1)}{(n+1)\Gamma(\frac{1}{2}n+\frac{1}{2})}c_n a^n . \tag{2.2.34}$$

By using the parameters obtained by using Sneddon's approach to contact problems, the surface displacement is derived below to express the function explicitly without the integration over the loaded circular surface. The surface displacement, Eq. (2.2.28), within the contact area is then given in terms of the contact pressure, $\bar{\sigma}_{zz}(r)$, Eq. (2.2.32):

$$\bar{u}_z(r) = J_{Sin}\bar{\sigma}_{zz}(\rho), \qquad r \le a \qquad (2.2.35)$$

where

$$J_{Sin} = \frac{\bar{u}_z(r)}{\bar{\sigma}_{zz}(\rho)} = -\frac{\frac{2}{\sqrt{\pi}}}{\frac{2\mu}{\sqrt{\pi}(1-\nu)a}} \sum_{n=1}^{\infty} \frac{\frac{\Gamma(\frac{1}{2}n+1)}{\Gamma(\frac{1}{2}n+\frac{1}{2})} c_n a^n j_n(\rho)}{\frac{n\Gamma(\frac{1}{2}n+1)}{\Gamma(\frac{1}{2}n+\frac{1}{2})} c_n a^n i_n(\rho)}$$

$$= -\frac{1-\nu}{\mu}\left[a\sum_{n=1}^{\infty}\frac{j_n(\rho)}{n i_n(\rho)}\right]. \qquad (2.2.36)$$

By recalling Eq. (2.1.11),

$$\bar{u}_z = \frac{(1-\nu)}{\mu}\left[\frac{1}{2\pi}\iint_S p(s_c,\phi)ds_c d\phi\right],$$

and defining $p_C(r)$, the contribution of the pressure over the loaded circular surface to the displacement, as

$$p_C(r) = \left[\frac{1}{2\pi}\iint_S p(s_c,\phi)ds_c d\phi\right], \qquad (2.2.37)$$

then

$$\bar{u}_z = \frac{(1-\nu)}{\mu} p_C. \qquad (2.2.38)$$

By comparing Eqs. (2.2.38) and (2.2.35), we have

$$\bar{u}_z(r) = J_{Sin}\bar{\sigma}_{zz}(\rho)$$

$$= \frac{1-\nu}{\mu}\left\{ a \times \frac{2\mu}{\sqrt{\pi}\,(1-\nu)a} \sum_{n=1}^{\infty} \frac{j_n(\rho)}{n i_n(\rho)} \frac{n\Gamma(\frac{1}{2}n+1)}{\Gamma(\frac{1}{2}n+\frac{1}{2})} c_n a^n i_n(\rho) \right\}$$

$$= \frac{(1-\nu)}{\mu} p_{Cin}, \tag{2.2.39}$$

where

$$p_{Cin} = \frac{2\mu}{\sqrt{\pi}(1-\nu)} \sum_{n=1}^{\infty} \frac{\Gamma\left(\frac{1}{2}n+1\right)}{\Gamma\left(\frac{1}{2}n+\frac{1}{2}\right)} c_n a^n j_n(\rho). \tag{2.2.40}$$

Without integrating over the loaded circular surface, as shown in section 2.1, a function is obtained for the contact pressure that acts on a circular surface to give the corresponding surface displacement of a semi-infinite elastic body. By assigning $n = 2$ and $c_2 = 1/2R$ in Eq. (2.2.40), where R is the radius of a spherical indenter, to have the contact profile consistent with Eq. (2.1.4), one obtains

$$p_{Cin\,n=2} = \frac{\mu c_2}{(1-\nu)}\left(2a^2 - a^2\rho^2\right)$$

$$= \frac{\mu}{2R(1-\nu)}\left(2a^2 - r^2\right). \qquad r \le a \tag{2.2.41}$$

Substituting the above equation into Eq. (2.2.39) yields

$$\bar{u}_z(r) = \frac{(1-\nu)}{\mu}\left\{ \frac{\mu}{2R(1-\nu)}\left(2a^2 - r^2\right) \right\}, \qquad r \le a \tag{2.2.42}$$

which agrees with the equation obtained by substituting Eq. (2.1.35) into Eq. (2.1.21); i.e.,

$$\bar{u}_z(r) = \frac{(1-\nu)}{\mu}\left\{ \frac{\mu}{2R(1-\nu)}\left(2a^2 - r^2\right) \right\}. \qquad r \le a \tag{2.2.43}$$

Eq. (2.2.39) suggests that once the contact profile has been approximated by using a polynomial function, one can find the corresponding relationship between the normal surface displacement and the contact pressure within the contact area.

The surface displacement outside the contact area can also be obtained by using an approach analogous to the above. Again, the surface displacement, Eq. (2.2.30), can be expressed as a function of the contact pressure, Eq. (2.2.32):

$$\bar{u}_z(r) = J_{Sout}\bar{\sigma}_{zz}(\rho), \qquad r \geq a \qquad (2.2.44)$$

where

$$J_{Sout} = \frac{\bar{u}_z(r)}{\bar{\sigma}_{zz}(\rho)} = \frac{\frac{2}{\sqrt{\pi}}}{\frac{2\mu}{\sqrt{\pi}(1-\nu)a}} \sum_{n=1}^{\infty} \frac{\frac{\Gamma(\frac{1}{2}n+1)}{\Gamma(\frac{1}{2}n+\frac{1}{2})} c_n a^n \left[\sin^{-1}\left(\frac{1}{\rho}\right) - k_n(\rho)\right]}{\frac{n\Gamma(\frac{1}{2}n+1)}{\Gamma(\frac{1}{2}n+\frac{1}{2})} c_n a^n i_n(\rho)}$$

$$= -\frac{(1-\nu)}{\mu} a \sum_{n=1}^{\infty} \frac{\sin^{-1}\left(\frac{1}{\rho}\right) - k_n(\rho)}{n i_n(\rho)}. \qquad (2.2.45)$$

By isolating the terms related to the contact pressure in Eq. (2.2.44), one obtains

$$\bar{u}_z(r) = J_{Sout}\bar{\sigma}_{zz}(\rho)$$

$$= \frac{(1-\nu)}{\mu}\left\{ a \times \frac{2\mu}{\sqrt{\pi}(1-\nu)a} \sum_{n=1}^{\infty} \frac{\sin^{-1}\left(\frac{1}{\rho}\right) - k_n(\rho)}{n i_n(\rho)} \frac{n\Gamma(\frac{1}{2}n+1)}{\Gamma(\frac{1}{2}n+\frac{1}{2})} c_n a^n i_n(\rho) \right\}$$

$$= \frac{(1-\nu)}{\mu} P_{Cout}. \qquad (2.2.46)$$

Thus,

$$p_{Cout} = \frac{2\mu}{\sqrt{\pi}(1-\nu)} \sum_{n=1}^{\infty} \frac{\Gamma(\frac{1}{2}n+1)}{\Gamma(\frac{1}{2}n+\frac{1}{2})} c_n a^n \left[\sin^{-1}\left(\frac{1}{\rho}\right) - k_n(\rho)\right]. \qquad (2.2.47)$$

By assigning $n = 2$ and $c_2 = 1/2R$ in Eq. (2.2.47), one obtains

$$p_{Cout} = \frac{\mu}{\pi R(1-\nu)}\left\{ (2a^2 - r^2)\sin^{-1}\left(\frac{a}{r}\right) + r^2\left(\frac{a}{r}\right)\left(1 - \frac{a^2}{r^2}\right)^{1/2} \right\}. \qquad r \geq a \qquad (2.2.48)$$

Then, the surface displacement outside the contact area is given by

$$\bar{u}_z(r)=\frac{(1-\nu)}{\mu}\left[\frac{\mu}{\pi R(1-\nu)}\left\{(2a^2-r^2)\sin^{-1}\left(\frac{a}{r}\right)+r^2\left(\frac{a}{r}\right)\left(1-\frac{a^2}{r^2}\right)^{1/2}\right\}\right]. \quad r\geq a \qquad (2.2.49)$$

This surface displacement can be made to agree with the one obtained in section 2.1, Eq. (2.1.27), by substituting Eq. (2.1.35); i.e.,

$$\bar{u}_z(r)=\frac{(1-\nu)}{\mu}\left[\frac{\mu}{\pi R(1-\nu)}\left\{(2a^2-r^2)\sin^{-1}\left(\frac{a}{r}\right)+r^2\left(\frac{a}{r}\right)\left(1-\frac{a^2}{r^2}\right)^{1/2}\right\}\right]. \quad r\geq a \qquad (2.2.50)$$

The above derivation for the relationship between the contact pressure and surface displacement is equivalent to the derivation used in section 2.1. However, unlike the one in section 2.1, this process does not require the cumbersome surface integral but is still applicable to a wider range of contact problems.

2.3 Linear Viscoelastic Materials

2.3.1 Classification of Materials

The term "viscoelasticity" is used for materials which have the combined characteristics of viscous fluids and elastic solids. An elastic solid is the idealized model for the materials which can store all work applied to a body as strain energy, provided that no other form of energy dissipation occurs. Viscous fluid is also an idealized model for the materials which can transport momentum in shear, but the momentum is a linear function of the strain rate in Newtonian fluid (following the linear stress-strain rate relationship) so the momentum will eventually be dissipated if the strain rate is zero. This

phenomenon is called "relaxation"; i.e., the stress will decrease with time under a constant strain. In a pure shear stress state, a Newtonian viscous fluid dissipates energy, but cannot store it.

The characteristics of viscoelastic materials are

1. Instantaneous response to suddenly applied stress/strain
2. Creep to constant stress excitation/ stress relaxation to constant strain excitation

In this study, only viscoelastic solids are considered. One characteristic of a viscoelastic solid is that the stresses go to a finite value as $t \to \infty$ under the applied constant strain. In reality, time t cannot be an infinite value. The measurement of stress for the applied constant strain must be terminated.

No simple or exact distinction exists between a "solid" and a "fluid", but we can model the materials as an ideal liquid, a perfectly elastic solid, or viscoelastic material, depending on the time scale in concern. The quantitative classification can be done by using the Deborah Number, N_D, defined as

$$N_D = \frac{\tau_{relax}}{\tau_{obs}}, \tag{2.3.1}$$

where τ_{relax} is relaxation time, and τ_{obs} is the time scale of observation, i.e., the time scale of interest for a particular problem. For an ideal liquid, $\tau_{relax} = 0$, and hence, $N_D = 0$. For a perfectly elastic solid $\tau_{relax} = \infty$, and hence, $N_D = \infty$. The Deborah number for any liquid or solid is therefore somewhere between 0 and ∞. If the Deborah number has the order of unity, the material should be treated as a viscoelastic material

because the contribution from the viscosity is significant. Therefore, the approach introduced in this chapter is not restricted by the time scale, but the Deborah number.

2.3.2 Constitutive Equation

The linearity of the stress-strain relationship is essential for applying the superposition principle to obtain the constitutive equations and is also a key for applying the solution technique, the correspondence principle (to be discussed in the next section). The constitutive equation for the viscoelastic materials is derived based on the infinitesimal deformation theory; i.e., the strain field is given by

$$\varepsilon_{ij} = \frac{1}{2}\left(u_{i,j} + u_{j,i}\right), \tag{2.3.2}$$

which is the same as the one needed in linear elastic cases, defined by Eq. (2.1.6). Here, viscoelasticity is treated by using the continuum mechanics approach.

As this study is concerned with indentation on an isotropic homogeneous material, the constitutive equations for an isotropic homogeneous material will be used here. Also, the material is assumed to be isothermal; i.e., the temperature distribution in the body is uniform and does not change during the deformation, so that the material properties are functions only of time. This assumption enables one to solve viscoelastic boundary value problems by using the correspondence principle.

Assuming that one is using an isotropic homogenous viscoelastic solid, two independent material properties that are functions of time are required to construct the stress-strain relationships. The two functions chosen here are the shear relaxation

function, $G(t)$, and the bulk relaxation function, $K(t)$. The two independent functions are not limited to these two. As a perfectly elastic solid is the limiting case of a viscoelastic solid, an analogy exists between the constitutive equations of elastic and viscoelastic solids. For a perfectly elastic solid, two of the four elastic constants should be independent of each other. This rule can also be applied to a viscoelastic solid. In order to easily distinguish the effects of the two types of deformation, i.e., distortion and volume change, shear and bulk relaxation functions are chosen as the two independent parameters. They can be obtained, respectively, by applying the strain step functions; i.e.,

$$\varepsilon_{12}(t) = \varepsilon_0 U(t) \tag{2.3.3}$$

and

$$\varepsilon_{ii}(t) = \varepsilon_{ii} U(t), \tag{2.3.4}$$

On the other hand, the shear and bulk creep functions can be obtained, respectively, by applying the stress step functions

$$\sigma_{12} = \sigma_0 U(t) \tag{2.3.5}$$

and

$$\sigma_{ii}(t) = \sigma_{ii} U(t). \tag{2.3.6}$$

$U(t)$ is the unit step function defined as

$$U(t) = \begin{cases} 1 & t \geq 0 \\ 0 & t < 0 \end{cases}. \tag{2.3.7}$$

The shear relaxation and creep functions are schematically depicted in Figures 2-3-1 and 2-3-2, respectively. The bulk relaxation and creep functions also have the same characteristics; i.e., the relaxation function is monotonically decreasing while the creep function is monotonically increasing with respect to time.

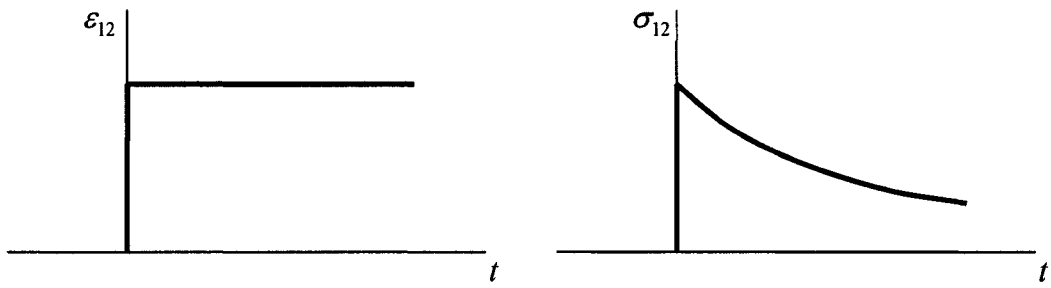

Figure 2-3-1. Shear relaxation function. Left: shear strain step function, and right: corresponding shear stress response.

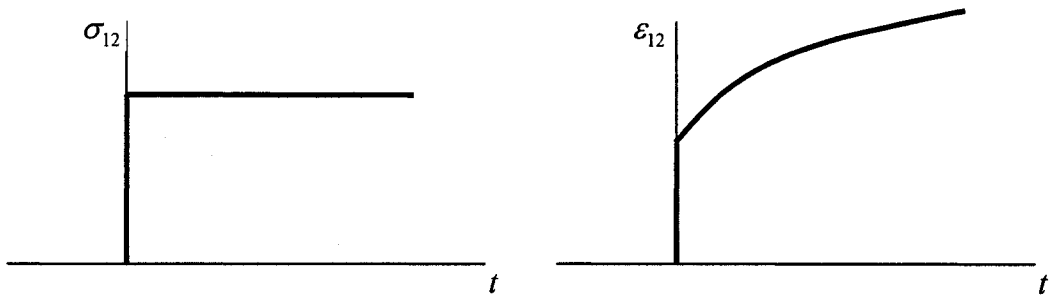

Figure 2-3-2. Shear creep function. Left: shear stress step function, and right: corresponding shear strain response.

The response of these functions to an arbitrary input of stress/strain can be determined by using Boltzman's superposition principle. Figure 2-3-3 provides a graphical explanation of this principle. In a linear behavior regime, the applied stress and the strain response can be superimposed. The strain corresponding to the applied stress step function, $\sigma_1 U(t-\tau_1)$, is given by

$$\varepsilon(t) = \sigma_1 J(t-\tau_1) U(t-\tau_1), \tag{2.3.8}$$

where $J(t)$ is a shear creep function. When the stress input is an arbitrary function of time, the arbitrary stress input can be approximated by the sum of the step functions as

shown in Figure 2-3-4. The response to the sum of the discretized stress step functions is obtained by the sum of all of these responses; i.e.,

$$\varepsilon_{12}(t)=\sum_{i=1}^{n}\Delta\sigma_i J(t-\tau_i)U(t-\tau_i). \tag{2.3.9}$$

By taking the limit of Eq. (2.3.9), the expression is rewritten as

$$\varepsilon_{12}(t)=\lim_{\max\Delta\sigma_i\to 0}\sum_{i=1}^{n}\Delta\sigma_i J(t-\tau_i)U(t-\tau_i)=\int_{0^-}^{t}J(t-\tau)d\sigma_{12}, \tag{2.3.10}$$

where $U(t-\tau)$ is always unity because t is always larger than or equal to the value of τ. The lower limit, 0^-, of the integration suggests that the body is not disturbed when $t<0$. By doing so, the integration still takes into account the instantaneous response at $t=0$. Thus, the well known form of the constitutive equation for the shear stress-strain relationship of a viscoelastic material can be written as

$$\varepsilon_{12}(t)=\int_{0^-}^{t}J(t-\tau)\frac{\partial\sigma_{12}}{\partial\tau}d\tau. \tag{2.3.11}$$

In an analogous procedure, the shear stress response to an arbitrary shear strain input can be written as

$$\sigma_{12}(t)=\int_{0^-}^{t}G(t-\tau)\frac{\partial\varepsilon_{12}}{\partial\tau}d\tau. \tag{2.3.12}$$

Similarly, the bulk relaxation and creep responses to an arbitrary input are given by

$$\sigma_{ii}(t)=\int_{0^-}^{t}K(t-\tau)\frac{\partial\varepsilon_{ii}}{\partial\tau}d\tau \tag{2.3.13}$$

$$\varepsilon_{ii}(t)=\int_{0^-}^{t}B(t-\tau)\frac{\partial\sigma_{ii}}{\partial\tau}d\tau, \tag{2.3.14}$$

where $K(t)$ and $B(t)$ are the bulk relaxation and creep functions, respectively.

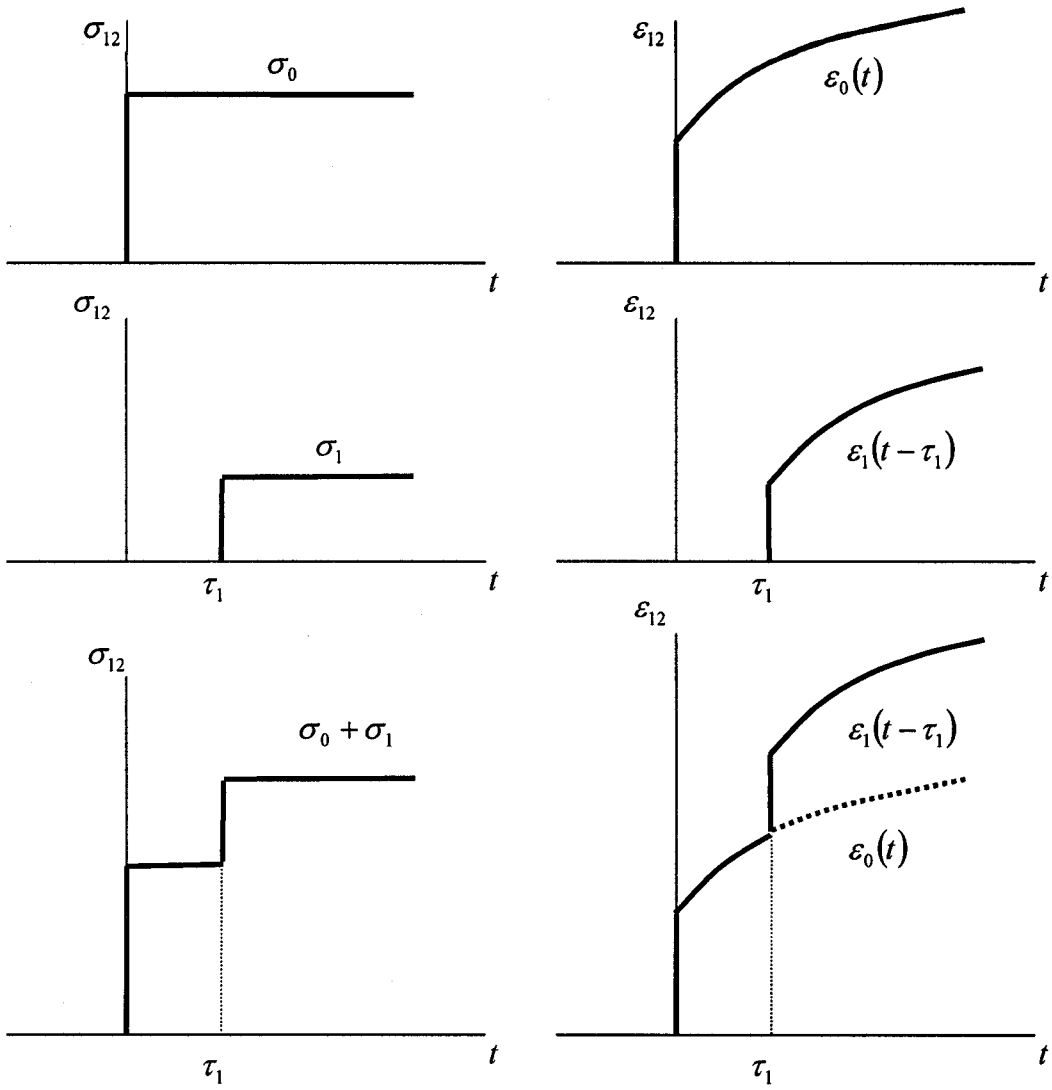

Figure 2-3-3. Boltzman's superposition principle, from Findley et al. [11]

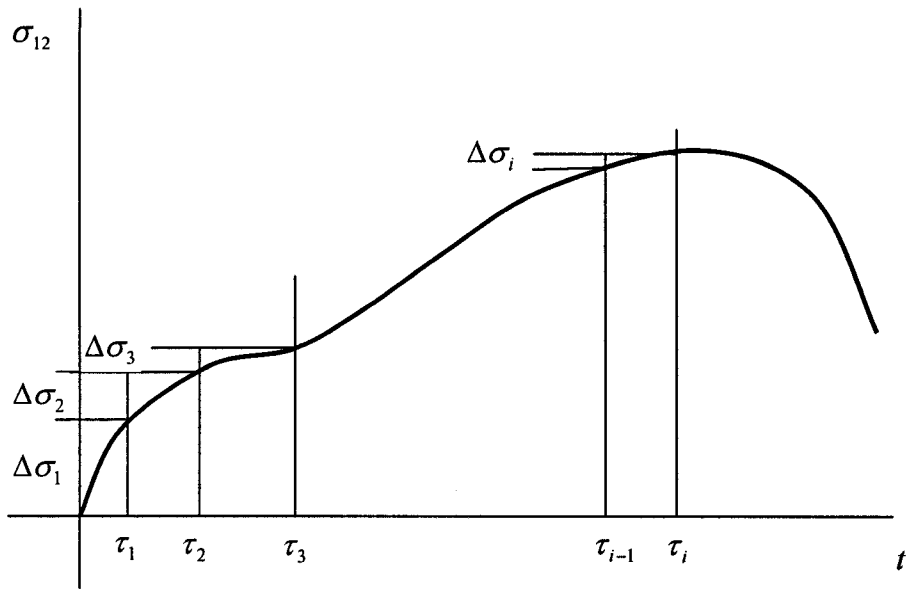

Figure 2-3-4. An arbitrary shear stress input function approximated by the discretized stress step functions, from Findley et al. [11]

The generalized constitutive equation is, therefore, given by

$$\varepsilon_{ij} = \int_{0^-}^{t} S_{ijkl}(t-\tau)\frac{\partial \sigma_{kl}}{\partial \tau} d\tau , \tag{2.3.15}$$

where $S_{ijkl}(t)$ are creep functions.

Alfrey [12] proposed the differential forms of the constitutive equations. Also, the stress-strain relationship for the linear isotropic viscoelastic material can be expressed in the following form:

$$P(D)s_{ij}(t) = Q(D)e_{ij}(t), \tag{2.3.16}$$

where

$$s_{ij} = \sigma_{ij} - \frac{1}{3}\delta_{ij}\sigma_{kk}, \quad s_{ii} = 0 \tag{2.3.17}$$

$$e_{ij} = \varepsilon_{ij} - \frac{1}{3}\delta_{ij}\varepsilon_{kk},\ e_{ii} = 0 \tag{2.3.18}$$

$$P(D) = \sum_{k=0}^{N} p_k D^k \tag{2.3.19}$$

$$Q(D) = \sum_{k=0}^{N} q_k D^k \tag{2.3.20}$$

and

$$D^k = \frac{\partial^k}{\partial t^k}. \tag{3.2.21}$$

s_{ij} is the deviatoric components of the stress, and e_{ij} is the deviatoric components of the strain. This approach can also be applied to dilational components of stress and strain as

$$P'(D)\sigma_{ii} = Q'(D)\varepsilon_{ii}, \tag{2.3.22}$$

where

$$P'(D) = \sum_{k=0}^{N} p'_k D^k \tag{2.3.23}$$

$$Q'(D) = \sum_{k=0}^{N} q'_k D^k\ . \tag{2.3.24}$$

The prime was used for distinguishing the parameters for bulk properties from those for shear properties. In those constitutive equations, the elastic constants are given when $k = 0$. In the elastic case, shear and bulk stress-strain relationships are given, respectively, by

$$p_0 s_{ij}(t) = q_0 e_{ij}(t)$$

$$s_{ij}(t) = \frac{q_0}{p_0} e_{ij}(t) \tag{2.3.25}$$

and

$$p_0'\sigma_{ij}(t) = q_0'\varepsilon_{ij}(t)$$

$$\sigma_{ij}(t) = \frac{q_0'}{p_0'}\varepsilon_{ij}(t). \tag{2.3.26}$$

By comparing Eqs. (2.3.25) and (2.3.26) to the elastic constitutive equations, the elastic constants are given by

$$\mu = \frac{q_0}{p_0} \tag{2.3.27}$$

$$\kappa = \frac{q_0'}{p_0'}, \tag{2.3.28}$$

where μ is the shear modulus and κ is the bulk modulus.

2.4 Viscoelastic Contact Problems

Lee and Radok [2] first studied the linear viscoelastic contact problem by using the correspondence principle, as shown in Figure 2-4-1.

$$F_c(t) = \frac{8\sqrt{R}\,\mu}{3(1-\nu)}\delta(t)^{3/2}$$

Laplace Transform and $\mu \to sG^*(s)$

$$F_c^*(s) = \frac{8\sqrt{R}}{3(1-\nu)}sG^*(s)\delta^*(s)^{3/2}$$

Inverse Laplace Transform

$$F_c(t) = \frac{8\sqrt{R}}{3}\int_{0^-}^{t}\frac{G(t-\tau)}{1-\nu}d\delta^{3/2}(\tau)$$

Figure 2-4-1. The procedure of the correspondence principle.

Read [13] and Lee [14] solve the viscoelastic boundary value problems by using the Fourier transform and by using the Laplace transform, respectively. The Laplace transform of a function, $f_L(t)$, is defined as

$$f_L^*(s) = \mathcal{L}(f_L) = \int_0^\infty f_L(t) e^{-st} dt, \tag{2.4.1}$$

where the superscript * indicates the Laplace transform, and s is the Laplace transform parameter. The inverse Laplace transform is defined as

$$f_L(t) = \mathcal{L}^{-1}(f_L^*). \tag{2.4.2}$$

The correspondence principle, used to obtain linear viscoelastic solutions by using the corresponding linear elastic solution with the use of the Laplace transform, has the following equations:

$$P(s)\sigma_{ij}^* = Q(s)e_{ij}^* \tag{2.4.3}$$

$$P'(s)\sigma_{ii}^* = Q'(s)\varepsilon_{ii}^* \tag{2.4.4}$$

$$\sigma_{ij,j}^* = f_i^*(x_k, s) \tag{2.4.5}$$

$$\varepsilon_{ij}^* = \frac{1}{2}\left(u_{i,j}^* + u_{j,i}^*\right) \tag{2.4.6}$$

$$T_i^*(x_i, s) = \sigma_{ij}^* n_j. \tag{2.4.7}$$

The Laplace transformed viscoelastic variables are associated with the corresponding elastic variables.

The linear viscoelastic solution obtained by Lee and Radok is restricted to cases in which the contact area does not decrease. This limitation is due to the contact pressure cannot be obtained by using the correspondence principle when the contact area decreases, due to the violation of the traction-free condition outside the contact area, as

will be explained later in section 2.5 after explaining the procedure for using the correspondence principle.

Graham [15] proposed a more general linear viscoelastic solution by using the generalized Papkovich Neuber solution. The solutions were obtained for arbitrary normal pressure on the surface of a semi-infinite viscoelastic body. When dealing with contact problems, the ideas behind these two techniques, i.e., those of Lee and Radok, and of Graham, are the same because both obtain the viscoelastic contact pressure distribution from the corresponding elastic contact pressure distribution. For axisymmetric cases, Ting [5] studied axisymmetric viscoelastic contact problems by using the Laplace transformation of Boussinesq's solution.

Here, Lee and Radok's approach is used to obtain the viscoelastic contact law for a more general case; i.e., Poisson's ratio is not constant. While Lee and Radok started with Eq. (2.1.36) by changing its material properties to operators, Q and P, and assuming $\nu = 1/2$, the following derivation will start with Eq. (2.1.11) to obtain the surface displacement due to arbitrary normal pressure distribution.

Recall Eq. (2.1.11),

$$\bar{u}_z(r,t) = \frac{(1-\nu)}{\mu}\frac{1}{2\pi}\iint_{\Omega_{max}} p(s_c,\phi,t)\,ds_c\,d\phi,$$

where Ω_{max} is the maximum contact area.

By using the isotropic elastic moduli relationship,

$$\bar{u}_z(r,t) = \frac{(3\kappa+4\mu)}{\mu(6\kappa+2\mu)}\frac{1}{2\pi}\iint_{\Omega_{max}} p(s_c,\phi,t)\,ds_c\,d\phi, \tag{2.4.8}$$

where

$$\nu = \frac{3\kappa - 2\mu}{6\kappa + 2\mu}. \tag{2.4.9}$$

The elastic constants are replaced using Eqs.(2.3.27) and (2.3.28).

$$\bar{u}_z(r,t) = \frac{(3\kappa + 4\mu)}{\mu(6\kappa + 2\mu)} \frac{1}{2\pi} \iint_{\Omega_{\max}} p(s_c,\phi,t) ds_c d\phi$$

$$= \left(3\frac{q_0'}{p_0'} + 4\frac{q_0}{p_0} \right) \left(6\frac{q_0'}{p_0'} + 2\frac{q_0}{p_0} \right)^{-1} \left(\frac{q_0}{p_0} \right)^{-1} \frac{1}{2\pi} \iint_{\Omega_{\max}} p(s_c,\phi,t) ds_c d\phi. \tag{2.4.10}$$

After applying the Laplace transform to the functions of pressure distribution $p(s_c,\phi,t)$ and surface displacement $\bar{u}_z(r,t)$, and replacing the symbols for the constants as follows, $q_0' \to Q'^*$, $p_0' \to P'^*$, $q_0 \to Q^*$ and $p_0 \to P^*$, we have

$$\bar{u}_z^*(r,s) = \left(3\frac{Q'^*}{P'^*} + 4\frac{Q^*}{P^*} \right) \left(6\frac{Q'^*}{P'^*} + 2\frac{Q^*}{P^*} \right)^{-1} \left(\frac{Q^*}{P^*} \right)^{-1} \frac{1}{2\pi} \iint_{\Omega_{\max}} p^*(s_c,\phi,s) ds_c d\phi. \tag{2.4.11}$$

The Laplace transformed constitutive equations of Eqs. (2.3.12) and (2.3.13) are determined as follows. By applying the Laplace transform to Eq. (2.3.12) and (2.3.16), one obtains

$$\sigma_{12}^*(s) = sG^*(s)\varepsilon_{12}^*(s) \tag{2.4.12}$$

and

$$P^*(s)s_{ij}(s) = Q^*(s)e_{ij}(s). \tag{2.4.13}$$

Therefore,

$$P^* = 1 \tag{2.4.14}$$

$$Q^* = sG^*. \tag{2.4.15}$$

One can find the similar relationship for a bulk relaxation function as that for the shear relaxation function. From Eqs. (2.3.13) and (2.3.22), we have

$$\sigma_{ii}^{*}(s) = sK^{*}(s)\varepsilon_{ii}^{*}(s) \tag{2.4.16}$$

$$P'^{*}(s)\sigma_{ii}^{*} = Q'^{*}(s)\varepsilon_{ii}^{*}. \tag{2.4.17}$$

Therefore,

$$P'^{*} = 1 \tag{2.4.18}$$

$$Q'^{*} = sK^{*}. \tag{2.4.19}$$

By replacing the transformed operator in Eq.(2.4.11) and using Eqs. (2.4.14), (2.4.15), (2.4.18) and (2.4.19), one obtains

$$\bar{u}_z^{*}(r,s) = \left(3K^{*} + 4G^{*}\right)\left\{s\left(6K^{*} + 2G^{*}\right)\right\}^{-1}\left(sG^{*}\right)^{-1} s\left[\frac{1}{2\pi}\iint_{\Omega_{\max}} p^{*}(s_c,\phi,s)ds_c d\phi\right]. \tag{2.4.20}$$

Applying the inverse Laplace transform to Eq. (2.4.20) yields

$$\bar{u}_z(r,t) = \int_{0^{-}}^{t}\Phi(t-\tau)d\left[\frac{1}{2\pi}\iint_{\Omega_{\max}} p(s_c,\phi,\tau)ds_c d\phi\right], \tag{2.4.21}$$

where

$$\Phi(t) = \left[\ \Gamma_m * d\Lambda^{-1} * dG^{-1}\right](t) \tag{2.4.22}$$

$$\Lambda(t) = 6K(t) + 2G(t) \tag{2.4.23}$$

$$\Gamma_m(t) = 3K(t) + 4G(t). \tag{2.4.24}$$

Note:

For f_N and g_N, which are functions of position and time, $f_N * dg_N$ indicates the Riemann-Stieltjes integral, defined as

$$[f_N * dg_N](\mathbf{x},t) = \int_{-\infty}^{t} f_N(\mathbf{x},t-t')\,dg_N(\mathbf{x},t'). \tag{2.4.25}$$

If either $f_N(\mathbf{x},t)=0$ or $g_N(\mathbf{x},t)=0$ when $t<0$, the above expression is equivalent to

$$[f_N * dg_N](\mathbf{x},t) = \int_{0^-}^{t} f_N(\mathbf{x},t-t')\,dg_N(\mathbf{x},t'). \tag{2.4.26}$$

In this study, no function is defined when $t<0$. Therefore, Eq.(2.4.26) is used to express $f_N * dg_N$.

The surface displacement of a semi-infinite viscoelastic body, due to the arbitrary normal pressure distribution on a circular surface that has been derived here, is the same as the one that Graham [15] obtained by using the generalized Papkovich Neuber solution.

Eq.(2.4.21) suggests that by knowing the pressure distribution history, the corresponding surface displacement can be obtained. The terms inside the bracket in Eq. (2.4.21) are actually the same as p_C defined in Eq. (2.2.37). Thus,

$$\bar{u}_z(r,t) = \int_{0^-}^{t} \Phi(t-\tau)\,dp_C(r,\tau). \tag{2.4.27}$$

This equation is the general form of the surface displacement due to the normal pressure applied to a circular surface on a semi-infinite viscoelastic body.

The viscoelastic contact pressure distribution is obtained by using the corresponding elastic contact pressure distribution and the correspondence principle in the case in which the contact area does not decrease. By substituting Eq. (2.1.35) into Eq. (2.1.7), the contact pressure distribution for a rigid sphere indenter and a semi-infinite elastic body is given by

$$p(r,t) = p_0\left\{1-(r/a(t))^2\right\}^{1/2}$$

$$= \frac{4\mu}{(1-\nu)R\pi}\sqrt{a^2(t)-r^2}\ . \tag{2.4.28}$$

By applying the analogous procedure for the previous case to the above equation, one obtains

$$p(t) = \frac{4}{R\pi}\frac{\mu(6\kappa+2\mu)}{(3\kappa+4\mu)}\sqrt{a^2(t)-r^2}$$

$$= \frac{4}{R\pi}\frac{q_0}{p_0}\left(6\frac{q_0'}{p_0'}+2\frac{q_0}{p_0}\right)\left(3\frac{q_0'}{p_0'}+4\frac{q_0}{p_0}\right)^{-1}\sqrt{a^2(t)-r^2}$$

$$p^*(s) = \frac{4}{R\pi}\frac{Q^*}{P^*}\left(6\frac{Q'^*}{P'^*}+2\frac{Q^*}{P^*}\right)\left(3\frac{Q'^*}{P'^*}+4\frac{Q^*}{P^*}\right)^{-1}\sqrt{a^{*2}(s)-r^2}$$

$$= \frac{4}{R\pi}sG^*\left(6K^*+2G^*\right)\left\{s\left(3K^*+4\ G^*\right)\right\}^{-1}s\sqrt{a^{*2}(s)-r^2}$$

$$p(r,t) = \frac{4}{R\pi}\int_{0^-}^{t}\Psi(t-\tau)d\sqrt{a^2(\tau)-r^2}\ , \tag{2.4.29}$$

where

$$\Psi(t) = \left[\ G^* d\Lambda^* d\Gamma_m^{-1}\right](t). \tag{2.4.30}$$

By defining p_e, Eq. (2.4.29) becomes

$$p(r,t)=\int_{0^-}^{t}\Psi(t-\tau)dp_e(r,\tau), \tag{2.4.31}$$

where p_e is the form of the pressure distribution without material constants. In Eq.(2.4.31), $p_e(r,\tau)=\frac{4}{R\pi}\sqrt{a^2(\tau)-r^2}$, from Eq. (2.4.29). Thus, the viscoelastic contact pressure can be obtained from the elastic contact pressure when the contact area does not decrease. The contact load for a viscoelastic material can be obtained by integrating the pressure distribution over the current contact area:

$$F_c(t)=\frac{4}{R\pi}\int_{0^-}^{a(\tau)}\left\{\int_{0^-}^{t}\Psi(t-\tau)d\sqrt{a^2(\tau)-r^2}\right\}2\pi r dr$$

$$=\frac{8}{3R}\int_{0^-}^{t}\Psi(t-\tau)da^3(\tau). \tag{2.4.32}$$

For the loading phase of the indentation test on a viscoelastic material, the contact area-indentation depth is same as that for the elastic case. An procedure analogous to the elastic case is applied to obtain the relationship between the indentation depth and the contact area in the contact-area-increasing phase.

First, the viscoelastic surface displacements in terms of the contact pressure distribution are obtained as a function of the elastic contact pressure by using Eqs. (2.4.21) and (2.4.31):

$$\bar{u}_z(r,t)=\int_{0^-}^{t}\Phi(t-\tau)d\left[\frac{1}{2\pi}\iint_{\Omega_{\max}}p(s_c,\phi,\tau)ds_c d\phi\right]$$

$$=\int_{0^-}^{t}\Phi(t-\tau)d\left[\int_{0^-}^{\tau}\Psi(\tau-\theta_t)d\left\{\frac{1}{2\pi}\iint_{\Omega_{\max}}p_e(s_c,\phi,\theta_t)ds_c d\phi\right\}\right]. \tag{2.4.33}$$

The surface integral can be obtained by using the elastic solution. By comparing Eqs. (2.1.21), (2.1.27) and (2.4.33), the surface displacements within and outside the contact area are, respectively, given by

$$\bar{u}_z(r,t)=\int_{0^-}^{t}\Phi(t-\tau)d\left[\int_{0^-}^{\tau}\Psi(\tau-\theta_t)d\left\{\frac{1}{2R}\left(2a^2(\theta_t)-r^2\right)\right\}\right] \tag{2.4.34}$$

$$\bar{u}_z(r,t)=\int_{0^-}^{t}\Phi(t-\tau)$$

$$d\left[\int_{0^-}^{\tau}\Psi(\tau-\theta_t)d\left\{\frac{1}{\pi R}\left\{\left(2a^2(\theta_t)-r^2\right)\sin^{-1}\left(\frac{a(\theta_t)}{r}\right)+r^2\left(\frac{a(\theta_t)}{r}\right)\left(1-\frac{a^2(\theta_t)}{r^2}\right)^{1/2}\right\}\right\}\right]. \tag{2.4.35}$$

Thus, the surface displacement on a semi-infinite viscoelastic body is given by a function of the solution of the elastic contact problem when the contact area is not decreasing.

For the approximation of a spherical indenter conforming to the surface, the normal surface displacement should meet the following conditions:

$$\bar{u}_z(r)=\delta-f(r)$$

$$\int_{0^-}^{t}\Phi(t-\tau)d\left[\int_{0^-}^{\tau}\Psi(\tau-\theta_t)d\left\{\frac{1}{2R}\left(2a^2(\theta_t)-r^2\right)\right\}\right]=\delta(t)-\frac{1}{2R}r^2. \tag{2.4.36}$$

By substituting Eq. (2.4.22) and Eq. (2.4.30) into Eq. (2.4.36) and applying the Laplace transformation, one obtains

$$\Gamma_m(s\Lambda)^{-1}(sG)^{-1}sGs\Lambda(s\Gamma_m)^{-1}s\left\{\frac{1}{2R}\left(2a^2(s)-r^2\right)\right\}=\delta(s)-\frac{1}{2R}r^2$$

$$\left\{\frac{1}{2R}\left(2a^2(s)-r^2\right)\right\}=\delta(s)-\frac{1}{2R}r^2\ . \tag{2.4.37}$$

By applying the inverse Laplace transform and substituting $r=0$,

$$\frac{a^2(t)}{R} = \delta(t)$$

$$a(t) = \sqrt{\delta(t)R} \tag{2.4.38}$$

By substituting Eq. (2.4.38) into Eq. (2.4.32), the relationship between the contact load and the indentation depth is given by

$$F_c(t) = \frac{8\sqrt{R}}{3} \int_{0^-}^{t} \Psi(t-\tau)\, d\delta^{3/2}(\tau). \tag{2.4.39}$$

The contact pressure, Eq. (2.4.29), satisfies the displacement boundary condition, Eq. (2.1.5). This relationship can be verified by using the surface displacement obtained by substituting Eq. (2.4.29) into Eq. (2.4.21). Therefore, the viscoelastic contact problem can be solved by using the Laplace transform to obtain the viscoelastic solutions from the corresponding elastic solutions with the restriction that the contact area is not decreasing.

The viscoelastic contact solutions obtained by using the correspondence principle contain the Stieljet integral. Thus, the contact area cannot have discontinuity or be a constant contact area. For example,

$$a(t) = a_0 U(t), \tag{2.4.40}$$

where $U(t)$ is the unit step function defined in Eq. (2.3.7). Substituting Eq. (2.4.40) into Eq. (2.4.32) gives

$$F_c(t) = \frac{8a_0^3}{3R} \int_{0^-}^{t} \psi(t-\tau) \frac{\partial U(\tau)}{\partial \tau} d\tau. \tag{2.4.41}$$

The discontinuity at time $t = 0$ causes difficulty in obtaining the corresponding contact load due to the derivative of the unit step function, i.e., the delta function, in the integral. While the contact area is kept constant in Eq. (2.4.41), this area does not contribute to the

pressure distribution because the derivative of a constant contact area is zero. This problem can be resolved by applying the integration by parts to Eq. (2.4.41):

$$F_c(t) = \frac{8}{3R}\int_{0^-}^{t}\psi(t-\tau)da^3(\tau)$$

$$= \frac{8}{3R}\left[a^3(\tau)\psi(t-\tau)\Big|_{0^-}^{t} - \int_{0^-}^{t}a^3(\tau)d\psi(t-\tau)\right]$$

$$= \frac{8}{3R}\left[a^3(t)\psi(0) + \int_{0}^{t}a^3(t-\theta)d\psi(\theta)\right], \qquad (2.4.42)$$

where a at $\tau = 0^-$ is equal to 0, and $\theta = t - \tau$. Thus, the solution does not have a difficulty in integration as long as $\psi(t)$ is a smooth, continuous function. Also, the constant contact area is also taken into account to obtain the contact load. The analogous procedure can be applied to any viscoelastic contact solutions.

2.5 Previous Work on Viscoelastic Contact Problems

Hunter [16] expanded Lee and Radok's work to the contact problem of a semi-infinite viscoelastic body possessing a single maximum contact area, i.e., involving an unloading phase. Graham [15] and Ting [5] obtained the same results by using the inverse of the Stieljet integral equation. Graham and Ting found that the contact pressure during the contact-area-decreasing phase can be obtained by using the contact pressure during the contact-area-increasing phase and using the radius of the contact area as an independent variable. Hunter proposed the basic idea which Graham and Ting expanded

to more complicated problems; i.e., problems in which the radius of the contact area is given by an arbitrary smooth function.

The idea that the contact area can be an independent variable comes from the following equation in Hunter's paper [16]:

$$F_c(t) = \frac{8}{3R(1-\nu)} \int_{0^-}^{t_1} G(t-\tau) da^3(\tau), \tag{2.5.1}$$

where $a(t) = a(t_1)$, and t_1 is the time before t_{max} is reached; i.e., $t_1 \le t_{max}$. t is the time after t_{max} is reached; i.e., $t > t_{max}$ where t_{max} is the time when the contact area is maximum. Eq. (2.5.1) suggests that if we know the size of the contact area, $a(t)$, the corresponding contact load can be determined independently of whether it is in the loading or the unloading phase. This approach is based on the concept that the same contact area gives the same contact pressure distribution, regardless of the loading history from $a(t_1)$ to $a(t)$.

The above contact problem was solved by using dual integral equations. In the linear elastic case, the dual integral equations have the mixed-boundary conditions: the normal surface displacement is prescribed within the contact area while the traction-free condition is prescribed outside the contact area. The dual integral equations have, for example, the following general forms equivalent to Eqs. (2.2.15) and (2.2.16):

$$\int_0^\infty \xi^{-1} \psi(\xi) J_0(\xi\rho) d\xi = \delta - f(\rho) \qquad 0 \le \rho \le 1 \tag{2.5.2}$$

$$\int_0^\infty \psi(\xi) J_0(\xi\rho) d\xi = 0. \qquad \rho > 1 \tag{2.5.3}$$

Eq. (2.5.2) satisfies the surface displacement $\delta - f(\rho)$ condition within the contact area while Eq.(2.5.3) satisfies the traction-free condition outside the contact area. The dual equations are solved for an unknown function $\psi(\xi)$, which satisfies both boundary conditions.

The correspondence principle requires the region(s) of the Laplace transformed displacement/traction boundary condition or mixed boundary condition to be independent of time, so that the viscoelastic problem has a unique solution. Therefore, the use of the dual integral equations with the correspondence principle to solve the corresponding viscoelastic contact problem has a restriction due to the uniqueness requirement. Onat and Breuer [17] have studied the uniqueness in the mixed boundary problems of viscoelastic materials. The mixed boundary conditions are

$$\sigma_{ij} n_j = T_i = \hat{T}_i(x,t) \quad \text{on } \partial\Re^T, \quad t \geq 0 \tag{2.5.4}$$

$$u_i = \hat{u}_i(x,t) \qquad \text{on } \partial\Re^D = \partial\Re - \partial\Re^T, \quad t \geq 0, \tag{2.5.5}$$

where $\partial\Re$ is the entire boundary of a body, $\partial\Re^T$ is the boundary where the traction boundary condition is applied, and $\partial\Re^D$ is the boundary where the displacement boundary condition is applied. Also, both $\partial\Re^D$ and $\partial\Re^T$ are time-independent. This restriction suggests that the indentation problem in which the contact area varies with time cannot maintain the required condition that $\partial\Re^T$ is time-independent. Therefore, using the dual integral equations which deal with the mixed boundary condition is not a suitable method for solving the viscoelastic contact problem possessing the contact-area-decreasing phase.

Hunter [16] also used the dual integral equations for the viscoelastic contact problem. He obtained the same solution as that by Lee and Radok [2] for the contact-area-

increasing phase. The use of the correspondence principle for the dual integral equations for the contact-area-increasing phase by Hunter is actually the same as that for obtaining viscoelastic contact pressure from the corresponding elastic solution. No special procedure was applied to obtain the solution.

The boundary condition during the contact-area-increasing phase can be interpreted as

$$\left.\begin{array}{ll} \bar{\sigma}_{zz}(t)=0 & \\ \bar{\sigma}_{rz}(t)=0 & 0\le\rho(t)\le 1 \\ \bar{\sigma}_{zz}(t)\neq 0 & \\ \bar{\sigma}_{zz}(t)=0 & 1\le\rho(t) \\ \bar{\sigma}_{rz}(t)=0 & \end{array}\right\} \quad \text{on } \partial\Re^T, \tag{2.5.6}$$

rather than the mixed-boundary conditions expressed as in Eqs. (2.1.1) to (2.1.3). Since no displacement boundary condition is applied, $\partial\Re^T = \partial\Re$. Even though the normal traction is a function of time so that the area on which the traction is applied varies with time, the region $\partial\Re^T$ where the traction boundary condition is applied does not change over time. Onat and Breuer [17] reported the uniqueness of this type of boundary condition. Therefore, the contact problem can be completely solved by using the correspondence principle for the contact-area-increasing phase.

Without violating the uniqueness condition, the viscoelastic contact pressure obtained by the elastic solution still satisfies the prescribed normal displacement condition, as if normal displacement were prescribed with a traction-free condition outside the contact area. Hunter [16] explained the restriction that the contact area is increasing. The traction boundary condition transformed using the correspondence principle is given by

$$\int_0^t \Psi(t-\tau)\,dp_e(\tau)=0, \qquad r>a(t) \tag{2.5.7}$$

where $p_e(\tau)$ is defined as in Eq. (2.4.31). During the contact-area-increasing phase, the boundary condition is satisfied because $p_e(\tau) = 0$ outside the contact area. In contrast, during the contact-area-decreasing phase, the boundary condition Eq. (2.5.6) is not satisfied because the history of $p_e(\tau)$ outside the current contact area still has non-zero value by the indentation. Therefore, the correspondence principle cannot be applied to the contact-area-decreasing phase to determine the pressure distribution.

Hunter used the idea of dual integral equations, with the correspondence principle, to obtain the viscoelastic contact pressure distribution for the contact-area-decreasing phase. His solution still satisfies the prescribed displacement boundary condition within the contact area. He also obtained the contact pressure distribution, which is exactly the same as the one with the same contact area in the contact-area-increasing phase. However, the uniqueness of the mixed boundary conditions is only valid when $\partial\Re^T$ is time-independent, as explained above. Hunter used the normal displacement within the contact area to confirm that the contact pressure distribution obtained is a unique solution, but this condition is not sufficient because only the displacement within the contact area is confirmed. This boundary condition is given by

$$\bar{u}_z(\rho(t)) = \delta - f(\rho(t)). \qquad 0 \le \rho(t) \le 1 \quad (2.5.8)$$

Since $\rho(t) = r/a(t)$, the region where the above boundary condition is applicable is also a function of time, so that

$$\bar{u}_z(\rho(t)) = \delta - f(\rho(t)) \qquad \text{on } \partial\Re^D(t), \qquad (2.5.9)$$

where $\partial\Re^D$ is the region where the displacement boundary condition is specified. However, this boundary condition is not sufficient to solve the viscoelastic problem by

using the correspondence principle, due to the time-dependence of $\partial\Re^D(t)$. Thus, the displacement within the contact is not a sufficient boundary condition to give the corresponding pressure distribution for the contact-area-decreasing phase, resulting in incorrect contact pressure. Since Graham [15] and Ting [5] used Hunter's results for the further development of viscoelastic contact problems, their work is not correct, either.

3. Semi-Analytical Algorithm for Viscoelastic Contact Problems

As mentioned in the last chapter, the viscoelastic contact pressure cannot be obtained from the elastic contact pressure by using the correspondence principle in the contact-area-decreasing phase. Accordingly, the viscoelastic contact load-indentation depth relationship for the unloading (contact-area-decreasing) phase cannot be expressed as a closed form solution in terms of the indentation depth. Numerical techniques such as finite element methods (FEM) offer alternative ways for such a viscoelastic contact problem. In this chapter, a semi-analytical technique is introduced to deal with the contact between an axisymmetric rigid body and a semi-infinite viscoelastic body. The technique can be applied to viscoelastic contact problems without the restriction of the contact-area-increasing or decreasing phase.

The technique for approximating the viscoelastic contact load at an instant of time by the solution of the equivalent elastic boundary value problem is introduced in this chapter. The technique allows the approximate viscoelastic contact load at the next time step in the contact-area-decreasing phase to be predicted by using the elastic solution, i.e., for the contact load-indentation depth relationship in the semi-analytical algorithm. Then, an algorithm for the numerical simulation is proposed based on the equivalent elastic boundary value problem.

A computationally effective numerical convolution integral algorithm that is useful for the semi-analytical algorithm of the viscoelastic contact is derived.

3.1 A viscoelastic Solution at an Instant of Time from an Elastic Solution

The fundamental concept of the proposed technique is to obtain the linear viscoelastic solution at an instant of time from the linear elastic solution by using Stieljet integrals, Eq. (2.3.15). Since only linear viscoelastic and linear elastic problems are discussed, the term "linear" is omitted hereafter.

Recall Eq. (2.3.15):

$$\varepsilon_{ij} = \int_{0^-}^{t} S_{ijkl}(t-\tau)\frac{\partial \sigma_{kl}(\tau)}{\partial \tau} d\tau ,$$

To separate the elastic response and viscosity contribution of the total strain, integration by parts is applied to Eq. (2.3.15):

$$\varepsilon_{ij} = S_{ijkl}(0)\sigma_{kl}(t) + \int_{0}^{t} \sigma_{kl}(t-\theta)\frac{\partial S_{ijkl}(\theta)}{\partial \theta} d\theta . \tag{3.1.1}$$

where $\theta = t - \tau$, and σ_{kl} at $\tau = 0^-$ is equal to 0. From Eq. (3.1.1), the total strain can be separated into two components; i.e.,

$$\varepsilon_{ij}(t) = \varepsilon_{ij}^{I}(t) + \varepsilon_{ij}^{D}(t), \tag{3.1.2}$$

where ε_{ij}^{I} is the instantaneously recoverable strain, defined as

$$\varepsilon_{ij}^{I}(t) = S_{ijkl}(0)\sigma_{kl}(t), \tag{3.1.3}$$

and ε_{ij}^{D} is the delayed recoverable strain, defined as

$$\varepsilon_{ij}^{D} = \int_{0}^{t} \sigma_{kl}(t-\theta)\frac{\partial S_{ijkl}(\theta)}{\partial \theta} d\theta . \tag{3.1.4}$$

By knowing the instantaneously recoverable strain at time t and the instantaneous elasticity of a viscoelastic material given by

$$C_{ijkl}(0) = S^{-1}_{ijkl}(0), \tag{3.1.5}$$

the stress σ_{kl} at time t can be obtained by using the instantaneously recoverable strain and the instantaneous elasticity of a viscoelastic material. By rearranging Eq. (3.1.3) and using the relationship given by Eq. (3.1.5), we have

$$\sigma_{kl}(t) = C_{ijkl}(0)\varepsilon^{I}_{ij}(t), \tag{3.1.6}$$

Thus the stresses at time t at a point of a viscoelastic body can be reproduced by its instantaneously elastic properties and instantaneously recoverable strains.

As the instantaneous elasticity of a viscoelastic material is used to obtain the instantaneously recoverable strain, the magnitude of the corresponding components of the $S_{ijkl}(0)$ should be larger than 0. Furthermore, to obtain the stress from the known instantaneously recoverable strain, the corresponding components of the $C_{ijkl}(0)$ for the strains should be larger than 0. Also, an instantaneously recoverable strain should exist. These requirements are violated when the generalized Kelvin-Voigt model, which does not show the instantaneous elastic response, is used to represent the viscoelastic material properties. Also, the Burgers model, which does not allow for instantaneous recovery, cannot be used in this method. More discussion of viscoelastic models can be fund in Findley et al. [11].

3.2 Application to Viscoelastic Contact Problems

The idea introduced in the previous section may be applied to the viscoelastic boundary value problems as well. In an indentation problem, i.e., a problem in which contact occurs between a rigid indenter and a semi-infinite viscoelastic body, the boundary conditions are applied to the surface of a semi-infinite viscoelastic body, and the rest of the body is not bounded; i.e., no other boundary surfaces are present. It is postulated that the instantaneously recoverable normal surface displacement of a semi-infinite viscoelastic body may give enough information to reproduce the solution of the viscoelastic boundary value problem at an instant of time. Since only normal surface displacement is discussed in this chapter, the term "normal surface" is omitted hereafter.

The applicability to the viscoelastic contact problem is verified by comparing the contact pressures obtained from the viscoelastic and the equivalent elastic problems. The procedure for applying the idea to the contact problem is performed in the following order. First, the instantaneously recoverable displacement is derived. Second, the equivalent elastic boundary value problem is obtained by using the instantaneously recoverable displacement. The term "the equivalent elastic problem" is used hereafter to represent the equivalent elastic boundary value problem. Last, the contact pressure distributions obtained from the viscoelastic boundary problem and from the equivalent elastic problem are compared.

Recall Eq. (2.4.21): the displacement on the surface of a semi-infinite viscoelastic body due to arbitrary normal pressure applied on the surface is given by

$$\bar{u}_z(r,t)=\int_{0^-}^{t}\Phi(t-\tau)d\left[\frac{1}{2\pi}\iint_{\Omega_{max}}p(s_c,\phi,\tau)ds_c d\phi\right].$$

Only arbitrary normal pressure distribution on a circular area is considered here because the available solution, i.e., Sneddon's solution, for the equivalent elastic problem is valid only for axisymmetric contact.

Applying integration by parts to Eq. (2.4.21) gives

$$\bar{u}_z(r,t)=\frac{1}{2\pi}\Phi(0)\iint_{\Omega_{max}}p(s_c,\phi,t)ds_c d\phi+\frac{1}{2\pi}\int_0^t\left[\iint_{\Omega_{max}}p(s_c,\phi,t-\theta)ds_c d\phi\right]\frac{\partial\Phi(\theta)}{\partial\theta}d\theta, \quad (3.2.1)$$

where $\theta=t-\tau$ and p at $\tau=0^-$ is equal to 0. Then the instantaneously recoverable displacement, $\bar{u}_z^I(r,t)$, is given by

$$\bar{u}_z^I(r,t)=\frac{1}{2\pi}\Phi(0)\iint_{\Omega_{max}}p(s_c,\phi,t)ds_c d\phi, \quad (3.2.2)$$

and the delayed recoverable displacement, $\bar{u}_z^D(r,t)$, is given by

$$\bar{u}_z^D(r,t)=\frac{1}{2\pi}\int_0^t\left[\iint_{\Omega_{max}}p(s_c,\phi,t-\theta)ds_c d\phi\right]\frac{\partial\Phi(\theta)}{\partial\theta}d\theta. \quad (3.2.3)$$

Eqs. (3.2.1) to (3.2.3) are displacements corresponding to arbitrary normal pressure distribution and its loading history on a semi-infinite viscoelastic body. By using the notation introduced in Eq. (2.2.37), we have

$$\bar{u}_z^I(r,t)=\Phi(0)p_C(r,t) \quad (3.2.4)$$

$$\bar{u}_z^D(r,t)=\int_0^t p_C(r,t-\theta)\frac{\partial\Phi(\theta)}{\partial\theta}d\theta, \quad (3.2.5)$$

where p_C is given by Eq. (2.2.41) when $r\le a(t)$ and by Eq. (2.2.48) when $r\ge a(t)$, for a spherical indenter approximated by a parabolic function.

Now that the two components of the total displacement are known, the equivalent elastic problem can be proposed as follows. First, let us define the equivalent elastic problem by using two of the three displacements (the instantaneously recoverable displacement, the delayed recoverable displacement, and the total displacement) for the viscoelastic solution because two of the three parameters are independent. The schematic description of two components of the total displacement and the total displacement obtained from the viscoelastic solution are shown in Figure 3-2-1. To generate the equivalent elastic problem, the instantaneously recoverable displacement is required to produce the surface contour. The undeformed original surface of the equivalent elastic problem is depicted by the broken line in Figure 3-2-2. The values of $g_{surface}$ are given by subtracting the instantaneously recoverable displacement, $\bar{u}_z^I$ in Figure 3-2-1, from the total displacement of the equivalent elastic problem, $\bar{u}_z^E$. The indentation depth in the equivalent elastic problem, δ_e, is equal to 0 when the indenter and the undeformed original surface are barely in contact at $r = 0$. Thus, the origin of the coordinate system is shifted down, as shown in Figure 3-2-2. The shifted coordinate system is used only to apply the indentation depth of the equivalent elastic problem to determine other quantities such as the contact area with changes of the indenter position and the contact pressure and to obtain the contact profile for the equivalent elastic boundary value problem. All other values are obtained by using the coordinate systems shown in Figure 3-2-1.

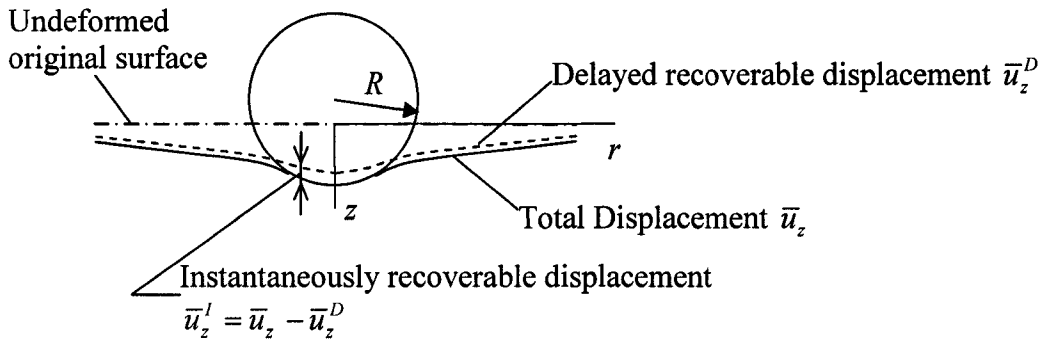

Figure 3-2-1. The schematic description of two components of the displacement.

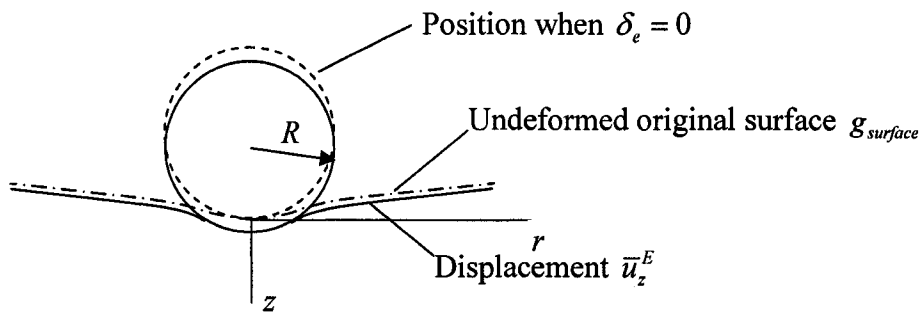

Figure 3-2-2. The schematic description of the equivalent elastic problem.

$g_{surface}(\rho,t)$ is defined as the difference obtained between the total displacement and the instantaneously recoverable displacement by using the coordinates in Figure 3-2-2; i.e.,

$$g_{surface}(\rho,t) = \bar{u}_z(\rho,t) - \bar{u}_z^I(\rho,t) - \left\{\bar{u}_z(\rho,t) - \bar{u}_z^I(\rho,t)\right\}\Big|_{\rho=0}. \qquad (3.2.6)$$

From Figure 3-2-2, the contact profile is defined by

$$f(\rho) = g(\rho) - g_{surface}(\rho), \qquad 0 \le \rho \le 1 \qquad (3.2.7)$$

where $\rho = r/a$, $g(\rho)$ is the indenter profile; i.e., $g(\rho) = \rho^2/2a^2R$ for the approximation of spherical indenter. $f(\rho)$ is obtained by using the shifted coordinate system shown in Figure 3-2-2. The boundary conditions for the equivalent elastic problem are given by

$$\bar{\sigma}_{rz}(\rho)=0 \qquad \rho \geq 0 \qquad (3.2.8)$$

$$\bar{u}_z(\rho)=\delta_e - f(\rho) \qquad 0 \leq \rho \leq 1 \qquad (3.2.9)$$

$$\bar{\sigma}_{zz}(\rho)=0, \qquad \rho > 1 \qquad (3.2.10)$$

where $\delta_e = \bar{u}_z'(r)\big|_{r=0}$ is used to reproduce the viscoelastic contact pressure distribution at an instant of time. The boundary conditions are exactly the same as those used to solve the generalized contact problem proposed by Sneddon [3], except that the undeformed surface is not flat. Sneddon's solution is originally for problems involving the contact between a rigid axisymmetric indenter and a semi-infinite body with the flat undeformed surface of a semi-infinite body. The equivalent elastic boundary value problem, however, does not have the flat undeformed surface. Thus, Sneddon's solution should serve at most as an approximate solution, with the boundary conditions given by Eqs. (3.2.8) to (3.2.10). The use of the same contact profile with a different undeformed surface geometry implies a change in the indenter shape. It can be understood to have been modified, so that the contact profile remains the same even though the modification is actually due to the change of the initial surface geometry.

For the equivalent elastic problem, the contact profile, $f(\rho)$ given by Eq. (3.2.7), is no longer a known function in advance because the value of $g_{surface}(\rho,t)$ changes with time. Since $g_{surface}(\rho,t)$ depends on the past history and varies with time, $f(\rho)$ should also be a function of time, i.e. $f(\rho,t)$. The approximation method available to use Sneddon's approach for an arbitrary function is a polynomial function, as discussed in Chapter 2. Since a polynomial function is a special case of a power series function, the power series function is applied to express $f(\rho,t)$ explicitly.

To obtain a close approximation by the power series function, it is usually best not to omit the linear term, $n=1$ in Eq. (2.2.25). However, when the linear term is used for the curve-fitting, this term gives the infinite contact pressure at $\rho=0$, due to the integration, Eq. (2.2.33), in Eq. (2.2.32), as shown in Eq. (3.2.11). The physical meaning of $n=1$ is for the indenter of a conical shape:

$$i_1(\rho)=\int_{\rho}^{1}\frac{1}{\sqrt{\vartheta^2-\rho^2}}d\vartheta$$

$$=-\ln(\rho)+\ln\left(1+\sqrt{1-\rho^2}\right). \tag{3.2.11}$$

Even thought the power series can approximate the contour of a smoothly curved indenter, the infinite contact pressure at $\rho=0$, due to the linear term in the powers series, makes it unsuitable for representing the contact pressure distribution caused by a spherical indenter. As a result, the linear term ($n=1$) in the power series was omitted. The loading conditions are given in Table 3-2-1. The material properties are given in Table 3-2-2 by using the viscoelastic model shown in Figure 3-2-3. The time increment, Δt, listed in Table 3-2-1 is used for the numerical convolution integral to obtain the two components of the total displacement used to generate the equivalent elastic problem.

Table 3-2-1. Loading conditions for the viscoelastic problem.

Maximum Indentation Depth, δ_{max} [m]	Time required to reach δ_{max} [sec]	Time increment, Δt [sec]	The indentation speed, V [m/sec]
0.5×10^{-6}	5	1×10^{-2}	1×10^{-7}
0.5×10^{-6}	5	5×10^{-3}	1×10^{-7}
0.5×10^{-6}	5	1×10^{-3}	1×10^{-7}

Table 3-2-2 Material properties and the radius of the spherical indenter.

G_0 [MPa]	G_1 [MPa]	Relaxation Time τ_{relax} [sec] $(=\eta/(G_0+G_1))$	Poisson's Ratio ν	The radius of the spherical indenter R [μm]
235	25.8	0.99	0.483	2

*The model used here is the same as the one in Figure 3-2-3. The material properties are taken from Cheng et al. [19].

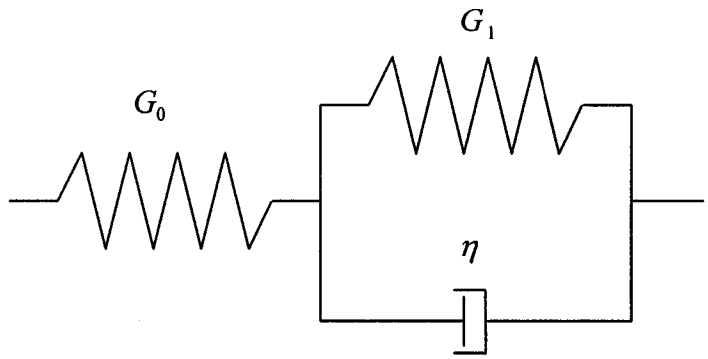

Figure 3-2-3 Three-element standard solid model by using the Kelvin-Voigt element.

The contact pressures distribution for the viscoelastic problem, Eq. (2.4.29), and the equivalent elastic problem, Eq. (2.2.32), are approximated by the power series with n from 2 to 12, and the results are plotted in Figure 3-2-4 at the maximum indentation depth. The pressure distribution near the center is enlarged in Figure 3-2-5.

The difference between the solution obtained for the viscoelastic problem and that for the equivalent elastic problem is the error introduced into the equivalent elastic problem, as shown in Figure 3-2-5. The error is caused mainly by the accumulated error of the total displacement within the contact area and the power series approximation of the contact profile, as will be explained in the following section.

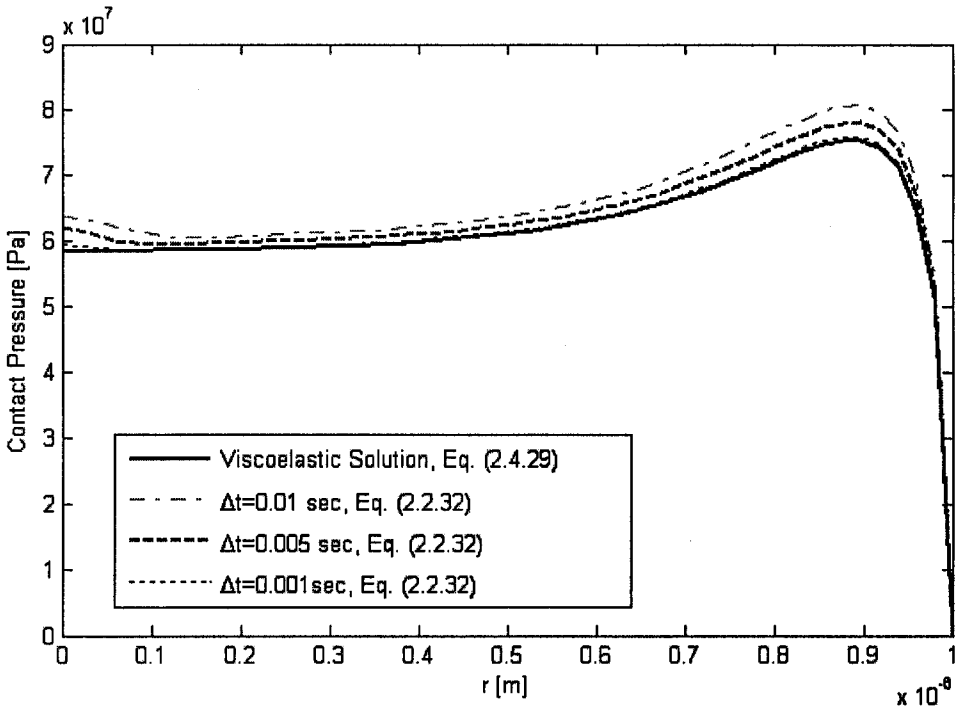

Figure 3-2-4. Comparison of contact pressures in the viscoelastic problem and the equivalent elastic problem at the maximum indentation depth.

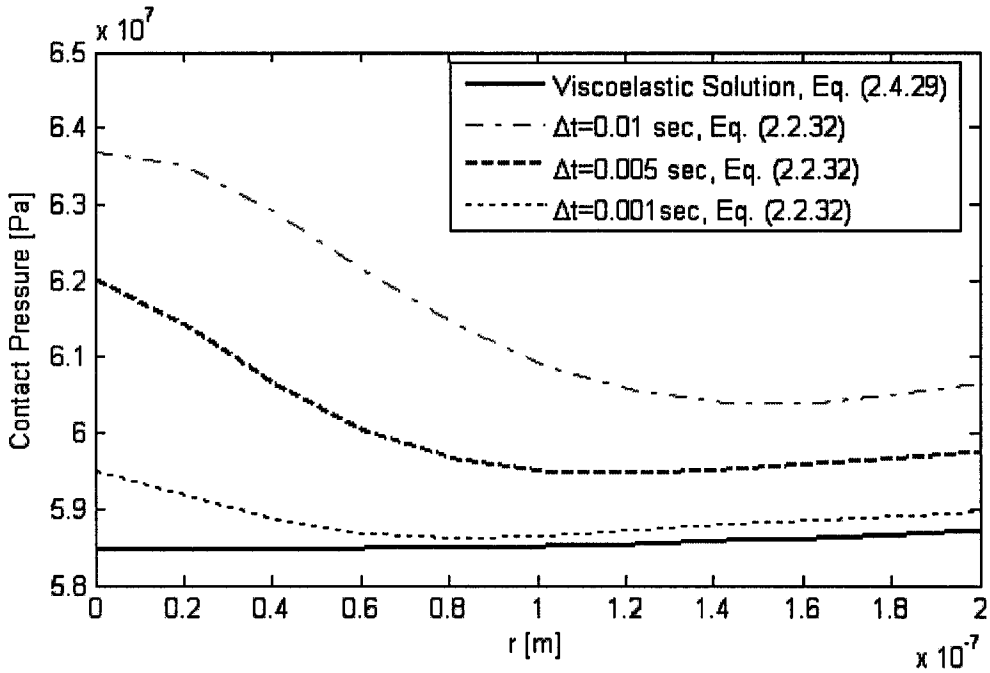

Figure 3-2-5. Enlarged contact pressures around $r = 0$, obtained by using the viscoelastic problem at the maximum indentation depth and the equivalent elastic problem.

First, the accumulated error in the total displacement is investigated by using the relative error of the total displacement within the contact area, defined as

$$E_{Disp} = \frac{\bar{u}_z - \{g(r) + \delta_{\max}\}}{\bar{u}_z}. \tag{3.2.12}$$

In principle, the total displacement within the contact area should conform to the indenter profile, $g(r)$. Thus, the relative error, E_{Disp}, should ideally be equal to zero within the contact area. The error may have been introduced when an numerical convolution integration was used to obtain the displacement, due to the numerical computation of the total displacement. Figure 3-2-6 shows the relative error with the total displacements calculated by using $\Delta t = 0.01$, $\Delta t = 0.005$, and $\Delta t = 0.001$ in the numerical convolution integral.

Figure 3-2-6 clearly shows the tendency of a smaller time increment to yield a smaller error. Since the total displacement is used in Eq. (3.2.6) and also in Eq. (3.2.7) to obtain the contact profile, the error of the total displacement may have affected the coefficient of the contact profile used in Eq. (2.2.32), and resulted in an error in the contact pressure. Accordingly, it is concluded that the convergence of the solution can be obtained when a sufficiently small time increment is used.

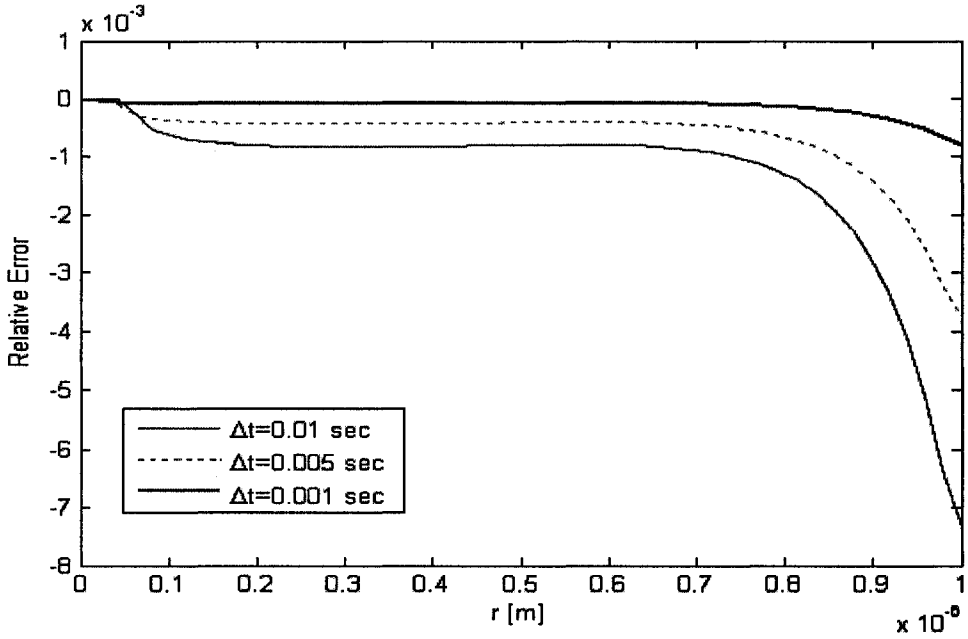

Figure 3-2-6. The relative error, Eq. (3.2.12), of the total displacement and the indenter profile with various time increments, Δt.

Second, a possible error in the contact pressure caused by the power series approximation is investigated in the following paragraphs. The power series approximation of the contact profile is given by Eq. (2.2.25). The increment of the power series terms in Eq. (2.2.32) should normally be 1 to obtain the contact pressure distribution, due to the availability of the closed form solution for Eq. (2.2.33). However,

the contact load that is the integration of the contact pressure over the contact area can be obtained without using Eq. (2.2.33). Thus, a non-integer increment of the power series terms may be used to calculate the contact load, as will be discussed later.

Also, the contact load should have a finite value in spite of the infinite pressure at $\rho = 0$ when the linear term is included. Since the algorithm uses only Sneddon's solution to simulate the contact load-indentation depth relationship, the linear term ($n = 1$) of the power series should be kept to provide a close approximation of the curve-fitting.

The approximate contact loads obtained by curve-fitting with various parameters are compared in Table 3-2-3. The viscoelastic solution of the contact load is given in column V. The loading condition, which is the same as the one used in comparing the contact pressure with the time increment $\Delta t = 0.001$, was chosen due to its accuracy in providing the contact pressure. The best approximate contact load for each configuration is listed in columns 1 to 3 of Table 3-2-3. The configuration of column 1 is with the increment of the power index of Eq. (2.2.35) of 0.5, and the first index of 1. By modifying Eq. (2.2.25), the power series used for the contact profile in column 1 of Table 3-2-3 is

$$f\left(\rho_{(q)}, t_{(m)}\right) = \sum_{n=2}^{12} c_{\frac{1}{2}n(m)} a_{(m)}^{\frac{1}{2}n} \rho_{(q)}^{\frac{1}{2}n} . \tag{3.2.13}$$

Similarly, by modifying Eq. (2.2.34), the contact load is given by

$$F_{c(m'+1)} = \frac{4\sqrt{\pi}\,\mu a_{(m'+1)}}{1-\nu} \sum_{n=2}^{12} \frac{\frac{1}{2}n\Gamma(\frac{1}{4}n+1)}{(\frac{1}{2}n+1)\Gamma(\frac{1}{4}n+\frac{1}{2})} c_{\frac{1}{2}n(m')} a_{(m'+1)}^{\frac{1}{2}n} . \tag{3.2.14}$$

The configuration of column 2 is based on Eq. (2.2.34), and the first index of the polynomial series is 1. The configuration of column 3 is similar to that of column 2, but

with the first index is 2 instead of 1. The configuration of column 3 is exactly the same as the one used in obtaining the contact pressure in Figure 3-2-4.

The goodness of curve-fitting for a set of N data points, x_i and the corresponding value y_i, $i = 1,2,3,...N$, by power series $f_{power}(x_i)$ is determined by using the coefficient of determination, R^2, defined as

$$R^2 = \sum_{i=1}^{N}\left[f_{power}(x_i) - \hat{y}\right]^2 \Big/ \sum_{i=1}^{N}\left[y_i - \hat{y}\right]^2 . \qquad (3.2.15)$$

where $\hat{y}_i$ is the sample mean of data points y_i.

As shown by Table 3-2-3, the coefficients of determinant of the curve-fittings are all very close to 1. Thus, the goodness of the curve-fitting, 1 – the coefficient of determination, is very close to zero. The numbers suggest that the curve-fittings are all very good. However, in terms of the contact load, the configuration of column 1 gives the closest value to that of the viscoelastic solution, and the relative error of 0.0051%. Therefore, it can be concluded that convergence of the solution can be obtained by using the power series used in column 1.

Table 3-2-3. Contact loads obtained by the viscoelastic solution and the solution of the equivalent elastic problem.

	V	1	2	3
	Viscoelastic problem Eq. (2.4.31)	The equivalent elastic problem Eq. (3.2.14) $n = 2$ to 12	The equivalent elastic problem Eq. (2.2.34) $n = 1$ to 8	The equivalent elastic problem Eq. (2.2.34) $n = 2$ to 8
Contact Load (N)	2.0368×10^{-4}	2.0367×10^{-4}	2.0335×10^{-4}	2.0350×10^{-4}
Goodness of the Curve-fitting (= 1 – Coefficient of determination)		7.5747×10^{-8}	1.8307×10^{-7}	2.1709×10^{-7}

The stress distribution within the two bodies, i.e., the viscoelastic and elastic bodies solved by the viscoelastic boundary value problem and the equivalent elastic boundary value problem, respectively, is also of interest. The stresses given by the integral equations, (2.2.10) and (2.2.11), cannot be obtained in the case of $z > 0$ due to the integration of the Bessel function in the equations. Thus, the closed form solution for the stresses within a body cannot be obtained. FEM has the advantage of obtaining the stress distributions within a body since the entire body has already been meshed, and the values of interest are obtained at each node. Thus, the stress distributions for the viscoelastic problem and the equivalent elastic problem were obtained by using commercial FEM software, ANSYS 10.0, University Advanced edition with the limitation of a maximum 128,000 nodes.

The FEM model used in the calculation of the viscoelastic model is shown in Figure 3-2-7 for the entire view and Figure 3-2-8 for the enlarged view around the contact point.

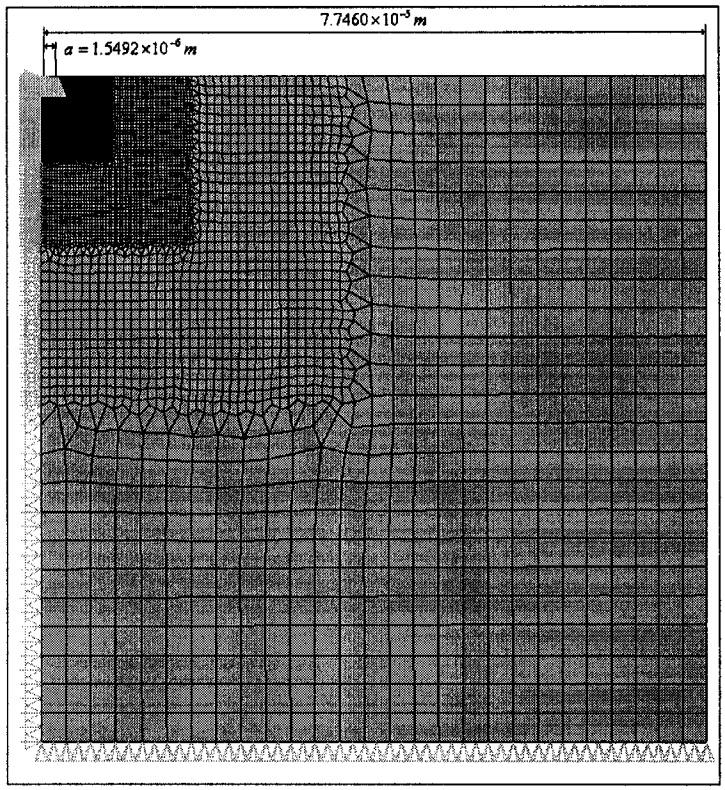

Figure 3-2-7. FEM model for the viscoelastic problem.

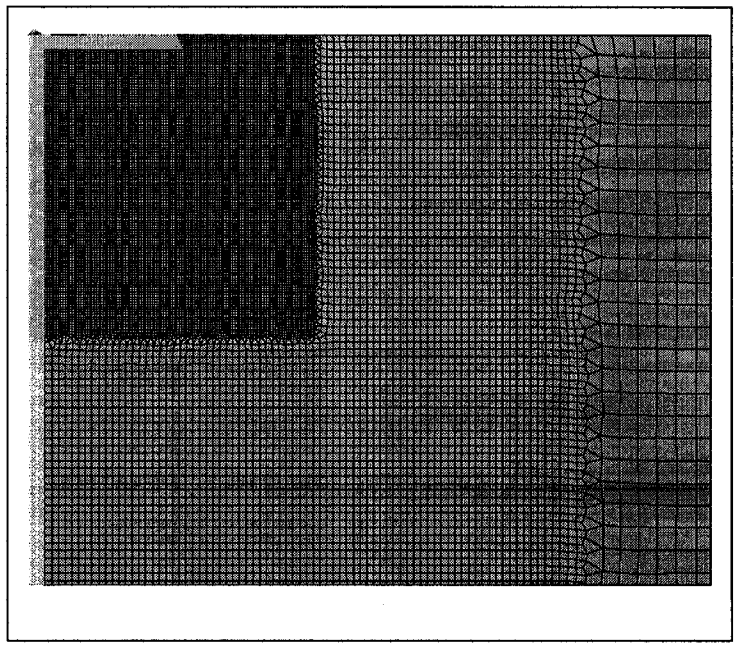

Figure 3-2-8. Enlarged FEM model around the loading point for the viscoelastic problem.

The indentation relaxation test, i.e., the boundary condition being $\delta(t) = \delta_0 U(t)$, was considered here to compare the stress distribution within the body obtained by the viscoelastic and the equivalent elastic problems, because this test requires less computational time than other tests. The stress distribution for the viscoelastic problem was taken at 10 seconds after the excitation by indentation. The equivalent elastic problem was modeled with the initial surface geometry obtained by Eq. (3.2.6) at 10 seconds after the contact area reached its maximum at a sufficiently fast loading rate.

As Swanson [8] explained, the approximation of a semi-infinite body in the FEM model is determined so that the ratios of the radius of the contact area to the thickness of the body indented and to the width and length, are larger than 50 to eliminate the effect of finite geometry. The FEM model has dimensions satisfying the requirement and was meshed with axisymmetric solid elements, PLANE183 in ANSYS. The total number of nodes used in the model is 44,286. Instead of using contact elements to simulate the actual contact between a rigid spherical indenter and a semi-infinite viscoelastic body, the following surface displacement boundary condition is applied:

$$u_z(r,t) = \left(\delta - \frac{1}{2R} r^2\right) U(t), \qquad r < a \qquad (3.2.16)$$

where $U(t)$ is the unit step function, defined by Eq. (2.3.7), $\delta = 1.2 \times 10^{-6} m$ and $a = 1.5492 \times 10^{-6} m$. By knowing the displacement boundary conditions in advance, a transient analysis without the inertia effect can be applied to simulate the indentation relaxation test without the use of contact elements. For this reason, the indentation relaxation test requires less computational time than those using contact elements with a

prescribed indenter position. The material properties used in the FEM model are given in Table 3-2-4.

Table 3-2-4. Material properties for the FEM calculation of the viscoelastic problem.

G_0' [GPa]	G_1' [GPa]	Relaxation Time τ'_{relax} [sec]	Poisson's Ratio ν
0.66757	0.1219	4.2794	0.33

The values in Table 3-2-4 are modified from those used by Cheng et al. [19] based on the model shown in Figure 3-2-3, after the original values were converted to those for the Maxwell model because ANSYS supports only the generalized Maxwell model, Figure 3-2-9.

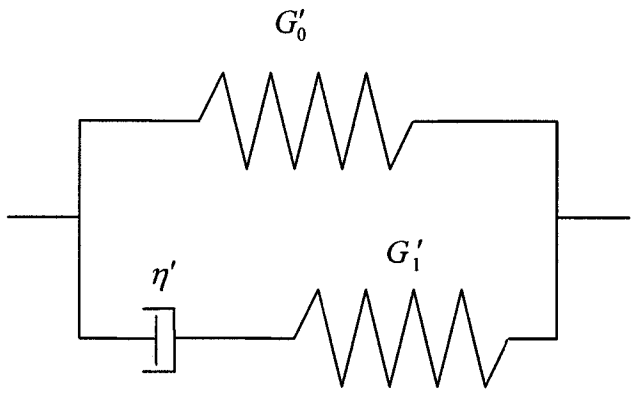

Figure 3-2-9. Three-element standard solid model by using the Maxwell element.

The following equations are used for the conversion, by comparing the relaxation functions of the two viscoelastic models:

$$G(t)=\frac{G_0G_1}{G_0+G_1}+\frac{G_0^2}{G_0+G_1}\exp\left(-\frac{t}{\tau_{relax}}\right) \tag{3.2.17}$$

for the viscoelastic model shown in Figure 3-2-3 and

$$G(t)=G_0'+G_1'\exp\left(-\frac{t}{\tau_{relax}'}\right) \tag{3.2.18}$$

for the viscoelastic model shown in Figure 3-2-9. By comparing Eqs. (3.2.17) and (3.2.18), the following relationships can be obtained:

$$G_0'=\frac{G_0G_1}{G_0+G_1} \tag{3.2.19}$$

$$G_1'=\frac{G_0^2}{G_0+G_1} \tag{3.2.20}$$

$$\tau_{relax}'=\tau_{relax}\,. \tag{3.2.21}$$

The equivalent elastic problem is modeled by using the displacements obtained by using Eqs. (2.4.34) and (2.4.35) with the loading condition listed in Table 3-2-5. The algorithm introduced in section 3.3 cannot properly take into account values at $t = 0$ except the values of material properties $t = 0$. Thus, the step function cannot be applied exactly in the algorithm. However, by using a sufficiently fast loading phase in Table 3-2-5, the quasi-instantaneous response can be reproduced. For the relaxation phase, Δt does not have to be as small as that used in the loading phase to ensure accuracy. Thus, a larger Δt was chosen for the relaxation phase. Chapter 4 includes a detailed discussion of the time increment, Δt. The indentation depth is kept constant for 10 seconds after reaching the maximum contact area. Then, $g_{surface}(r,t)$ is obtained by the instantaneously and delayed recoverable displacements, calculated by using the algorithm to be

introduced in the next section. $g_{surface}(r,t)$ was obtained within the range $0 < r \leq 50a$ by using Eq. (3.2.6) and was used to construct the initial FEM model's undeformed surface geometry, as shown in Figure 3-2-10 for the entire view of the model, and Figure 3-2-11 for the partially enlarged model. The number of nodes used in the model is 48,063, with element type PLANE183.

Table 3-2-5. Loading conditions for obtaining the surface geometry of the equivalent elastic problem.

	Maximum Indentation Depth, δ_{max} [m]	Time required to reach δ_{max} [sec]	Time increment, Δt [sec]	The indentation speed, V [m/sec]
Loading Phase	1.2×10^{-6}	0.1	1×10^{-4}	1.2×10^{-5}
Relaxation Phase	1.2×10^{-6}	n.a.	1×10^{-2}	0

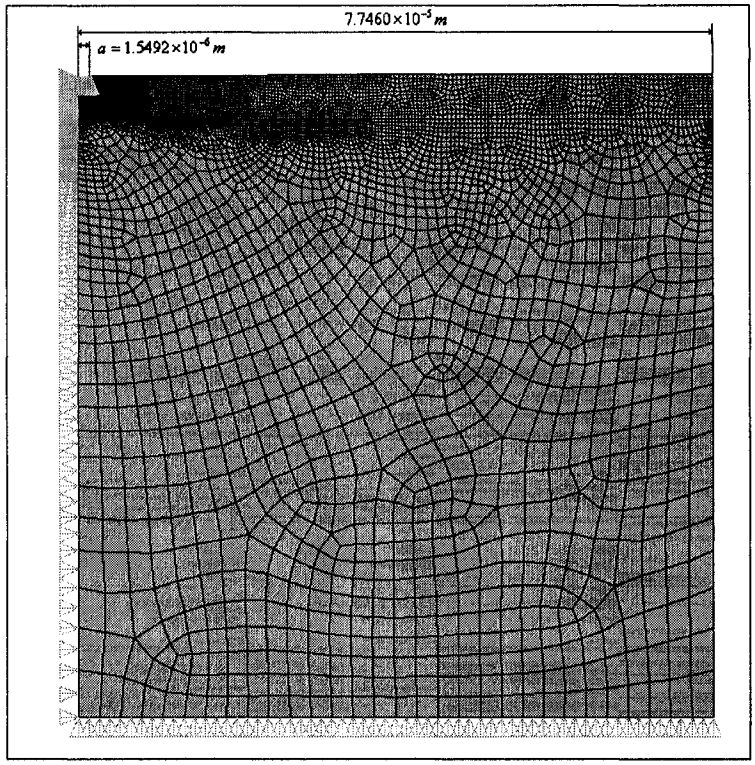

Figure 3-2-10. FEM model for the equivalent elastic problem.

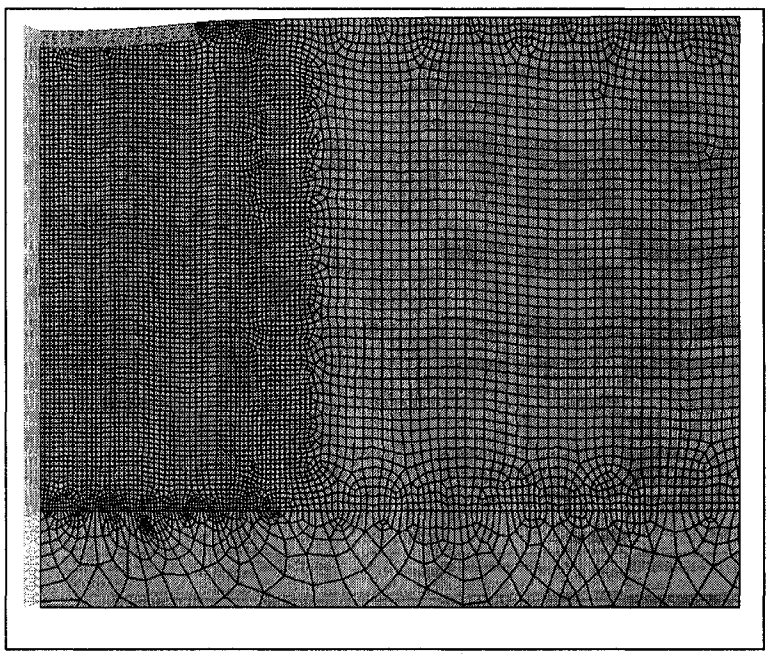

Figure 3-2-11. Enlarged FEM model around the loading point for the equivalent elastic problem.

The less regular shape of the elements in the FEM model of the equivalent elastic problem, as shown in Figures 3-2-10 and 3-2-11, is due to the use of key points to specify the curved surface. Since each key point has to be assigned a node, the model cannot be meshed with the regular-shaped elements such as the square ones. The material properties used in the equivalent elastic problem are the shear modulus, $G = 0.78947$ GPa, and Poisson's ratio, $v = 0.33$. G has the same value as that of the shear relaxation function $G(t)$ at $t = 0$.

The von Mises stress distribution of the viscoelastic problem and that of the equivalent elastic problem are compared by using their contour plots. The two contour plots in Figure 3-2-12 are similar in magnitude and these distribution of the stresses, regardless of the potential error of the FEM modeling. The FEM solutions likely suggest that the two models give the same pressure distribution inside the bodies.

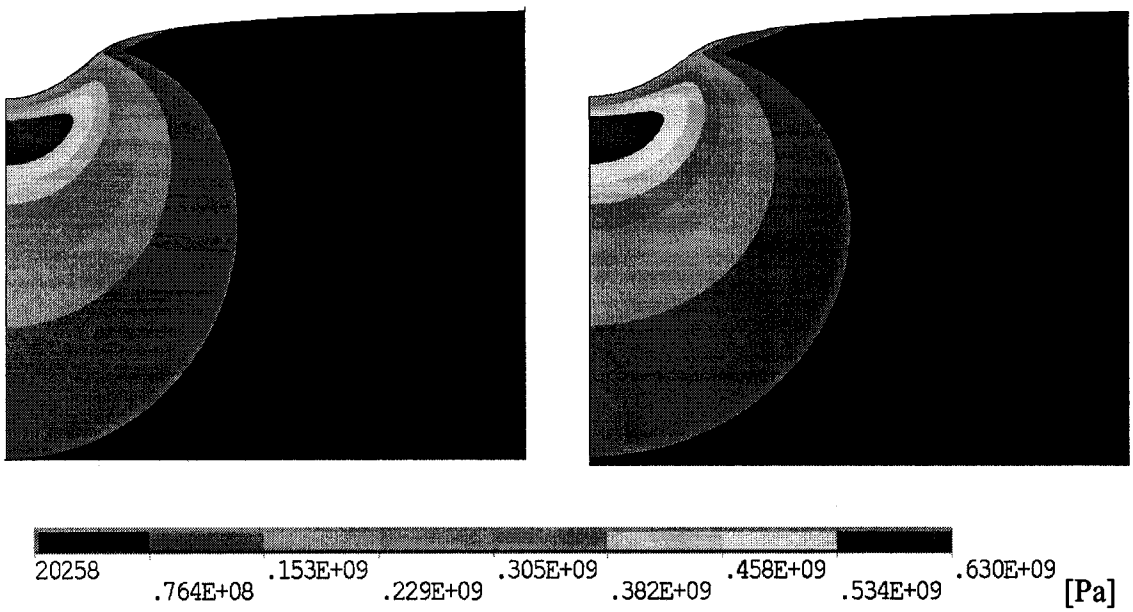

Figure 3-2-12. von Mises stress distribution. Left: the contour plot of the viscoelastic problem, and right: the contour plot of the equivalent elastic problem.

Accordingly, the equivalent elastic problem gives the same stress distribution of the viscoelastic solution at an instant of time, at least at the surface and, likely, also within the body. This idea was confirmed by comparing the contact pressure distributions at the contact surface, the contact loads, and the von Mises stress distribution within the two bodies. As well, the cause of error involved in using the equivalent elastic problem has also been discussed. Several different values of the parameters for the numerical integration and configuration of the parameters for the power series approximation have been investigated to examine the convergence of the numerical solution.

3.3 Prediction of the Contact Parameters for the Contact-Area-Decreasing Phase

A knowledge of the relationship between the contact area and the indentation depth is essential to obtain the contact load-indentation depth curve for the displacement-controlled indentation test; i.e., the indenter position, $\delta_{(t)}^{prescribed}$, is prescribed. As Sneddon's solution requires a knowledge of the contact area to obtain other values in the contact problem, i.e., the contact load and p_C, the contact area must be obtained from a known indenter position. For the contact-area-increasing phase, the contact area-indentation depth relationship is given by Eq. (2.1.31) for elastic and Eq. (2.4.38) for viscoelastic behavior, no matter what the material properties, i.e., elastic or viscoelastic, are. A viscoelastic material in the contact-area-decreasing phase does not have such a simple relationship due to the residual surface displacement generated by the viscoelastic

behavior. The mechanism can be explained as follows. The surface outside the contact area of a viscoelastic body that was once part of the contact area still shows a displacement due to the hereditary property of viscoelastic materials. In other words, the contact area-indentation depth relationship depends not only on the indenter profile, but also on the indenter position history.

However, the contact area in the contact-area-decreasing phase of the indentation test of a viscoelastic material may be approximated by using the equivalent elastic problem. The equivalent elastic problem discussed in the previous section suggests that the solution of a viscoelastic contact problem at an instant of time can also be obtained by using that of an elastic contact problem. That is, the solution of an elastic contact problem may be used to predict the contact area change within a sufficiently short time change, Δt, as depicted in Figure 3-3-1. This idea is supported by the Deborah Number, N_D, as explained in Chapter 2. If the concerned time range is very small compared to the time required for a material to complete stress relaxation, i.e., $\tau_{obs} << \tau_{relax}$ in Eq. (2.3.1), the Deborah Number will be very large, i.e., $N_D >> 1$. Thus, by choosing a very small Δt, the viscoelastic problem may be approximated by using an elastic problem within Δt, i.e., when $N_D (= \tau/\Delta t) >> 1$. This idea's validity is confirmed by simulation of the indentation relaxation test for which an analytical solution, Eq. (2.4.42), is available. This result will be shown in Chapter 4.

Like other numerical simulation methods, the proposed method also requires the discretization of space and time, so that infinite points in continuous space and time are treated as finite points in computation. Time is discretized throughout the indentation test, i.e., the contact-area-increasing and decreasing phases. The index m is used to indicate

the descretized time through $a_{(0)}$ to $a_{(m_{max})}$. To distinguish the contact-area-decreasing phase, the index m' is used for the time after reaching the maximum contact area, a_{max}, particularly when such a distinction is convenient for explaining the relationships valid only in the contact-area-decreasing phase.

Discretized space, i.e., the discretized surface of a semi-infinite viscoelastic body, is depicted in Figure 3-3-2. The values, i.e., $p_C(r_{(q)},t_{(m)})$, $\bar{u}_z^I(r_{(q)},t_{(m)})$ and $\bar{u}_z^D(r_{(q)},t_{(m)})$, required for the semi-analytical algorithm are computed at each grid point. The grids are predetermined within the maximum contact area because the entire history of the parameter at each grid point should be stored for the computation in the next time step due to the hereditary property of viscoelastic materials. This semi-analytical algorithm is introduced with the displacement-controlled indentation test, which possesses a single maximum contact area.

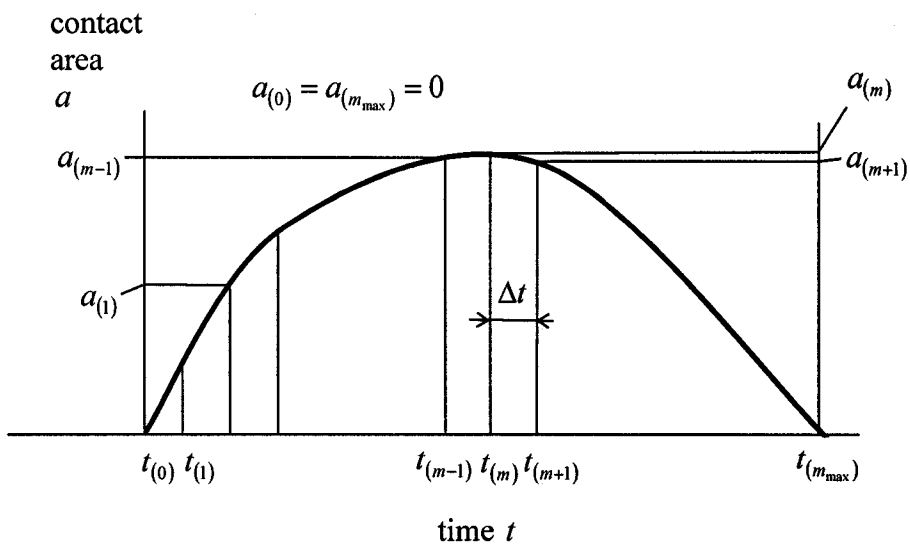

Figure 3-3-1. Schematic of contact area history.

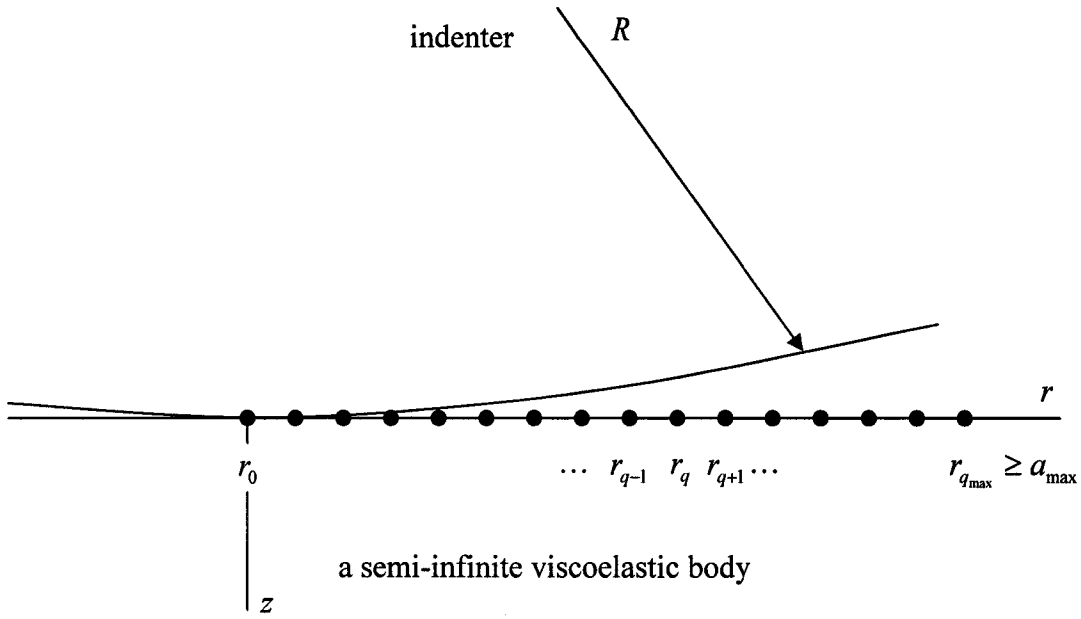

Figure 3-3-2. Schematic of the grids on the surface of a semi-infinite viscoelastic body for computation.

The flow chart of the proposed semi-analytical algorithm is shown in Figure 3-3-3. At first, two components of the total displacement, i.e., the instantaneously recoverable displacement and the delayed recoverable displacement, are obtained to generate the equivalent elastic problem. The contact profile for the equivalent elastic problem is obtained by using the undeformed surface obtained by using the two components of the total displacement and the indenter profile. The equivalent elastic problem is then generated by using the contact profile with the assumptions needed to apply Sneddon's solution. A change of the indenter position is applied, and the approximate solution is obtained by using the equivalent elastic problem. At the end, the viscosity contribution to the displacement is taken into account.

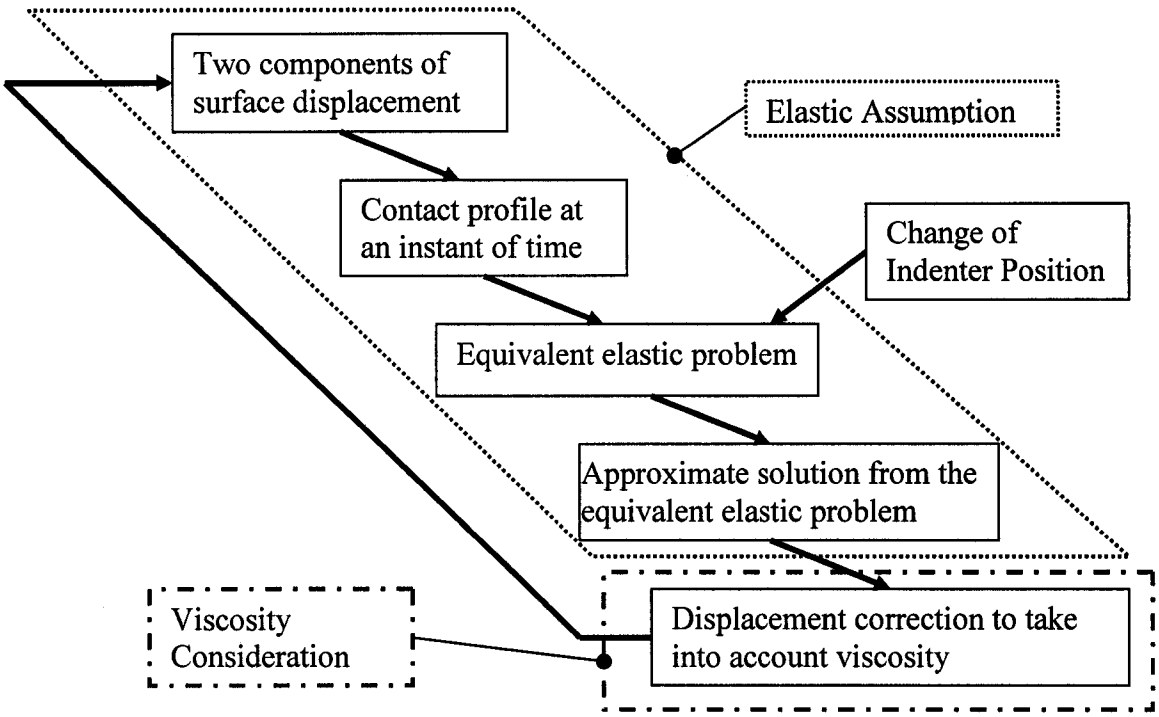

Figure 3-3-3. Brief flow chart of the semi-analytical algorithm.

3.3.1 Determination of the Contact Area

The following description of the contact area prediction is based on the assumption that the material can be considered as elastic within the time change, Δt, which is sufficiently small. Due to the better accuracy obtained by using the power series curve-fitting, expressed by Eq. (3.2.13), all of the following derivations are based on the power series approximation for the contact profile.

As discussed in the previous section, the solution of the equivalent elastic problem can be obtained with a great accuracy by using Sneddon's solution. The contact area can

also be obtained by using Sneddon's solution as a function of the indentation depth. By using Eq. (2.2.27), the indentation from the Sneddon's solution is given by

$$\delta_{(m)} = \sqrt{\pi} \sum_{n=2}^{N} \frac{\Gamma(\frac{1}{4}n+1)}{\Gamma(\frac{1}{4}n+\frac{1}{2})} c_{\frac{1}{2}n(m)} a_{(m)}^{\frac{1}{2}n}, \tag{3.3.1}$$

where $c_{\frac{1}{2}n(m)}$ is obtained by using the power series curve-fitting of the contact profile, i.e., Eq. (3.2.13). Recall Eq. (3.2.13),

$$f\left(\rho_{(q)}, t_{(m)}\right) = \sum_{n=2}^{N} c_{\frac{1}{2}n(m)} a_{(m)}^{\frac{1}{2}n} \rho_{(q)}^{\frac{1}{2}n},$$

where $f\left(\rho_{(q)}, t_{(m)}\right)$ is defined by using Eq. (3.2.7) for the contact-area-decreasing phase. The maximum number, N, is chosen so that the coefficient of determination of the contact profile is larger than 0.999. Thus, the relationship between the contact area and the indentation depth for the equivalent elastic problem can be given by Eq. (3.3.1) if the contact profile as shown by Eq. (3.2.13) is known. Since the indentation depth is a parameter controllable in the displacement-controlled indentation test, it is desirable to know the inverse relationship of Eq. (3.3.1), i.e., the contact area from the known indentation depth. The relationship of the two parameters is a monotonic function; i.e., the indentation depth increases with the increase of the contact area and decreases with the decrease of the contact area. Nevertheless, the inverse of Eq. (3.3.1) cannnot be obtained because of its non-linearity. The numerical technique, i.e., the secant method, is used here to determine the contact area corresponding to a given indentation depth.

With the assumption that the initially undeformed surface contour of the equivalent elastic problems at $t_{(m')}$ and $t_{(m'+1)}$ are the same, i.e., $g_{surface}\left(r_{(q)}, t_{(m')}\right) = g_{surface}\left(r_{(q)}, t_{(m'+1)}\right)$, Eq. (3.3.1) and (3.2.14) can be applied to the equivalent elastic problems at $t_{(m')}$ and $t_{(m'+1)}$

because the coefficients of the power series of the contact profiles, Eq. (3.2.7), are the same. Since the extrapolation of a power series approximation is not recommended, the coefficients, $c_{\frac{1}{2}n(m)}$, obtained for the larger contact area of either $a_{(m')}$ or $a_{(m'+1)}$, as defined in Figure 3-3-1, should be used. After the contact area reaches the maximum, it is expected to decrease monotonically. Therefore, it is always true that $a_{(m'+1)} < a_{(m')}$. Thus, the approximation of the contact area, $a_{(m'+1)}$, is obtained by finding the root of

$$\delta\left(a_{(m'+1)}\right)-\left(\delta\left(a_{(m')}\right)+\Delta\delta_{(m')}\right)=0, \tag{3.3.2}$$

where $\delta_{(m')}=\sqrt{\pi}\sum_{n=2}^{N}\frac{\Gamma(\frac{1}{4}n+1)}{\Gamma(\frac{1}{4}n+\frac{1}{2})}c_{\frac{1}{2}n(m')}a_{(m')}^{\frac{1}{2}n}$, $\delta_{(m'+1)}=\sqrt{\pi}\sum_{n=2}^{N}\frac{\Gamma(\frac{1}{4}n+1)}{\Gamma(\frac{1}{4}n+\frac{1}{2})}c_{\frac{1}{2}n(m')}a_{(m'+1)}^{\frac{1}{2}n}$, and $\Delta\delta$ is the change of the indentation depth during Δt; i.e.,

$$\Delta\delta_{(m')} = \delta_{(m'+1)}^{prescribed} - \delta_{(m')}^{prescribed} \tag{3.3.3}$$

from $t_{(m')}$ to $t_{(m'+1)}$. The sign of $\Delta\delta$ is negative when $\delta_{(m)}^{prescribed}$ is decreasing and positive when $\delta_{(m)}^{prescribed}$ is increasing. By using the contact area $a_{(m'-1)}$ and $a_{(m')}$ as the initial values for the secant method, the root of Eq. (3.3.2), $a_{(m'+1)}$, can usually be found by using several iterations.

3.3.2. Approximation of the Contact Load

As the semi-analytical algorithm determines the contact load by using Eq. (3.2.14) and the approximation of the contact area obtained following the procedure discussed in section 3.3.1, the contact load is also an approximate solution. That is, the contact load is given by

$$F_{c(m'+1)} = \frac{4\sqrt{\pi}\,\mu a_{(m'+1)}}{1-\nu}\sum_{n=2}^{N}\frac{\frac{1}{2}n\Gamma(\frac{1}{4}n+1)}{(\frac{1}{2}n+1)\Gamma(\frac{1}{4}n+\frac{1}{2})}c_{\frac{1}{2}n(m')}a_{(m'+1)}^{\frac{1}{2}n}. \tag{3.3.4}$$

The above contact load is obtained simply by substituting the approximation of the contact area, $a_{(m'+1)}$, and the coefficient of the power series approximation of the contact profile, $c_{n(m')}$.

3.3.3 Determination of p_C within the Contact Area

As the indentation test considered here possesses a single maximum contact area, computation must be avoided at unnecessary grid points, i.e., the grid points outside the current contact area in the contact-area-decreasing phase. p_C, defined in Eq. (2.2.37), is the nominal pressure term showing the relationship between the normal surface displacement and the pressure distribution. To determine the displacement within the current contact area, only p_C within the current contact area is used, under the same assumption as the one used to obtain the approximate contact area, i.e., when the Deborah

number is large enough to consider the deformation. Substituting discretized $r_{(q)}$ and $t_{(m)}$ into Eq. (2.2.38) gives

$$\bar{u}_z\left(r_{(q)},t_{(m)}\right)=\frac{(1-\nu)}{\mu}p_C\left(r_{(q)},t_{(m)}\right). \qquad r_{(q)}\le a_{(m)} \qquad (3.3.5)$$

In the equivalent elastic problem, $\bar{u}_z\left(r_{(q)},t_{(m)}\right)$ is replaced by $\bar{u}_z^E\left(r_{(q)},t_{(m)}\right)-g_{surface}\left(r_{(q)},t_{(m)}\right)$, where $\bar{u}_z^E\left(r_{(q)},t_{(m)}\right)$ and $g_{surface}\left(r_{(q)},t_{(m)}\right)$ are defined in Figure 3-3-4. Thus, Eq. (3.3.5) can be rewritten as

$$\bar{u}_z^E\left(r_{(q)},t_{(m)}\right)-g_{surface}\left(r_{(q)},t_{(m)}\right)=\frac{(1-\nu)}{\mu}p_C\left(r_{(q)},t_{(m)}\right). \qquad r_{(q)}\le a_{(m)} \qquad (3.3.6)$$

Under the assumption discussed in section 3.2, i.e., that the initially undeformed surface geometry is flat, the gap between $\bar{u}_z^E\left(r_{(q)},t_{(m)}\right)$ and $g_{surface}\left(r_{(q)},t_{(m)}\right)$ can be determined by using Sneddon's solution:

$$\bar{u}_z^e\left(r_{(q)},t_{(m)}\right)=\bar{u}_z^E\left(r_{(q)},t_{(m)}\right)-g_{surface}\left(r_{(q)},t_{(m)}\right), \qquad (3.3.7)$$

where $\bar{u}_z^e\left(r_{(q)},t_{(m)}\right)$ has the same value as the instantaneously recoverable displacement. Therefore,

$$\bar{u}_z^I\left(r_{(q)},t_{(m)}\right)=\bar{u}_z^e\left(r_{(q)},t_{(m)}\right). \qquad (3.3.8)$$

By using Eq. (3.3.7), Eq. (3.3.6) can be rewritten as

$$\bar{u}_z^e\left(r_{(q)},t_{(m)}\right)=\frac{(1-\nu)}{\mu}p_C\left(r_{(q)},t_{(m)}\right). \qquad r_{(q)}\le a_{(m)} \qquad (3.3.9)$$

The inverse relationship of Eq. (3.3.9) is then given by

$$p_C\left(r_{(q)},t_{(m)}\right)=\frac{\mu}{(1-\nu)}\left\{\bar{u}_z^e\left(r_{(q)},t_{(m)}\right)\right\}. \qquad r_{(q)}\le a_{(m)} \qquad (3.3.10)$$

To apply the procedure for determining p_C in the contact-area-decreasing phase, $\bar{u}_z^e\left(r_{(q)}, t_{(m'+1)}\right)$ is first given as a known parameter. Within the contact area, the normal surface displacement $\bar{u}_z^e\left(r_{(q)}, t_{(m'+1)}\right)$ should be the same as the indenter position change, $\Delta\delta_{(m')}$. Thus,

$$\bar{u}_z^e\left(r_{(q)}, t_{(m'+1)}\right) = \bar{u}_z^e\left(r_{(q)}, t_{(m')}\right) + \Delta\delta_{(m')}. \qquad r_{(q)} \le a_{(m'+1)} \quad (3.3.11)$$

Outside the current contact area, $a_{(m'+1)}$, on the other hand, the displacement no longer conforms to the indenter. For a indentation test with a single maximum contact area, the displacement outside the current contact area in the contact-area-decreasing phase is no longer used to obtain the contact profile for the equivalent elastic problem. Thus, the displacement outside the current contact area is not determined by using the algorithm.

By replacing $\bar{u}_z^e\left(r_{(q)}, t_{(m')}\right)$ in Eq. (3.3.10) by $\bar{u}_z^e\left(r_{(q)}, t_{(m'+1)}\right)$ and using Eq. (3.3.11), the $p_C\left(r_{(q)}, t_{(m'+1)}\right)$ is given by

$$p_C\left(r_{(q)}, t_{(m'+1)}\right) = \frac{\mu}{(1-\nu)}\left\{\bar{u}_z^e\left(r_{(q)}, t_{(m'+1)}\right)\right\}$$

$$= \frac{\mu}{(1-\nu)}\left\{\bar{u}_z^e\left(r_{(q)}, t_{(m')}\right) + \Delta\delta_{(m')}\right\}. \qquad r_{(q)} \le a_{(m'+1)} \quad (3.3.12)$$

Thus, the approximation of $p_C\left(r_{(q)}, t_{(m'+1)}\right)$ is given by Eq. (3.3.12).

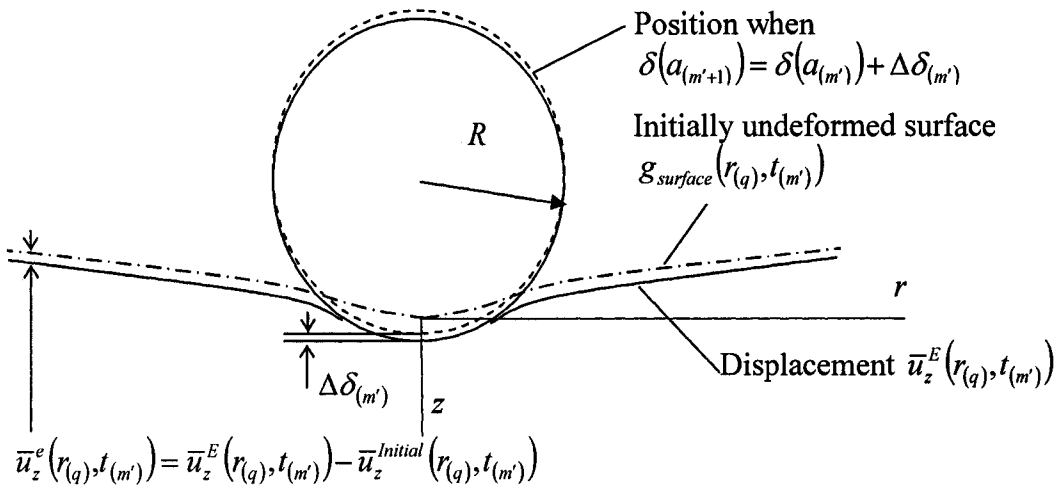

Figure 3-3-4. The parameters of the equivalent elastic problem at time $t_{(m')}$.

3.3.4. Approximation of the Two Components of the Surface Displacement

In the previous section, no consideration was given to the viscosity of a viscoelastic material. However, the contribution of the viscosity should be taken into account before proceeding to the next time step of the iteration. The viscosity contribution is considered here for the surface displacement due to the viscosity, by using the approximate $p_c(r_{(q)}, t_{(m'+1)})$. By using Eq. (3.2.5), the displacement contributed by the viscosity is expressed as

$$\bar{u}_z^D\left(r_{(q)},t_{(m'+1)}\right)=\int_0^{t_{(m'+1)}} p_C\left(r_{(q)},t_{(m'+1)}-\theta\right)\frac{\partial\Phi(\theta)}{\partial\theta}d\theta \qquad r_{(q)}\le a_{(m'+1)} \quad (3.3.13)$$

This equation is a continuous form of the convolution integral. Brigham [20] gives the discrete convolution integral:

$$\bar{u}_z^D\left(r_{(q)},t_{(m'+1)}\right)=\sum_{M=0}^{m'} p_C\left(t_{(m'+1-M)}\right)\frac{\Phi_{(M)}-\Phi_{(M-1)}}{\Delta\theta}\Delta\theta, \quad (3.3.14)$$

where the time derivative of $\Phi(\theta)$ is approximated by the one-sided first-order forward-difference formula. While Eq. (3.3.13) can deal only with analytical functions, the solution of the discrete convolution can be determined after learning the values at the discrete points. Therefore, $p_C\left(t_{(m')}\right)$ can be an arbitrary function of the time. Since $p_C\left(t_{(m')}\right)$ is unknown prior to the computation, the discrete convolution is used in this algorithm. To maintain this section's focus on the newly developed semi-analytical algorithm, the more computationally effective discrete convolution is discussed in the next section.

To approximate the values of the two components of the total displacement in the contact-area-decreasing phase, the instantaneously recoverable displacement is expressed in terms of $p_C\left(r_{(q)},t_{(m'+1)}\right)$ by using Eq. (3.2.4):

$$\bar{u}_z^{I(approx.)}\left(r_{(q)},t_{(m'+1)}\right)=\Phi_{(0)}p_C\left(r_{(q)},t_{(m'+1)}\right). \qquad r_{(q)}\le a_{(m'+1)} \quad (3.3.15)$$

The total displacement should be the summation of the two components

$$\bar{u}_z\left(r_{(q)},t_{(m'+1)}\right)=\bar{u}_z^{I(approx.)}\left(r_{(q)},t_{(m'+1)}\right)+\bar{u}_z^D\left(r_{(q)},t_{(m'+1)}\right). \qquad r_{(q)}\le a_{(m'+1)} \quad (3.3.16)$$

However, Eq. (3.3.16) may not satisfy the displacement boundary condition, due to the approximation error in $\bar{u}_z^{I(approx.)}\left(r_{(q)},t_{(m'+1)}\right)$ and $\bar{u}_z^D\left(r_{(q)},t_{(m'+1)}\right)$. Therefore, this equation

may also not satisfy the condition that the indenter should conform to the semi-infinite viscoelastic body, i.e., that

$$\bar{u}_z\left(r_{(q)},t_{(m'+1)}\right)\neq \delta\left(t_{(m'+1)}\right)-f\left(r_{(q)}\right). \qquad r_{(q)}\le a_{(m'+1)} \quad (3.3.17)$$

Eq. (3.3.17) means that the boundary condition is no longer satisfied in the approximation of $p_C\left(r_{(q)},t_{(m'+1)}\right)$ by using the elastic solution. Instead of correcting $p_C\left(r_{(q)},t_{(m'+1)}\right)$ to satisfy Eq. (3.3.16) by solving a nonlinear equation by using an iterative method, $\bar{u}_z^{I(approx.)}\left(r_{(q)},t_{(m'+1)}\right)$ is corrected by subtracting the difference of the displacement contributed by the viscosity, $\Delta\bar{u}_z^{D}\left(r_{(q)},t_{(m'+1)}\right)$, from $\bar{u}_z^{I(approx.)}\left(r_{(q)},t_{(m'+1)}\right)$, so that Eq.(3.3.16) satisfies the boundary condition; i.e.,

$$\bar{u}_z^{I(corrected)}\left(r_{(q)},t_{(m'+1)}\right)=\bar{u}_z^{I(approx.)}\left(r_{(q)},t_{(m'+1)}\right)-\Delta\bar{u}_z^{D}\left(r_{(q)},t_{(m'+1)}\right), \qquad r_{(q)}\le a_{(m'+1)} \quad (3.3.18)$$

where

$$\Delta\bar{u}_z^{D}\left(r_{(q)},t_{(m'+1)}\right)=\bar{u}_z^{D}\left(r_{(q)},t_{(m'+1)}\right)-\bar{u}_z^{D}\left(r_{(q)},t_{(m')}\right). \qquad r_{(q)}\le a_{(m'+1)} \quad (3.3.19)$$

Since the surface displacement conforms to the indenter within the contact area, the displacement in the next step is determined simply by adding the indenter position change to the instantaneously recoverable displacement:

$$\bar{u}_z^{I}\left(r_{(q)},t_{(m'+2)}\right)=\bar{u}_z^{I(corrected)}\left(r_{(q)},t_{(m'+1)}\right)+\Delta\delta_{(m'+1)}. \qquad r_{(q)}\le a_{(m'+1)} \quad (3.3.20)$$

This approximation approach is best explained by using the indentation relaxation test in which $\Delta\delta_{(m')}=0$. According to the approximate $p_c\left(r_{(q)},t_{(m')}\right)$, as discussed in section 3.3.3, when $\Delta\delta_{(m')}=0$, $p_c\left(r_{(q)},t_{(m'+1)}\right)=p_c\left(r_{(q)},t_{(m')}\right)$, which leads to $\bar{u}_z^{I}\left(r_{(q)},t_{(m'+1)}\right)=\bar{u}_z^{I}\left(r_{(q)},t_{(m')}\right)$ from Eq. (3.3.8).

The total displacement at $t_{(m'+1)}$ is given by Eqs. (3.3.18) and (3.3.20):

$$\bar{u}_z\left(r_{(q)},t_{(m'+1)}\right)=\bar{u}_z^{I(approx.)}\left(r_{(q)},t_{(m'+1)}\right)+\bar{u}_z^{D}\left(r_{(q)},t_{(m'+1)}\right)-\Delta\bar{u}_z^{D}\left(r_{(q)},t_{(m'+1)}\right). \qquad r_{(q)}\le a_{(m'+1)} \quad (3.3.21)$$

Since $\bar{u}_z^{I(approx.)}\left(r_{(q)},t_{(m'+1)}\right)=\bar{u}_z^{I}\left(r_{(q)},t_{(m')}\right)$ in Eq. (3.3.16) for the indentation relaxation test, the subtraction of $\Delta\bar{u}_z^{D}\left(r_{(q)},t_{(m'+1)}\right)$ from the total displacement $\bar{u}_z\left(r_{(q)},t_{(m'+1)}\right)$ gives the same displacement from $t_{(m')}$ to $t_{(m'+1)}$; i.e., $\bar{u}_z\left(r_{(q)},t_{(m'+1)}\right)=\bar{u}_z\left(r_{(q)},t_{(m')}\right)$ because $\bar{u}_z^{D}\left(r_{(q)},t_{(m')}\right)=\bar{u}_z^{D}\left(r_{(q)},t_{(m'+1)}\right)-\Delta\bar{u}_z^{D}\left(r_{(q)},t_{(m'+1)}\right)$.

It should be noted that instantaneously recoverable displacement, $\bar{u}_z^{I}\left(r_{(q)},t_{(m')}\right)$, may not be constant because the contact stress decreases with the increase of time in the indentation relaxation test. Therefore, the difference, Eq. (3.3.19), is subtracted from $\bar{u}_z^{I(approx.)}\left(r_{(q)},t_{(m'+1)}\right)$

$$\bar{u}_z^{I(corrected)}\left(r_{(q)},t_{(m'+1)}\right)=\bar{u}_z^{I(approx.)}\left(r_{(q)},t_{(m'+1)}\right)-\Delta\bar{u}_z^{D}\left(r_{(q)},t_{(m'+1)}\right). \quad (3.3.22)$$

Then, this corrected instantaneously recoverable displacement is carried over to the next time step. By using $\bar{u}_z^{I}\left(r_{(q)},t_{(m)}\right)=\bar{u}_z^{e}\left(r_{(q)},t_{(m)}\right)$ from Eq. (3.3.8), Eq. (3.3.22) is rewritten as

$$\bar{u}_z^{e(corrected)}\left(r_{(q)},t_{(m'+1)}\right)=\bar{u}_z^{e(approx.)}\left(r_{(q)},t_{(m'+1)}\right)-\Delta\bar{u}_{z(m'+1)}^{D}. \quad (3.3.23)$$

Thus,

$$\bar{u}_z^{e}\left(r_{(q)},t_{(m'+1)}\right)=\bar{u}_z^{e(corrected)}\left(r_{(q)},t_{(m'+1)}\right) \quad (3.3.24)$$

for the indentation relaxation test. For the general case of the indentation test, consider the change of the indenter position:

$$\bar{u}_z^{e}\left(r_{(q)},t_{(m'+1)}\right)=\bar{u}_z^{e(corrected)}\left(r_{(q)},t_{(m'+1)}\right)+\Delta\delta_{(m'+1)}, \quad (3.3.25)$$

The above procedure is used to correct the violation of the displacement boundary condition caused by the approximation of $p_C\left(r_{(q)},t_{(m'+1)}\right)$ by using the difference expressed

by Eq. (3.3.19). This procedure is graphically explained by Figure 3-3-5 as part of the algorithm for the semi-analytical algorithm.

The displacement $\bar{u}_z^E\left(r_{(q)}, t_{(m'+1)}\right)$ within the contact area is given by

$$\bar{u}_z^E\left(r_{(q)}, t_{(m'+1)}\right) = \delta\left(a_{(m'+1)}\right) - g\left(r_{(q)}\right), \qquad r_{(q)} \le a_{(m'+1)} \quad (3.3.26)$$

where $g(r)$ is the profile of the indenter. The initially undeformed surface in the next time step of the computation is given by rearranging Eq. (3.3.7); i.e.,

$$g_{surface}\left(r_{(q)}, t_{(m'+1)}\right) = \bar{u}_z^E\left(r_{(q)}, t_{(m'+1)}\right) - \bar{u}_z^e\left(r_{(q)}, t_{(m'+1)}\right). \qquad r_{(q)} \le a_{(m'+1)} \quad (3.3.27)$$

Substituting the initially undeformed surface into Eq. (3.2.7) to determine the new contact profile for the next step yields

$$f\left(\rho_{(q)}, t_{(m'+1)}\right) = g\left(\rho_{(q)}\right) - g_{surface}\left(\rho_{(q)}, t_{(m'+1)}\right). \quad (3.3.28)$$

The above contact profile $f\left(\rho_{(q)}, t_{(m'+1)}\right)$ is carried over to the next time step of computation. Thus, all the parameters, i.e., $a_{(m'+1)}$, $p_C\left(r_{(q)}, t_{(m'+1)}\right)$, $\bar{u}_z^D\left(r_{(q)}, t_{(m'+1)}\right)$, $\bar{u}_z^e\left(r_{(q)}, t_{(m'+1)}\right)$, and $f\left(\rho_{(q)}, t_{(m'+1)}\right)$, required to repetitively apply the procedures introduced in sections 3.3.1 to 3.3.4 over the time range considered are obtained by using those at time $t_{(m')}$. This iteration continues until the end of the prescribed indenter position history or stops when the contact area or the contact load is smaller than 0. Figure 3-3-5 depicts the algorithm in the form of flowcharts.

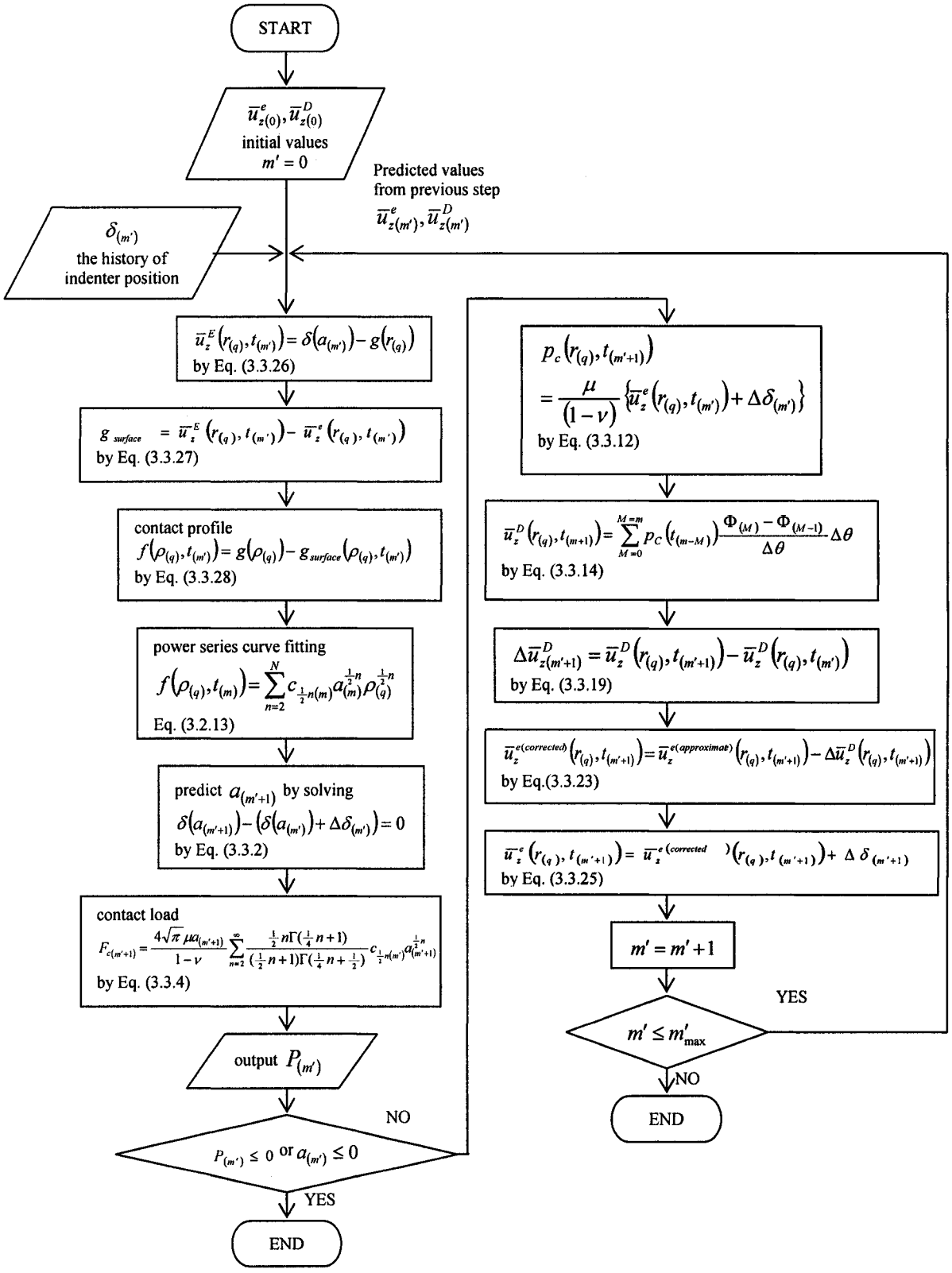

Figure 3-3-5 The algorithm of indentation simulation for the unloading phase.

3.4 Computationally Effective Convolution Integral

A brief computation time is always desirable for any kind of numerical simulation. In the algorithm depicted in Figure 3-3-4, computing the discrete convolution integral is the most time-consuming part of the process. For general cases, the FFT algorithm can be used more efficiently than Eq. (3.3.14) to compute the discrete convolution integral. However, all past history of $p_C\left(r_{(q)},t_{(m)}\right)$ and $\Phi\left(t_{(m)}\right)$ are still used to compute the value, $\bar{u}_z^D\left(r_{(q)},t_{(m+1)}\right)$. Therefore, this computation is not fast enough to be implemented in an algorithm using the convolution integral many times.

For viscoelastic constitutive equations which can be expressed by exponential function(s), Taylor et al. [21] proposed a more efficient algorithm. This algorithm is used in commercial FEM software such as ANSYS.

To apply the computationally efficient algorithm proposed by Taylor et al., the function $\Phi(t)$ is given in a form of exponential function. Recall Eq.(3.3.13):

$$\bar{u}_z^D\left(r_{(q)},t_{(m)}\right)=\int_0^{t_{(m)}} p_C\left(r_{(q)},t_{(m)}-\theta\right)\frac{\partial\Phi(\theta)}{\partial\theta}d\theta\,.$$

By changing the variable with $\theta=t_{(m)}-\tau$,

$$\bar{u}_z^D\left(r_{(q)},t_{(m)}\right)=\int_0^{t_{(m)}} \frac{\partial\Phi\left(t_{(m)}-\tau\right)}{\partial\tau}p_c\left(r_{(q)},\tau\right)d\tau\,. \tag{3.4.1}$$

By assuming that Poisson's ratio is constant and using the three element standard solid model with a Kelvin-Voigt element in Figure 3-2-3, the function, $\Phi(t)$, defined in Eq. (2.4.22), is given by

$$\Phi(\tau)=\frac{1-\nu}{G(\tau)}$$

$$=\frac{(1-\nu)}{G_0\widetilde{G}}\left\{1-\frac{G_0}{G_0+G_1}\exp\left(\frac{-\widetilde{G}}{\tau_{relax}}\tau\right)\right\}, \tag{3.4.2}$$

where

$$\widetilde{G}=\frac{G_1}{G_0+G_1}, \tag{3.4.3}$$

and τ is also a variable of time from 0 to the present time, $t_{(m)}$. $t_{(m)}$ can be treated as a constant in the following manipulation. By taking the time derivative of Eq. (3.4.2),

$$\frac{\partial\Phi(\tau)}{\partial\tau}=\frac{1-\nu}{(G_0+G_1)\tau_{relax}}\exp\left(\frac{-\widetilde{G}}{\tau_{relax}}\tau\right). \tag{3.4.4}$$

Substituting Eq. (3.4.4) into Eq. (3.4.1) yields

$$\bar{u}_z^D(r_{(q)},t_{(m)})=\frac{1-\nu}{(G_0+G_1)\tau_{relax}}\int_0^{t_{(m)}}\exp\left(\frac{-\widetilde{G}}{\tau_{relax}}(t_{(m)}-\tau)\right)p_C(r_{(q)},\tau)d\tau\,. \tag{3.4.5}$$

In the notation

$$h(\Delta\tau_{(M)})=\frac{1}{\Delta\tau_{(M)}}\int_{\tau_{(M-1)}}^{\tau_{(M)}}\exp\left(\frac{-\widetilde{G}}{\tau_{relax}}(\tau_{(M)}-\tau)\right)d\tau$$

$$=\frac{1}{\Delta\tau_{(M)}}\int_0^{\Delta\tau_{(M)}}\exp\left(\frac{-\widetilde{G}}{\tau_{relax}}\tau\right)d\tau, \tag{3.4.6}$$

$\tau_{(M)}$ is a discrete time variable of τ. The mathematical manipulation of Eq. (3.4.6) can be explained by the following relationships:

$$\int_{\tau_{(M-1)}}^{\tau_{(M)}}\exp\left(\frac{-\widetilde{G}}{\tau_{relax}}(\tau_{(M)}-\tau)\right)d\tau=\frac{\tau_{relax}}{\widetilde{G}}\left[1-\exp\left(\frac{-\widetilde{G}}{\tau_{relax}}\Delta\tau_{(M)}\right)\right] \tag{3.4.7}$$

$$\int_0^{\Delta\tau_{(M)}} \exp\left(\frac{-\widetilde{G}}{\tau_{relax}}\tau\right)d\tau = \frac{\tau_{relax}}{\widetilde{G}}\left[1-\exp\left(\frac{-\widetilde{G}}{\tau_{relax}}\Delta\tau_{(M)}\right)\right]. \tag{3.4.8}$$

Thus, the right hand side of Eq. (3.4.7) is equal to the right hand side of Eq. (3.4.8), so the left hand sides are also equal.

Eq. (3.4.5) is rewritten as

$$\bar{u}_z^D\left(r_{(q)},t_{(m)}\right) = \frac{1-\nu}{(G_0+G_1)\tau_{relax}}\int_0^{t_{(m)}} \exp\left(\frac{-\widetilde{G}}{\tau_{relax}}\left(t_{(m)}-\tau\right)\right)p_C\left(r_{(q)},\tau\right)d\tau$$

$$= \frac{1-\nu}{(G_0+G_1)\tau_{relax}}\exp\left(\frac{-\widetilde{G}}{\tau_{relax}}\left(t_{(m)}\right)\right)$$

$$\times \int_0^{t_{(m)}} \exp\left(\frac{\widetilde{G}}{\tau_{relax}}\left(\tau_{(M)}\right)\right)\exp\left(\frac{-\widetilde{G}}{\tau_{relax}}\left(\tau_{(M)}-\tau\right)\right)p_C\left(r_{(q)},\tau\right)d\tau\,. \tag{3.4.9}$$

The integration in Eq. (3.4.9) has the multiplication of three functions. The integration of the multiplication of the three functions is given by

$$\int_0^{t_{(m)}} \exp\left(\frac{\widetilde{G}}{\tau_{relax}}\left(\tau_{(M)}\right)\right)\exp\left(\frac{-\widetilde{G}}{\tau_{relax}}\left(\tau_{(M)}-\tau\right)\right)p_C\left(r_{(q)},\tau\right)d\tau$$

$$= \sum_{M=1}^{m}\exp\left(\frac{\widetilde{G}}{\tau_{relax}}\tau_{(M)}\right)h\left(\Delta\tau_{(M)}\right)p_C\left(r_{(q)},\tau_{(M)}\right)\Delta\tau_{(M)}\,. \tag{3.4.10}$$

Using Eq. (3.4.10), Eq. (3.4.9) is rewritten as

$$\bar{u}_z^D\left(r_{(q)},t_{(m)}\right) = \frac{1-\nu}{(G_0+G_1)\tau_{relax}}\exp\left(\frac{-\widetilde{G}}{\tau_{relax}}\left(t_{(m)}\right)\right)\sum_{M=1}^{m}\exp\left(\frac{\widetilde{G}}{\tau_{relax}}\tau_{(M)}\right)h\left(\Delta\tau_{(M)}\right)p_C\left(r_{(q)},\tau_{(M)}\right)\Delta\tau_{(M)}$$

$$= \frac{1-\nu}{(G_0+G_1)\tau_{relax}}\sum_{M=1}^{m}\exp\left(\frac{-\widetilde{G}}{\tau_{relax}}\left(t_{(m)}-\tau_{(M)}\right)\right)h\left(\Delta\tau_{(M)}\right)p_C\left(r_{(q)},\tau_{(M)}\right)\Delta\tau_{(M)}\,. \tag{3.4.11}$$

A new variable g_{rec} is defined by using the summation in Eq. (3.4.11) to construct a recursion formula. First, by rearranging the summation in Eq. (3.4.11), we have

$$\sum_{M=1}^{m}\exp\left(\frac{-\widetilde{G}}{\tau_{relax}}\left(t_{(m)}-\tau_{(M)}\right)\right)h\left(\Delta\tau_{(M)}\right)p_C\left(r_{(q)},\tau_{(M)}\right)\Delta\tau_{(M)}=$$

$$h\left(\Delta\tau_{(m)}\right)p_C\left(r_{(q)},\tau_{(m)}\right)\Delta\tau_{(m)}+\sum_{M=1}^{m-1}\exp\left(\frac{-\widetilde{G}}{\tau_{relax}}\left(t_{(m)}-\tau_{(M)}\right)\right)h\left(\Delta\tau_{(M)}\right)p_C\left(r_{(q)},\tau_{(M)}\right)\Delta\tau_{(M)}. \quad (3.4.12)$$

Then, define the variable, $g_{rec}\left(t_{(m)}\right)$, as

$$g_{rec}\left(t_{(m)}\right)=\sum_{M=1}^{m-1}\exp\left(\frac{-\widetilde{G}}{\tau_{relax}}\left(t_{(m)}-\tau_{(M)}\right)\right)h\left(\Delta\tau_{(M)}\right)p_C\left(r_{(q)},\tau_{(M)}\right)\Delta\tau_{(M)}, \quad (3.4.13)$$

and rearrange Eq. (3.4.13) to be

$$g_{rec}\left(t_{(m)}\right)=\exp\left(-\frac{\widetilde{G}}{\tau_{relax}}t_{(m)}\right)\left\{\sum_{M=1}^{m-1}\exp\left(\frac{\widetilde{G}}{\tau_{relax}}\tau_{(M)}\right)h\left(\Delta\tau_{(M)}\right)p_C\left(r_{(q)},\tau_{(M)}\right)\Delta\tau_{(M)}\right\}$$

$$=\exp\left(-\frac{\widetilde{G}}{\tau_{relax}}t_{(m)}\right)$$

$$\times\left\{\sum_{M=1}^{m-2}\exp\left(\frac{\widetilde{G}}{\tau_{relax}}\tau_{(M)}\right)h\left(\Delta\tau_{(M)}\right)p_C\left(r_{(q)},\tau_{(M)}\right)\Delta\tau_{(M)}\right.$$

$$\left.+\exp\left(\frac{\widetilde{G}}{\tau_{relax}}\tau_{(m-1)}\right)h\left(\Delta\tau_{(m-1)}\right)p_C\left(r_{(q)},\tau_{(m-1)}\right)\Delta\tau_{(m-1)}\right\}. \quad (3.4.14)$$

$g_{rec}\left(t_{(m-1)}\right)$ is

$$g_{rec}\left(t_{(m-1)}\right)=\sum_{M=1}^{m-2}\exp\left(\frac{-\widetilde{G}}{\tau_{relax}}\left(t_{(m-1)}-\tau_{(M)}\right)\right)h\left(\Delta\tau_{(M)}\right)p_C\left(r_{(q)},\tau_{(M)}\right)\Delta\tau_{(M)} \quad (3.4.15)$$

$$=\exp\left(-\frac{\widetilde{G}}{\tau_{relax}}t_{(m-1)}\right)\left\{\sum_{M=1}^{m-2}\exp\left(\frac{\widetilde{G}}{\tau_{relax}}\tau_{(M)}\right)h\left(\Delta\tau_{(M)}\right)p_C\left(r_{(q)},\tau_{(M)}\right)\Delta\tau_{(M)}\right\}. \quad (3.4.16)$$

Then

$$\left\{\sum_{M=1}^{m-2}\exp\left(\frac{\widetilde{G}}{\tau_{relax}}\tau_{(M)}\right)h\left(\Delta\tau_{(M)}\right)p_C\left(r_{(q)},\tau_{(M)}\right)\Delta\tau_{(M)}\right\}=g_{rec}\left(t_{(m-1)}\right)\exp\left(\frac{\widetilde{G}}{\tau_{relax}}t_{(m-1)}\right). \quad (3.4.17)$$

Substituting Eq. (3.4.17) into Eq. (3.4.14) and with $t_{(m)} = \tau_{(m)}$ yields

$$g_{rec}(t_{(m)}) = \exp\left(-\frac{\widetilde{G}}{\tau_{relax}}(t_{(m)} - t_{(m-1)})\right)\left\{g_{rec}(t_{(m-1)}) + h(\Delta\tau_{(m-1)})p_C(r_{(q)}, \tau_{(m-1)})\Delta\tau_{(m-1)}\right\}. \quad (3.4.18)$$

Since $\Delta\tau_{(m-1)} = t_{(m)} - t_{(m-1)}$, then

$$g_{rec}(t_{(m)}) = \exp\left(-\frac{\widetilde{G}}{\tau_{relax}}(\Delta\tau_{(m-1)})\right)\left\{g_{rec}(t_{(m-1)}) + h(\Delta\tau_{(m-1)})p_C(r_{(q)}, \tau_{(m-1)})\Delta\tau_{(m-1)}\right\}. \quad (3.4.19)$$

Thus, the delayed recoverable displacement is finally given by

$$\bar{u}_z^D(r_{(q)}, t_{(m)}) = \frac{1-\nu}{(G_1 + G_2)\tau_{relax}}\left\{h(\Delta\tau_{(m)})p_C(r_{(q)}, \tau_{(m)})\Delta\tau_{(m)} + g_{rec}(t_{(m)})\right\}. \quad (3.4.20)$$

Therefore, only $g_{rec}(t_{(m-1)})$ is required to obtain $g_{rec}(t_{(m)})$. $g_{rec}(t_{(m-1)})$ is obtained by recursive computation, so it has an accumulated value taking the past history into account. Consequently, the time-consuming integration of the entire past history is avoided by using Eq. (3.4.20).

3.5 Program with the Algorithm

An indentation relaxation test and an indentation test possessing a single maximum contact area are considered in the programming by using the viscoelastic solution, Eq. (2.4.32), obtained by the correspondence principle for the loading phase. The algorithm shown in Figure 3-3-5 is used for the relaxation phase of the indentation relaxation test and the unloading phase of the indentation test, with the indenter position, $\delta_{(t)}^{prescribed}$, prescribed. The computationally effective numerical convolution integral derived in section 3.4 is used in the algorithm, replacing the numerical convolution integral described in Figure 3-3-5.

4. Results and the Criteria

The semi-analytical numerical simulation algorithm for an indentation test is discussed in the previous chapter. The validation of the algorithm and the criteria to determine the parameters, i.e., the number of grids $q_{\max}$ within the maximum contact area and the time increment Δt, for the computation are presented in this chapter. The algorithm will be verified by comparing the computation results from the algorithm with those from the alternative methods, i.e., the analytical solution and FEM. The determination of the parameters used in the computation is also presented by using the computation results obtained by using the algorithm. The criteria to determine such parameters in advance of the computation are crucial to optimize the computational time. Here, the criteria are presented for the contact between a parabolic contact profile, i.e., the approximation of the rigid spherical indenter, and a semi-infinite viscoelastic body which is modeled as a three-element standard solid model by using the Kelvin-Voigt element, as shown in Figure 3-2-3.

4.1 Validation of the Algorithm

4.1.1 Indentation Relaxation Test

The indentation relaxation test is chosen for comparing the results obtained by using the algorithm, the analytical solution, i.e., Eq. (2.4.41), and FEM. Since the boundary condition for the indentation relaxation test, i.e., the displacement boundary condition, Eq. (3.2.16), is known in advance, the boundary condition is applied to the FEM model instead of using the contact elements. Without the errors due to the contact area search in FEM, a comparison of the results for the indentation relaxation tests verifies the part of the algorithm using the predicted p_C to determine viscoelastic behavior via the equivalent elastic problem, as introduced in sections 3.3.3 and 3.3.4. This approximate viscosity contribution is the core of the algorithm that simulates the viscoelastic response by the equivalent elastic problem. Without achieving great accuracy for the indentation relaxation test, the algorithm cannot be used for the indentation test, which involves an extensive contact area search that may cause a numerical error in the results.

The viscoelastic material properties used in the indentation relaxation test, which is modeled by the three-element standard solid model by using the Kelvin-Voigt element shown in Figure 3-2-3, are listed in Table 4-1-1. The material properties listed in Table 3-2-4, the FEM model shown in Figure 3-2-7, and the analysis option in ANSYS, i.e., transient analysis, are used to determine the viscoelastic response of the indentation relaxation test by using FEM.

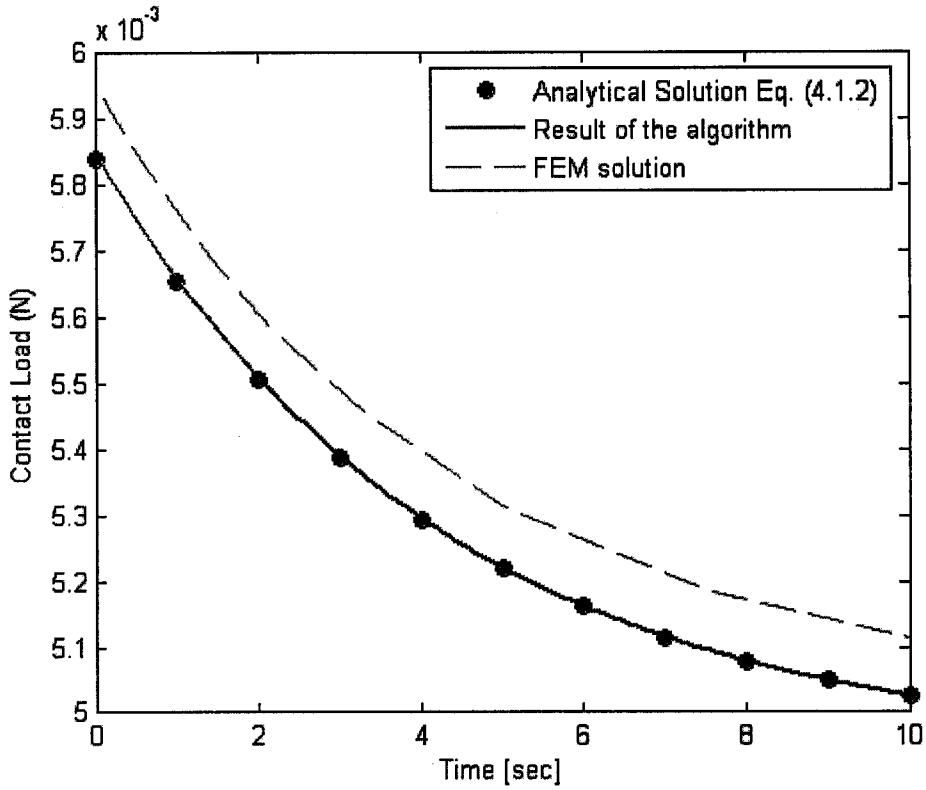

Figure 4-1-1. The comparison of the results of the various methods for the indentation relaxation test.

Table 4-1-1. Material properties used in the indentation relaxation test.

G_0 [GPa]	G_1 [GPa]	τ [sec]	ν
0.78947	4.3233	4.2794	0.33

The values are taken from Cheng et al. [19].

Table 4-1-2. The parameters used in the comparison of the results.

The radius of the spherical indenter R $[\times 10^{-6} m]$	The constant contact area a_0 $[\times 10^{-6} m]$	The maximum indentation depth δ_{max} $[\times 10^{-6} m]$
2	1.5492	1.2

The filled circles in Figure 4-1-1 represent the analytical solution, i.e., Eq. (2.4.42), by using the material properties in Table 4.1.1. The contact load, $F_c(t)$, for the indentation relaxation test is determined by using Eq. (3.2.17) and the following loading function

$$a(t) = a_0 U(t), \tag{4.1.1}$$

where $U(t)$ is the unit step function defined in Eq. (2.3.7). These functions are substituted into Eq. (2.4.42), yielding the following expression:

$$F_c(t) = 0.58415 \times 10^{-2} - 0.90190 \times 10^{-3} + 0.90190 \times 10^{-3} \exp(-0.23368t) \tag{4.1.2}$$

The filled circles in Figure 4-1-1 are obtained simply by substituting values of t into Eq. (4.1.2).

The solid line in Figure 4-1-1 represents the computational results from the algorithm. The values of the parameters used in the numerical simulation were carefully chosen to satisfy the criteria determined in section 4-2. The results have very good agreement to those of the analytical solution. Thus, the geometric assumption, i.e., of an initially flat undeformed surface accompanying with the use of Sneddon's solution for the equivalent elastic problem in section 3.2, does not cause any significant error in the computation. Also, the approximation used for obtaining p_C and the two components of the total displacement discussed in sections 3.3.3 and 3.3.4, respectively, also do not cause any significant error in the computation.

The dashed line in Figure 4-1-1 shows the results from the FEM simulation. These results are shifted slightly above those from the analytical solutions. The cause of such errors could have been the combination of the inherent error in the FEM simulation, and the finite geometry of the FEM model.

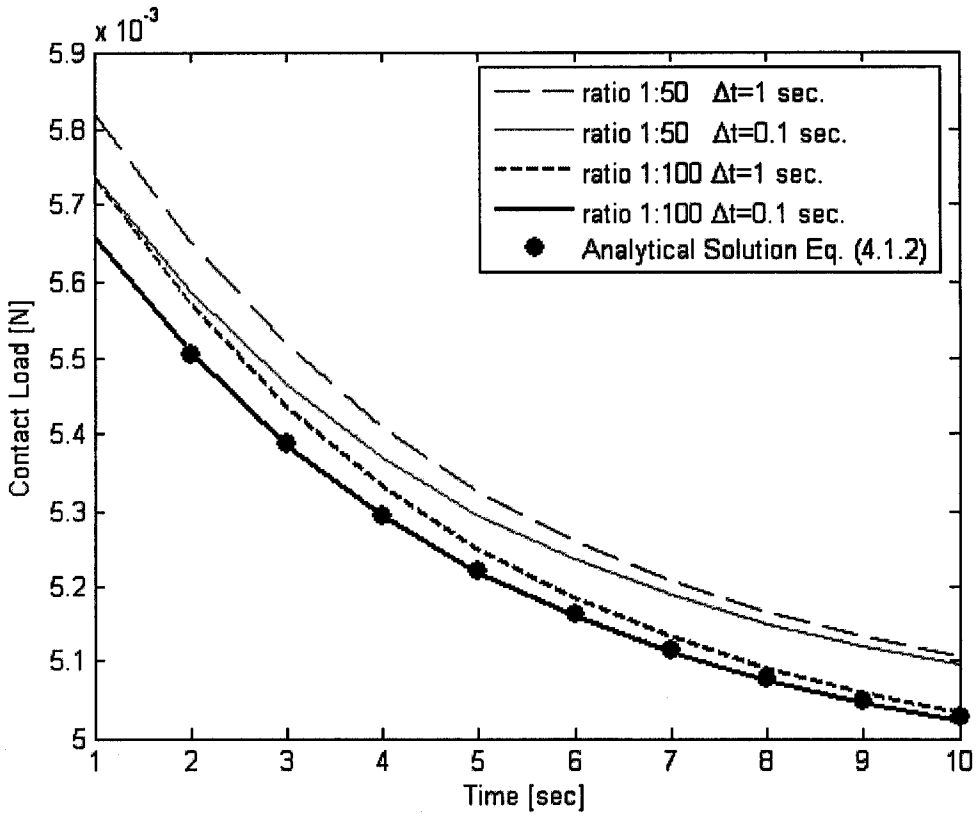

Figure 4-1-2. The convergence of the FEM solution and the analytical solution.

Figure 4-1-2. shows the convergence of the FEM solution and the analytical solution. This convergence was investigated by using two parameters, i.e., the time increment Δt, and the ratios of the radius of the contact area to the thickness of the body indented and to the width and length. Four sets of the parameters, i.e., the ratio 1:50 with $\Delta t = 0.1$ sec., the ratio 1:50 with $\Delta t = 1$ sec., the ratio is 1:100 with $\Delta t = 0.1$ sec., and the ratio is 1:100 with $\Delta t = 1$ sec., were used in the investigation, which clearly shows that the FEM solution approaches the analytical solution with a smaller time increment and a larger ratio. However, the computation time of the FEM simulation is 40 to 60 minutes while the algorithm requires less than a minute when using the same computer.

Thus, the algorithm gives a good approximation to the analytical solution of the viscoelastic contact problem, regardless of the assumptions made in sections 3.2 and 3.3. Also, the algorithm is very efficient in obtaining a good approximation.

4.1.2 Indentation Test

An algorithm is developed to simulate an indentation test with a single maximum contact area. The history of the indenter position is depicted in Figure 4-1-3. The algorithm is needed because the viscoelastic problem of the indentation test in the contact-area-decreasing phase cannot be solved analytically. In this section, the results from the FEM simulation and those from using the algorithm are compared.

The indentation history shown in Figure 4-1-3 is used so that the FEM results reported by Cheng et al. [18] can be used for the comparison. The material properties and the radius of the spherical indenter used in the FEM simulation are listed in Table 3-2-2. As the criteria to determine the parameters for the computation, i.e., $q_{\max}$ and Δt, have not been introduced, they will be specified in this chapter. The results from the use of the algorithm are shown in Figure 4-1-4.

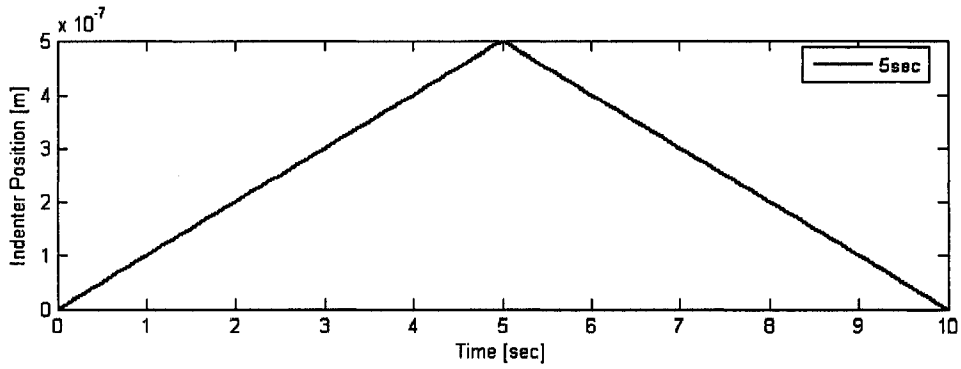

Figure 4-1-3. Indenter position history.

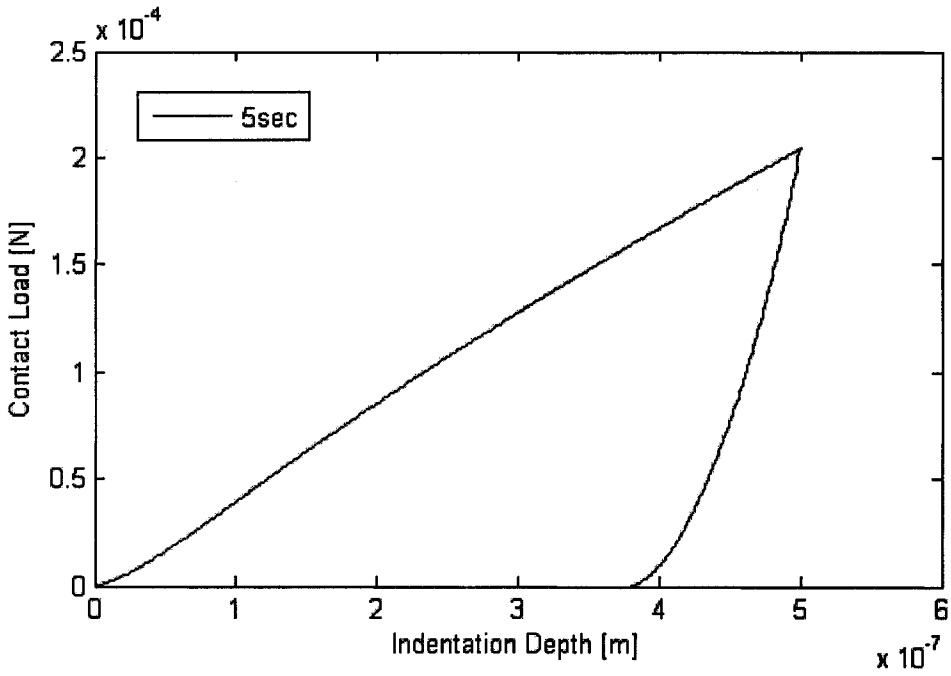

Figure 4-1-4. The result of the computation by using the algorithm.

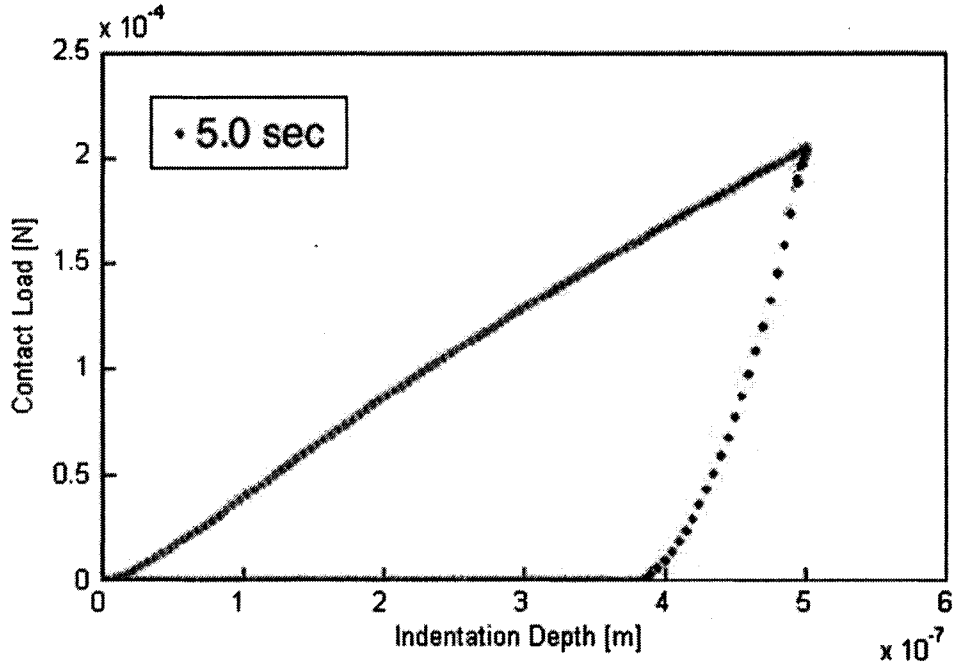

Figure 4-1-5. The result of the FEM calculations, from Cheng et al. [18]

The computation time of the semi-analytical algorithm is around 16 seconds when using a personal computer equipped with Intel Pentium 4, 2.80GHz and1.00GBytes of DDR2-400. This computation time may vary with the time increment and the number of grids used for the indentation test. The results from the computation using the algorithm and that from FEM simulation have good agreement. Therefore, it is concluded that the algorithm can be used to simulate the indentation test with a great accuracy and high efficiency, just as the algorithm can be used with the indentation relaxation test.

4.2 Determination of the Computational Parameters

The discretization of continuous space and time is essential for a digital computation. As the discretized points approximate a continuous function, the size of the increment of the discretized grids in space and in time influences the numerical error of the results from the computation. The closer the number of points to the infinity, the smaller the error of the result from the computation. However, the increase of the number of discretized points increases the computation time Therefore, a reasonable balance is required between the computation accuracy and the computation time.

The change of the number of grids $q_{\max}$ influences:

G-1. The approximation (smoothness) of the contact profile.

G-2. The resolution of the boundary of the contact area for the displacement computation.

G-3. The number of grids computed iteratively.

The time increment Δt influences:

T-1. The accuracy of the displacement computation.

T-2. The magnitude of the change of the indenter position within a time step.

T-3. The number of iterations throughout the indentation test simulation.

G-1, G-2, and T-1 are not independent because all of them are related to displacements. The relationships can be explained as follows. The accuracy of the displacement computation affects the approximation of the contact profile, i.e., T1 and G1. Then, the boundary of the contact area determines the range of grids for the displacement computation. Thus, G-2 governs the number of grid points used for the

contact profile approximation, i.e., G1 and G2. Through the iteration, all these parameters affect the accuracy. Therefore, the number of grids and the time increment cannot be determined separately.

A parametric study was conducted to explore the approach for determining the two parameters. All of the indentation tests considered possess a single maximum contact area because this algorithm is developed for such contact problems.

The program code for the algorithm is developed to obtain the contact load for the contact-area-increasing phase by using Eq. (2.4.32). The algorithm is then used to obtain the contact load after reaching the maximum contact area, i.e., the beginning of the unloading.

The parameters, i.e., five indentation position histories, three ratios of G_0 to G_1, three numbers of grids, and three time increments, are used. The five indenter position histories are obtained by changing the values of the two parameters shown in Figure 4-2-1, i.e., $T_{loading}$: time required to reach the maximum indentation depth and $T_{unloading}$: time required to return to the initial indenter position. By using these parameters, the five indenter position histories were listed as in Table 4-2-1.

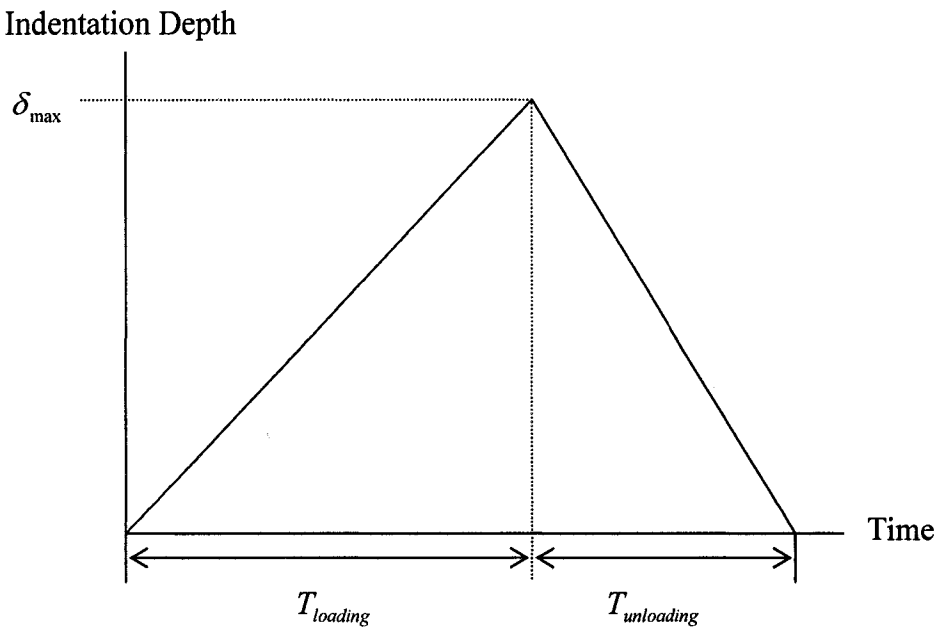

Figure 4-2-1. The schematic of the indenter position history used in the parametric study.

Table 4-2-1. Five indentation position histories used in the parametric study.

	$T_{loading}$ [sec]	$T_{unloading}$ [sec]	Maximum Indenter Depth δ_{max} [$\times 10^{-6}$ m]
H-1	1	1	1
H-2	5	5	1
H-3	10	10	1
H-4	1	5	1
H-5	1	10	1

The parameter of the material properties, i.e., the ratios of G_0 to G_1, is obtained by using the viscoelastic model shown in Figure 3-2-3. The 3 ratios used in the parametric study are listed in Table 4-2-2. The three numbers of the grids used in the parametric study are listed in Table 4-2-3. The three time increments and the corresponding Deborah numbers within the time increment, given by

$$N_D = \frac{\tau_{relax}}{\Delta t} \tag{4.2.1}$$

are listed in Table 4-2-4.

Table 4-2-2. Three ratios of the viscoelastic material properties used in the parametric study.

	G_0 [MPa]	G_1 [MPa]	Ratio G_0 to G_1	Relaxation Time τ_{relax} [sec]
R-1	200	200	1	1
R-2	200	20	0.1	1
R-3	200	2	0.01	1

Table 4-2-3. Three numbers of grids used in the parametric study.

	Number of Grid q_{max}
NG-1	50
NG-2	100
NG-3	200

Table 4-2-4. Three time increments used in the parametric study.

	Time Increment Δt [sec]	Deborah Number N_D
TI-1	0.02	50
TI-2	0.01	100
TI-3	0.005	200

The completeness of the simulation was checked by using these parameters. It was mentioned that the Deborah number should be large enough to be able to apply the equivalent elastic problem without a large error of approximation. However, the Deborah number does not seem to govern the simulation's completeness, because it has stricter

parameter conditions than those for the applicability of the equivalent elastic problem. A discussion of the results will follow their presentation.

Here, the completeness of the simulation is demonstrated by using the testing parameters H-5, R-2, NG-1, and TI-1.

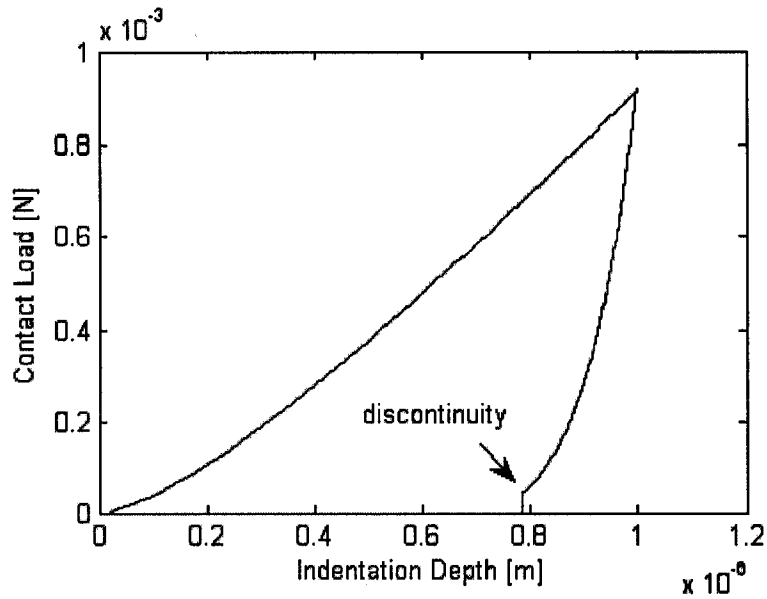

Figure 4-2-2. An example of the discontinuity in the unloading phase.

Figure 4-2-2 demonstrates a case of incomplete simulation, in which the discontinuity appears at the end of the contact load-indentation depth curve. The simulation is complete if the discontinuity does not occur. All parameters for R-1 generated a complete simulation. Therefore, any combination of the number of grids $q_{\max}$ (from 50 to 200) and the time increment Δt (from 0.02 to 0.005sec) provides a complete simulation. However, results for R-2 and R-3 have discontinuities, especially for the H-4 and H-5 types of the indenter position history, as depicted in Figure 4-2-3.

Table 4-2-5. Results of the parametric study #1.

H-1 R-1

N_D \ q_{max}	50	100	200
50	Y	Y	Y
100	Y	Y	Y
200	Y	Y	Y

H-1 R-2

N_D \ q_{max}	50	100	200
50	Y	Y	Y
100	Y	Y	Y
200	Y	Y	Y

H-2 R-1

N_D \ q_{max}	50	100	200
50	Y	Y	Y
100	Y	Y	Y
200	Y	Y	Y

H-2 R-2

N_D \ q_{max}	50	100	200
50	Y	N	Y
100	Y	Y	Y
200	Y	Y	Y

H-3 R-1

N_D \ q_{max}	50	100	200
50	Y	Y	Y
100	Y	Y	Y
200	Y	Y	Y

H-3 R-2

N_D \ q_{max}	50	100	200
50	Y	Y	Y
100	Y	Y	Y
200	Y	Y	Y

H-4 R-1

N_D \ q_{max}	50	100	200
50	Y	Y	Y
100	Y	Y	Y
200	Y	Y	Y

H-4 R-2

N_D \ q_{max}	50	100	200
50	Y	Y	Y
100	Y	N	Y
200	Y	Y	Y

H-5 R-1

N_D \ q_{max}	50	100	200
50	Y	Y	Y
100	Y	Y	Y
200	Y	Y	Y

H-5 R-2

N_D \ q_{max}	50	100	200
50	N	N	N
100	N	N	N
200	N	N	N
400	Y	Y	Y

Table 4-2-6. Results of the parametric study #2.

H-1 R-3

N_D \ q_{max}	50	100	200
50	Y	Y	Y
100	Y	Y	Y
200	Y	Y	Y

H-2 R-3

N_D \ q_{max}	50	100	200
50	Y	Y	Y
100	Y	Y	Y
200	Y	Y	Y

H-3 R-3

N_D \ q_{max}	50	100	200
50	Y	Y	Y
100	Y	Y	Y
200	Y	Y	Y

H-4 R-3

N_D \ q_{max}	50	100	200
50	N	N	N
100	N	N	N
200	N	N	Y
400	Y	Y	Y

H-5 R-3

N_D \ q_{max}	50	100	200
50	N	N	N
100	N	N	N
200	N	N	N
400	Y	Y	Y

Also, certain ratios of G_0 to G_1 may cause the discontinuity, which can be removed by using a shorter time increment. For example, by using $\Delta t = 0.0025$ (or $N_D = 400$), the discontinuity was removed in the cases of H-5 R-2, H-4 R-3, and H-5 R-3.

The discontinuity was found to occur when no root could be found for Eq. (3.3.2). The smaller time increment gives the smaller $\Delta\delta_{(m')}$, defined by Eq. (3.3.3). Also, the smaller time increment reduces the errors for the numerical convolution integral and results in a good approximation with the true contact profile. Since the numerical integration error and the approximate contact profile result in an inaccurate representation of the true contact profile, the difficulty in the root-finding for Eq. (3.3.2) can be removed

by using a smaller time increment.

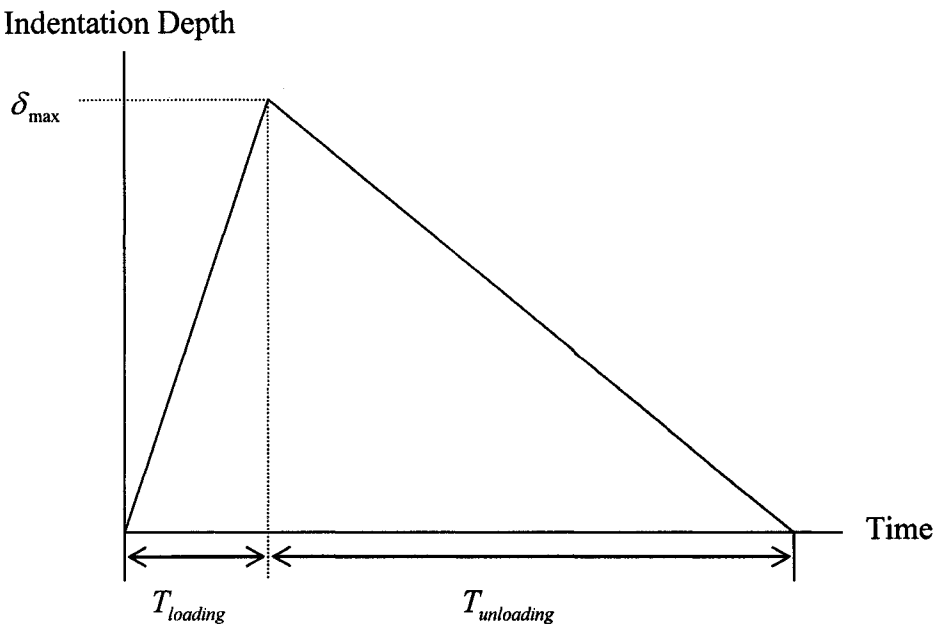

Figure 4-2-3. The indentation position history that takes a longer time to reach the initial position than that to reach the maximum indentation depth.

It is recommended to reduce the time increment when discontinuity arises.

Also, discontinuities are observed in the cases when $q_{max} = 100$ and $N_D = 100$ in the table for the H-4 R-2 condition and $q_{max} = 100$ and $N_D = 50$ in the table for the H-2 R-2 condition. Clear conclusions cannot be drawn from the two discontinuities because they appeared when the number of grids was increased in the H-2 R-2 condition and the Deborah number was increased in H-4 R-2. From H-4 R-3, it may be concluded that the use of a higher number of grids resolves the discontinuity problem. Moreover, the idea of using a smaller time increment to resolve the discontinuity problem cannot be applied to the discontinuity in H-4 R-2 condition because it appears even after increasing the

Deborah number from 50 to 100. However, the discontinuity was removed by using $N_D = 200$.

From the two discontinuities, it may be concluded that discontinuity may arise when the Deborah number and the number of grids are less than 100. This conclusion might not apply to the other loading conditions and material properties used in the parametric study. However, the discontinuities were removed by using a higher number of grids and a higher Deborah number than those that caused the discontinuities

The above discussion leads to the following criteria. For the number of grids, it is recommended to use $q_{\max} \geq 200$ to avoid the instable discontinuity arising when the ratio of G_0 to G_1 is less than 1. For the Deborah number, it is recommended to use at least $N_D \geq 200$ when $T_{loading}/T_{unloading} = 1$. When $T_{loading} < T_{unloading}$ and the ratio of G_0 to G_1 is less than 1, it is recommended to use $N_D \geq 400$. When the ratio of G_0 to G_1 is larger or equal to 1, $q_{\max}$ should be larger than 50, and N_D should be larger than 50 to ensure a complete simulation by the parametric study. These criteria are listed in Table 4-2-7. These criteria are valid within the loading conditions and material properties considered in the parametric study. However, the strategy for removing the discontinuity, i.e., by increasing the number of grids and the Deborah number, can be used for any other loading conditions and material properties.

Table 4-2-7. Proposed computational parameters criteria.

		Number of Grids q_{max}	Deborah Number N_D
$G_1/G_0 = 1$		≥ 50	≥ 50
$G_1/G_0 < 1$	$T_{loading}/T_{unloading} = 1$	≥ 200	≥ 200
	$T_{loading} < T_{unloading}$	≥ 200	≥ 400

5. Conclusion and Future Studies

A semi-analytical algorithm for the quasi-static contact between a rigid axisymmetric body and a semi-infinite viscoelastic body was discussed in this study. The algorithm is particularly useful for contact problems involving a contact-area-decreasing phase, because no closed form solution is available for the contact load-indentation depth relationship. The algorithm was developed based on the indentation test in which the rigid indenter has a spherical tip. The semi-analytical algorithm greatly reduces the computation time. With a reasonable choice of the computational parameters, this algorithm can be used to compute the contact load-indentation depth of an indentation test very quickly. The computational parameters recommended for particular loading conditions and material properties were determined in a parametric study.

5.1 Summary and Conclusions

The algorithm is based on the idea that the pressure applied to a linear viscoelastic problem at an instant of time can be reproduced by using a linear elastic solution. This idea was expanded for the viscoelastic boundary value problem by using the instantaneously recoverable surface displacement and delayed recoverable surface displacement for the contact between a rigid body and a semi-infinite viscoelastic body. The solution of the equivalent elastic problem was given by the generalized solution of the elastic contact with assumptions. The use of the idea for the boundary value problem

was verified by the contact pressure distributions obtained from the viscoelastic boundary value problem and the equivalent elastic problem.

The solutions of the equivalent elastic problem were used to predict the contact area and p_c, which was used to obtain the displacements, i.e., the instantaneously recoverable displacement and the delayed recoverable displacement. The imperfection of the predicted instantaneously recoverable displacement was corrected to meet the displacement boundary value specified by the indentation depth and the contact profile. Then the iteration to obtain the contact load, the contact area, and the displacement from those of the previous time step was carried over while the contact area or the contact load was positive.

Verification of the result of using the algorithm was conducted by comparing the results of the indentation relaxation tests obtained by the algorithm, the closed form solution and FEM. Also, the results of the indentation test, which has a contact-area-decreasing phase, obtained by using the algorithm and FEM were compared. The results from the indentation relaxation test of the algorithm and the closed form solution have good agreement while the result from FEM has some numerical errors. The results of the indentation test of the algorithm and FEM have good agreement. Accordingly, the algorithm can simulate the contact problem with great accuracy.

The criteria for the time increment and the grids within the maximum contact area were also discussed. The criteria were determined in a parametric study for the particular loading conditions and the material properties. The discontinuity in the contact load-indentation depth curve, which was caused by numerical difficulty, i.e., root-finding, can be resolved by increasing the number of grids and the Deborah number. It is suggested

that the strategy to remove the discontinuity in the curve can be applied to any other loading conditions and material properties.

5.2 Future Studies

The semi-analytical algorithm was restricted to the quasi-static contact between an axisymmetric rigid body and a semi-infinite viscoelastic body. Therefore, the recommended further studies could attempt to remove this restriction. There studies could examine

1. the body force for dynamic contact problems
2. elastic-viscoelastic contact problems
3. viscoelastic-viscoelastic contact problems
4. the arbitrary shape of the contact profile
5. frictional contact problems
6. the finite geometries of the bodies in contact

Two or more of contact problems are sometimes combined, thus increasing the difficulty of solving a problem. For any types of contact problems involving viscoelastic material, the solution of the equivalent elastic problem can be useful to predict the contact pressure at the next time step if the input is displacement, and the contact load is unknown.

Bibliography

[1] Hertz, H. "On the Contact of Elastic Solids," in "Miscellaneous Papers by Heinrich Hertz," Macmillan, 1896. pp.146-162.

[2] Lee, E.H. and Radok, J.R.M. "The Contact Problem for Viscoelastic Bodies," Journal of Applied Mechanics, Vol. 27, 1960, pp.438-444.

[3] Sneddon, I.N. "The Relation Between Load and Penetration in the Axisymmetric Boussinesq Problem for a Punch of Arbitrary Profile," International Journal of Engineering Science, Vol. 3, 1965, pp.45-57.

[4] Johnson, K.L. "Contact Mechanics," Cambridge University Press, 1985. pp.1-93.

[5] Ting, T.G.T. "The Contact Stresses Between a Rigid Indenter and a Viscoelastic Half-Space," Journal of Applied Mechanics, Vol. 33, 1966, pp.845-854.

[6] Zwillinger, D . "CRC Standard Mathematical Tables and Formulae 31st edition," CRC Press Compnay, 2002, Table of Indefinite Integrals, Section 5.4.12

[7] Meijers, P. "The Contact Problem of a Rigid Cylinder On an Elastic Layer," Applied Science Research, Vol. 18, 1968, pp.353-383.

[8] Swanson, S.R. "Herztian Contact of Orthotropic Materials," International Journal of Solids and Structures, Vol. 41, 2004, pp.1945-1959.

[9] Sneddon, I.N. "The Elementary Solution of Dual Integral Equations," Proceedings of the Glasgow Mathematical Association, Vol. 4, 1960, pp108-110.

[10] Zabreyko, P.P. et al. "Integral Equations," Noordhoff International Publishing, 1975, pp.20

[11] Findley, W.N, LAI, J.S., and Onaran, K. "Creep and Relaxation of Nonlinear Viscoelastic Materials with an Introduction of Linear Viscoelasticity," North-Holland Publishing Company, 1976, pp.82-83.

[12] Alfrey, T. "Non-Homogeneous Stresses in Visco-Elastic Media," Quarterly of Applied Mathematics, Vol.2, 1944, pp.113-119.

[13] Read, W.T. "Stress Analysis for Compressible Viscoelastic Materials," Journal of Applied Physics, Vol. 21, 1950, pp.671-674.

[14] Lee, E.H. "Stress Analysis in Visco-Elastic Bodies," Quarterly of Applied Mathematics, Vol.13, 1955, pp.183-190.

[15] Graham, G.A.C. "The Contact Problem in the Linear Theory of Viscoelasticity," International Journal of Engineering Science, Vol. 3, 1965, pp.27-46.

[16] Hunter, S.C. "The Hertz Problem for a Rigid Spherical Indenter and a Viscoelastic Half-Space," Journal of the Mechanics and Physics of Solids, Vol.8, 1960, pp.219-234.

[17] Onat, E.T. and Breuer, S. "On Uniqueness in Linear Viscoelasticity," Progress in Applied Mechanics, 1963, pp.349-353.

[18] Cheng, T.Y. and Cheng, C.M. "Relationship Between Initial Unloading Slope, Contact Depth, and Mechanical Properties for Spherical Indentation in Linear Viscoelastic Solids," Materials Science and Engineering A, Vol. 409, 2005 pp93-99.

[19] Cheng, L. Xia, X, Scriven, L.E. and Gerberich, W.W. "Spherical-tip Indentation of Viscoelastic Material," Mechanics of Materials, Vol. 37, 2005, pp.213-226.

[20] Brigham, E. O. "The Fast Fourier Transform and Its Applications," Prentice Hall, 1988. pp.121.

[21] Taylor, R.L., Pister, K.S. and Goudreau, G. L. "Thermomechanical Analysis of Viscoelastic Solids," International Journal for Numerical Methods in Engineering, Vol.2, 1970, pp.45-59.

[22] Sneddon, N. I. "Fourier Transforms," McGraw-Hill Book Company, 1951, pp. 450-457. pp.62.

[23] Timoshenko, S. "Theory of Elasticity," McGraw-Hill Book Company, 1934, pp.310-311.

[24] Watoson, G.N. "A Treatise On the Theory of Bessel Functions second edition," Cambridge University Press, 1966, pp.405

Appendix A

In this appendix, the entire derivation of Sneddon's approach [3] is presented. The formulations of the governing equations are taken from Sneddon [23].

The axisymmetrical linear elastic boundary value problem can be solved by using the Hankel transform, which reduces the biharmonic equation in r and z into a 4^{th} order ordinary differential equation in z.

First, the biharmonic equation is derived by using the compatibility equation for the axisymmetric linear elastic problem. Then the biharmonic equation is reduced to a 4th order ordinary differential equation by using the Hankel transform. Furthermore, by using the boundary conditions, the arbitrary coefficients in the general solution of 4th order differential equation are determined, leaving one of them still undetermined. Then the mixed-boundary value problem is expressed by using the dual integral equations, which have the undetermined coefficient of the general solution as an arbitrary function. The solution of the arbitrary function which satisfies the dual integral equations is known. Then the contact pressure, the contact load, the indentation depth, the displacement within the contact area, and the displacement outside the contact area are derived based on the solution of the dual integral equations.

A-1. Governing Filed Equations for Axisymmetric Linear Elastic Problem

The equilibrium equations for an axysimmetric problem are

$$\frac{\partial \sigma_{rr}}{\partial r}+\frac{\partial \sigma_{rz}}{\partial z}+\frac{\sigma_{rr}-\sigma_{\theta\theta}}{r}=0 \tag{A-1.1}$$

and

$$\frac{\partial \sigma_{rz}}{\partial r}+\frac{\partial \sigma_{zz}}{\partial z}+\frac{\sigma_{rz}}{r}=0\,. \tag{A-1.2}$$

The compatibility equations for the axisymmetric problem are obtained by applying coordinate transformation to those for Cartesian coordinates, as explained by Timoshenko [23]. The compatibility equations for Cartesian coordinates are

$$(1+\nu)\nabla^2\sigma_{xx}+\frac{\partial^2}{\partial x^2}\left(\sigma_{xx}+\sigma_{yy}+\sigma_{zz}\right)=0\,. \tag{A-1.3}$$

The stress components in x and y are expressed in r and θ; i.e.,

$$\sigma_{xx}=\sigma_{rr}\cos^2\theta+\sigma_{\theta\theta}\sin^2\theta \tag{A-1.4}$$

$$\sigma_{yy}=\sigma_{rr}\sin^2\theta+\sigma_{\theta}\cos^2\theta\,. \tag{A-1.5}$$

Then

$$\nabla^2\sigma_{xx}=\left(\frac{\partial^2}{\partial r^2}+\frac{1}{r}\frac{\partial}{\partial r}+\frac{1}{r^2}\frac{\partial^2}{\partial\theta^2}+\frac{\partial^2}{\partial z^2}\right)\left(\sigma_{rr}\cos^2\theta+\sigma_{\theta\theta}\sin^2\theta\right)$$

$$=\left(\frac{\partial^2}{\partial r^2}+\frac{1}{r}\frac{\partial}{\partial r}+\frac{\partial^2}{\partial z^2}\right)\left(\sigma_{rr}\cos^2\theta+\sigma_{\theta\theta}\sin^2\theta\right)-\frac{2}{r^2}\left(\sigma_{rr}-\sigma_{\theta\theta}\right)\left(\cos^2\theta-\sin^2\theta\right) \tag{A-1.6}$$

and

$$\frac{\partial^2}{\partial x^2}(\sigma_{xx}+\sigma_{yy}+\sigma_{zz})=\left(\frac{\partial}{\partial r}\cos\theta-\frac{1}{r}\sin\theta\frac{\partial}{\partial\theta}\right)$$

$$\times\left\{\frac{\partial}{\partial r}(\sigma_{rr}+\sigma_{\theta\theta}+\sigma_{zz})\cos\theta-\frac{1}{r}\frac{\partial}{\partial\theta}(\sigma_{rr}+\sigma_{\theta\theta}+\sigma_{zz})\sin\theta\right\}. \quad \text{(A-1.7)}$$

For an axisymmetric problem, $\partial/\partial\theta$ is a null operator. Therefore, Eq.(A-1.7) is rewritten as

$$\frac{\partial^2}{\partial x^2}(\sigma_{xx}+\sigma_{yy}+\sigma_{zz})=\left(\frac{\partial}{\partial r}\cos\theta-\frac{1}{r}\sin\theta\frac{\partial}{\partial\theta}\right)\left\{\frac{\partial}{\partial r}(\sigma_{rr}+\sigma_{\theta\theta}+\sigma_{zz})\cos\theta\right\}$$

$$=\frac{\partial^2}{\partial r^2}(\sigma_{rr}+\sigma_{\theta\theta}+\sigma_{zz})\cos^2\theta+\frac{1}{r}\frac{\partial}{\partial r}(\sigma_{rr}+\sigma_{\theta\theta}+\sigma_{zz})\sin^2\theta. \quad \text{(A-1.8)}$$

Substituting (A-1.6) and (A-1.8) into (A-1.3) gives

$$\left\{\left(\frac{\partial^2}{\partial r^2}+\frac{1}{r}\frac{\partial}{\partial r}+\frac{\partial^2}{\partial z^2}\right)\sigma_{rr}-\frac{2}{r^2}(\sigma_{rr}-\sigma_{\theta\theta})+\frac{1}{1+\nu}\frac{\partial^2}{\partial r^2}(\sigma_{rr}+\sigma_{\theta\theta}+\sigma_{zz})\right\}\cos^2\theta$$

$$+\left\{\left(\frac{\partial^2}{\partial r^2}+\frac{1}{r}\frac{\partial}{\partial r}+\frac{\partial^2}{\partial z^2}\right)\sigma_{\theta\theta}-\frac{2}{r^2}(\sigma_{rr}-\sigma_{\theta\theta})+\frac{1}{1+\nu}\frac{\partial^2}{\partial r^2}(\sigma_{rr}+\sigma_{\theta\theta}+\sigma_{zz})\right\}\sin^2\theta=0. \quad \text{(A-1.9)}$$

This equation holds for any value of θ. Thus, the following equations should be satisfied:

$$\left\{\nabla^2\sigma_{rr}-\frac{2}{r^2}(\sigma_{rr}-\sigma_{\theta\theta})+\frac{1}{1+\nu}\frac{\partial^2}{\partial r^2}(\sigma_{rr}+\sigma_{\theta\theta}+\sigma_{zz})\right\}=0 \quad \text{(A-1.10)}$$

$$\left\{\nabla^2\sigma_{\theta\theta}-\frac{2}{r^2}(\sigma_{rr}-\sigma_{\theta\theta})+\frac{1}{1+\nu}\frac{\partial^2}{\partial r^2}(\sigma_{rr}+\sigma_{\theta\theta}+\sigma_{zz})\right\}=0, \quad \text{(A-1.11)}$$

where

$$\nabla^2=\frac{\partial^2}{\partial r^2}+\frac{1}{r}\frac{\partial}{\partial r}+\frac{\partial^2}{\partial z^2} \quad \text{(A-1.12)}$$

is the Laplacian operator for an axisymmetric problem in cylindrical coordinates. This definition of Laplacian operator is used hereafter unless otherwise noted.

The equations (A-1.10) and (A-1.11) are two of the four compatibility equations for an axisymmetric problem. The other two compatibility equations for this problem are omitted here because the result will end up with the same biharmonic equation by using any one of the compatibility equations.

The stress-strain relationship of the linear elastic problem can be given by

$$\sigma_{ij} = 2\mu\varepsilon_{ij} + \lambda\varepsilon_{kk}\delta_{ij}\,. \tag{A-1.13}$$

The strain-displacement relationships for an axisymmetric problem are given by

$$\varepsilon_{rr} = \frac{\partial u_r}{\partial r},\ \varepsilon_{\theta\theta} = \frac{u_r}{r},\ \varepsilon_{zz} = \frac{\partial u_z}{\partial z},\ \text{and}\ \varepsilon_{rz} = \frac{1}{2}\left(\frac{\partial u_r}{\partial z} + \frac{\partial u_z}{\partial r}\right). \tag{A-1.14}$$

Substituting Eqs (A-1.14) into (A-1.13) gives

$$\sigma_{rr} = \left\{(\lambda+2\mu)\frac{\partial}{\partial r} + \frac{\lambda}{r}\right\}u_r + \lambda\frac{\partial u_z}{\partial z} \tag{A-1.15}$$

$$\sigma_{\theta\theta} = \left(\lambda\frac{\partial}{\partial r} + \frac{\lambda+2\mu}{r}\right)u_r + \lambda\frac{\partial u_z}{\partial z} \tag{A-1.16}$$

$$\sigma_{\theta\theta} = \lambda\left(\frac{\partial}{\partial r} + \frac{1}{r}\right)u_r + (\lambda+2\mu)\frac{\partial u_z}{\partial z} \tag{A-1.17}$$

$$\sigma_{rz} = \mu\left(\frac{\partial u_r}{\partial z} + \frac{\partial u_z}{\partial r}\right). \tag{A-1.18}$$

Defining the displacements as a function of an arbitrary function, $\Phi(r,z)$, i.e.,

$$u_r = -\frac{\lambda+\mu}{\mu}\Phi_{,rz} \tag{A-1.19}$$

$$u_z = \frac{\lambda+2\mu}{\mu}\nabla^2\Phi - \frac{\lambda+\mu}{\mu}\Phi_{,zz}\,, \tag{A-1.20}$$

and substituting Eqs. (A-1.19) and (A-1.20) into Eqs. (A-1.15) to (A-1.18) give

$$\sigma_{rr} = \lambda\nabla^2\Phi_{,z} - 2(\lambda+\mu)\Phi_{,rrz} \tag{A-1.21}$$

$$\sigma_{\theta\theta} = \lambda\nabla^2\Phi_{,z} - \frac{2}{r}(\lambda+\mu)\Phi_{,rz} \tag{A-1.22}$$

$$\sigma_{zz} = (3\lambda+4\mu)\nabla^2\Phi_{,z} - 2(\lambda+\mu)\Phi_{,zzz} \tag{A-1.23}$$

$$\sigma_{rz} = (\lambda+2\mu)\frac{\partial}{\partial r}\nabla^2\Phi - 2(\lambda+\mu)\Phi_{,rzz}. \tag{A-1.24}$$

The equilibrium equations are verified by substituting (A-1.21) to (A-1.24) into Eqs. (A-1.1) and (A-1.2). Substituting Eqs. (A-1.21) to (A-1.24) into Eqs. (A-1.10) and (A-1.11) gives the same expression; i.e.,

$$\nabla^4\Phi = 0. \tag{A-1.25}$$

This expression is satisfied if the arbitrary function Φ is a solution of the biharmonic equation (A-1.25). Then the axisymmetric problem is reduced to that of finding the solution of the biharmonic function in r and z.

A-2. Solution of the Equilibrium Equation by Using Hankel Transform

Integral transformation is used to eliminate partial derivatives with respect to one of the variables. Thus, the equation that the integral transformation is applied to has one less variable. The Hankel transform, defined by Eq. (A-2.1), was applied to Eq. (A-1.25) to reduce the biharmonic equation in r and z to a fourth-order ordinary differential equation in z. The Hankel transform of the derivatives of a function are explained, and the derivation of the forth-order ordinary differential equation follows.

A Hankel transform of order n is defined by

$$\hat{g}(\xi)=\int_0^\infty rg(r)J_n(\xi r)dr, \tag{A-2.1}$$

where $J_n(r)$ denotes a Bessel function of the first kind of order n, and the hat $\hat{g}(\xi)$ denotes the Hankel transformation of function $g(r)$. Also, the inverse of Hankel transform is defined by

$$g(r)=\int_0^\infty \xi\hat{g}(\xi)J_n(\xi r)d\xi. \tag{A-2.2}$$

For the contact between a axisymmetric rigid body and a semi-infinite elastic body, r ranges from 0 to infinite. The Hankel transform of the derivatives of a function $g(r,z)$ is obtained by Sneddon [22] as follows:

$$\int_0^\infty r\left(\frac{d^2g(r,z)}{dr^2}+\frac{1}{r}\frac{dg(r,z)}{dr}\right)J_0(\xi r)dr=-\xi^2\hat{g}(\xi,z). \tag{A-2.3}$$

The fourth-order ordinary differential equation is obtained by using Eq. (A-2.3) and Eq. (A-2.1). The following expression is obtained from Eqs. (A-2.3) and (A-2.1).

$$\int_0^\infty r\nabla^2 f(r,z)J_0(\xi r)dr=\left(\frac{\partial^2}{\partial z^2}-\xi^2\right)\int_0^\infty rf(r,z)J_0(\xi r)dr \tag{A-2.4}$$

Replacing $f(r,z)$ by $\nabla^2\Phi(r,z)$ and applying the same result as that from Eq. (A-2.4) gives

$$\int_0^\infty r\nabla^4\Phi(r,z)J_0(\xi r)dr=\left(\frac{\partial^2}{\partial z^2}-\xi^2\right)^2\int_0^\infty r\Phi(r,z)J_0(\xi r)dr. \tag{A-2.5}$$

The left hand side of Eq. (A-2.5) can also be obtained by multiplying Eq. (A-1.25) by $rJ_0(\xi r)$ and integrating over r from 0 to ∞; i.e.,

$$\int_0^\infty r\nabla^4\Phi J_0(\xi r)dr = 0 \tag{A-2.6}$$

From Eqs. (A-2.5) and (A-2.6), one can find a fourth-order ordinary differential equation; i.e.,

$$\left(\frac{\partial^2}{\partial z^2} - \xi^2\right)^2 G(\xi, z) = 0, \tag{A-2.7}$$

where

$$G(\xi, z) = \int_0^\infty r\Phi(r, z)J_0(\xi r)dr. \tag{A-2.8}$$

The general solution of Eq. (A-2.7) is expressed by

$$G(\xi, z) = (A + Bz)e^{\xi} + (C + Dz)e^{-\xi}, \tag{A-2.9}$$

where A, B, C and D are determined from the boundary conditions.

The same procedure is applied to Eqs. (A-1.20), (A-1.23) and (A-1.24) to express u_z, σ_{zz} and σ_{rz}, which are used to specify the boundary condition of the contact problem, in terms of the derivatives with respect to z.

Multiplying both sides of Eq. (A-1.20) by $rJ_0(\xi r)$ and integrating over r from 0 to ∞ gives

$$\int_0^\infty ru_z J_0(\xi r)dr = \frac{\lambda + 2\mu}{\mu}\int_0^\infty r\nabla^2\Phi J_0(\xi r)dr - \frac{\lambda + \mu}{\mu}\frac{d^2}{dz^2}\int_0^\infty r\Phi J_0(\xi r)dr. \tag{A-2.10}$$

By using Eq. (A-2.4) and Eq. (A-2.8), Eq. (A-2.10) is rewritten as

$$\int_0^\infty r u_z J_0(\xi r)dr = \frac{\lambda+2\mu}{\mu}\left(\frac{d^2}{dz^2}-\xi^2\right)G - \frac{\lambda+\mu}{\mu}\frac{d^2G}{dz^2}. \tag{A-2.11}$$

By using the inverse of Hankel transform Eq. (A-2.2), the displacement in z direction is given by

$$u_z = \int_0^\infty \xi\left(\frac{d^2G}{dz^2} - \frac{\lambda+2\mu}{\mu}\xi^2 G\right)J_0(\xi r)d\xi. \tag{A-2.12}$$

Multiplying Eq. (A-1.23) by $rJ_0(\xi r)$, integrating over r from 0 to ∞, and applying the inverse of the Hankel transform gives

$$\sigma_{zz} = \int_0^\infty \xi\left\{(\lambda+2\mu)\frac{d^3G}{dz^3} - (3\lambda+4\mu)\xi^2\frac{dG}{dz}\right\}J_0(\xi r)d\xi. \tag{A-2.13}$$

The derivation of the shear stress σ_{rz} requires the following equation from Sneddon [22]:

$$\int_0^\infty r\frac{dg(r)}{dr}J_1(\xi r)dr = -\xi\int_0^\infty rg(r)J_0(\xi r)dr. \tag{A-2.14}$$

Multiplying Eq. (A-1.24) by $rJ_1(\xi r)$, integrating over r from 0 to ∞, and using Eq. (A-2.14) and Eq. (A-2.3) yields

$$\begin{aligned}\int_0^\infty r\sigma_{rz}J_1(\xi r)dr &= \int_0^\infty r\left\{(\lambda+2\mu)\frac{\partial}{\partial r}\nabla^2\Phi - 2(\lambda+\mu)\Phi_{,rzz}\right\}J_1(\xi r)dr \\ &= (\lambda+2\mu)\int_0^\infty r\frac{\partial}{\partial r}\left(\frac{\partial^2\Phi}{\partial r^2}+\frac{1}{r}\frac{\partial\Phi}{\partial r}\right)J_1(\xi r)dr - \lambda\frac{d^2}{dz^2}\int_0^\infty r\frac{\partial\Phi}{\partial r}J_1(\xi r)dr \\ &= -(\lambda+2\mu)\xi\int_0^\infty r\left(\frac{\partial^2\Phi}{\partial r^2}+\frac{1}{r}\frac{\partial\Phi}{\partial r}\right)J_0(\xi r)dr + \lambda\xi\frac{d^2}{dz^2}\int_0^\infty r\Phi J_0(\xi r)dr \\ &= (\lambda+2\mu)\xi^3 G + \lambda\xi\frac{d^2G}{dz^2}.\end{aligned} \tag{A-2.15}$$

Applying the inverse of the Hankel transform to Eq. (A-2.15) gives

$$\sigma_{rz} = \int_0^\infty \xi^2 \left\{ \xi^2 (\lambda + 2\mu) G + \lambda \frac{d^2 G}{dz^2} \right\} J_1(\xi r) d\xi \,. \qquad \text{(A-2.16)}$$

A, B, C and D in Eq. (A-2.9) are now determined by using the boundary conditions. Recall the boundary condition for contact between a rigid body and a semi-infinite body:

$$\bar{\sigma}_{rz}(\rho) = 0 \qquad \rho \geq 0 \qquad \text{(A-2.17)}$$

$$\bar{u}_z(\rho) = \delta - f(\rho) \qquad 0 \leq \rho \leq 1 \qquad \text{(A-2.18)}$$

$$\bar{\sigma}_{zz}(\rho) = 0, \qquad \rho > 1 \qquad \text{(A-2.19)}$$

where $f(\rho)$ is a contact profile, $\rho = r/a$, and a is the radius of the contact area. First, since the stress and displacement tend to zero when $z \to \infty$, so that $A = B = 0$. Thus,

$$G(\xi, z) = (C + Dz) e^{-\xi z} \,. \qquad \text{(A-2.20)}$$

The relationship between C and D is obtained by applying the boundary condition Eq. (A-2.17). Substituting Eq. (A-2.20) into Eq. (A-2.16) gives

$$\sigma_{rz} = \int_0^\infty \xi^2 \left\{ \xi^2 (\lambda + 2\mu)(C + Dz) e^{-\xi z} + \lambda (C\xi^2 - 2D\xi + Dz\xi) e^{-\xi z} \right\} J_1(\xi r) d\xi \qquad \text{(A-2.21)}$$

By using Eq. (A-2.17), Eq. (A-2.21) must satisfy

$$\sigma_{rz}\big|_{z=0} = 2 \int_0^\infty \xi^3 \{ (\lambda + \mu) C\xi - \lambda D \} J_1(\xi r) d\xi = 0 \,. \qquad \text{(A-2.22)}$$

In order for the integration to be zero,

$$(\lambda + \mu) C\xi = \lambda D \,. \qquad \text{(A-2.23)}$$

By substituting Eq. (A-2.23) into Eq. (A-2.20),

$$G(\xi, z) = \frac{D}{\xi} \left(\frac{\lambda}{\lambda + \mu} + z\xi \right) e^{-\xi z} \,. \qquad \text{(A-2.24)}$$

Substituting Eq. (A-2.24) into Eqs. (A-2.12) and (A-2.13) yields

$$u_z(r,z)=\frac{a}{2(1-\nu)}\mathcal{H}_0\left[\{2(1-\nu)+\xi z\}\xi^{-1}\psi(\xi a)e^{-\xi z};\ \xi\to r\right] \tag{A-2.25}$$

$$\sigma_{zz}(r,z)=-\frac{\mu a}{1-\nu}\mathcal{H}_0\left[(1+\xi z)\psi(\xi a)e^{-\xi z};\ \xi\to r\right], \tag{A-2.26}$$

where

$$\psi(\xi a)=-\frac{\lambda+2\mu}{\mu a^3}(\xi a)^2 D \tag{A-2.27}$$

and uses the following notation

$$\mathcal{H}_n[f(\xi,z);\ \xi\to r]=\int_0^\infty \xi f(\xi,z)J_n(\xi r)d\xi \tag{A-2.28}$$

to denote the Hankel transform of order n of the function $f(\xi,z)$.

By changing the variable from r to $\rho=r/a$, Eq. (A-2.28) can be rewritten as

$$\frac{1}{a^2}\mathcal{H}_n[f(\xi,z);\ \zeta\to\rho]=\frac{1}{a^2}\int_0^\infty \zeta f(\zeta,z)J_n(\zeta\rho)d\rho. \tag{A-2.29}$$

Applying this notation to Eqs. (A-2.25) and (A-2.26), the boundary values, i.e., the displacement and stress at $z=0$, are given by

$$\bar{u}_z(r)=\mathcal{H}_0\left[\zeta^{-1}\psi(\zeta);\ \zeta\to\rho\right] \tag{A-2.30}$$

$$\bar{\sigma}_{zz}(r)=-\frac{\mu}{a(1-\nu)}\mathcal{H}_0[\psi(\zeta);\ \zeta\to\rho], \tag{A-2.31}$$

where

$$\psi(\zeta)=-\frac{\lambda+2\mu}{\mu a^5}\zeta^2 D. \tag{A-2.32}$$

Thus, the boundary conditions (A-2.17), (A-2.18) and (A-2.19) will be satisfied by solving

$$\mathcal{H}_0\left[\zeta^{-1}\psi(\zeta);\quad \zeta\to\rho\right]=\delta-f(\rho) \qquad 0\le\rho<1 \quad \text{(A-2.33)}$$

$$\mathcal{H}_0[\psi(\zeta);\ \zeta\to\rho]=0. \qquad 1<\rho \quad \text{(A-2.34)}$$

These equations are alternatively expressed as

$$\int_0^\infty \psi(\zeta)J_0(\rho\zeta)d\zeta=\delta-f(\rho) \qquad 0\le\rho<1 \quad \text{(A-2.35)}$$

$$\int_0^\infty \zeta\psi(\zeta)J_0(\rho\zeta)d\zeta=0. \qquad 1<\rho \quad \text{(A-2.36)}$$

The solution of the dual integration equations, (A-2.35) and (A-2.36), was obtained by Sneddon [9]. The following form of solution was proposed:

$$\psi(\zeta)=\int_0^1 \chi(\vartheta)\cos(\zeta\vartheta)d\vartheta. \qquad \text{(A-2.37)}$$

For the function $\psi(\zeta)$,

$$\int_0^\infty \zeta\psi(\zeta)J_0(\rho\zeta)d\zeta=\int_0^\infty J_0(\zeta\rho)d\zeta\int_0^1 \zeta\chi(\vartheta)\cos(\zeta\vartheta)d\vartheta$$

$$=\chi(1)\int_0^\infty J_0(\zeta\rho)\sin(\zeta)d\zeta-\int_0^\infty J_0(\zeta\rho)d\zeta\int_0^1\frac{d\chi}{d\vartheta}\sin(\zeta\vartheta)d\vartheta. \qquad \text{(A-2.38)}$$

By using Watson's [24] result, i.e.,

$$\int_0^\infty J_0(\zeta\rho)\sin(\zeta\vartheta)d\zeta=0, \qquad \vartheta<\rho \quad \text{(A-2.39)}$$

it can be verified that Eq. (A-2.37) satisfies Eq. (A-2.36) because $\vartheta\le1$ and $\rho>1$, so the condition of Eq. (A-2.39) is always satisfied for Eq. (A-2.36).

Substituting Eq. (A-2.37) into Eq. (A-2.35) gives

$$\int_0^\infty J_0(\rho\zeta)d\zeta \int_0^1 \chi(\vartheta)\cos(\zeta\vartheta)d\vartheta = \delta - f(\rho). \qquad 0 \le \rho < 1 \quad \text{(A-2.40)}$$

By using Watson's [24] result, i.e.,

$$\int_0^\infty J_0(\zeta\rho)\cos(\zeta\vartheta)d\zeta = \begin{cases} 0 & 0 < \rho < \vartheta \\ (\rho^2 - \vartheta^2)^{-1/2}. & \rho > \vartheta \end{cases} \quad \text{(A-2.41)}$$

Eq. (A-2.40) must satisfy

$$\int_0^\rho \frac{\chi(\vartheta)}{\sqrt{\rho^2 - \vartheta^2}} d\vartheta = \delta - f(\rho). \qquad 0 \le \rho < 1 \quad \text{(A-2.42)}$$

This form of integration is called "the Abel integral equation", and its solution can be obtained from Zabreyko et al. [10]:

$$\chi(\vartheta) = \frac{2\delta}{\pi} - \frac{2}{\pi}\frac{d}{d\vartheta}\left[\int_0^\vartheta \frac{\rho f(\rho)}{\sqrt{\vartheta^2 - \rho^2}} d\rho\right]. \quad \text{(A-2.43)}$$

Thus, the solution of the dual integral equation is given by Eq. (A-2.37) with Eq. (A-2.43).

A-3. Contact Pressure, Indentation Depth, and Displacements within/outside the Contact Area

First, the stress distribution within the contact area is determined by using the solution of the dual integral equations. Substituting Eq. (A-2.37) into Eq. (A-2.31) gives

$$\bar{\sigma}_{zz}(r) = -\frac{\mu}{a(1-\nu)}\mathcal{H}_0\left[\int_0^1 \chi(\vartheta)\cos(\zeta\vartheta)d\vartheta;\ \zeta \to \rho\right]. \tag{A-3.1}$$

By using the following relation,

$$\frac{1}{\rho}\frac{d}{d\rho}\rho\mathcal{H}_1[\zeta^{-1}g(\zeta);\ \zeta \to \rho] = \mathcal{H}_0[g(\zeta);\ \zeta \to \rho]. \tag{A-3.2}$$

Eq. (A-3.1) is rewritten as

$$\bar{\sigma}_{zz}(r) = -\frac{\mu}{a\rho(1-\nu)}\frac{d}{d\rho}\rho\mathcal{H}_1\left[\zeta^{-1}\int_0^1 \chi(\vartheta)\cos(\zeta\vartheta)d\vartheta;\ \zeta \to \rho\right]. \tag{A-3.3}$$

The bracket in Eq. (A-3.3) is given by

$$\mathcal{H}_1\left[\zeta^{-1}\int_0^1 \chi(\vartheta)\cos(\zeta\vartheta)d\vartheta;\ \zeta \to \rho\right] = \int_0^1 \chi(\vartheta)d\vartheta\int_0^\infty J_1(\zeta\rho)\cos(\zeta\vartheta)d\zeta$$

$$= \frac{1}{\rho}\int_0^\rho \chi(\vartheta)d\vartheta + \frac{1}{\rho}\int_\rho^1 \chi(\vartheta)\left\{1 - \frac{\vartheta}{\sqrt{\vartheta^2-\rho^2}}\right\}d\vartheta$$

$$= \frac{1}{\rho}\int_0^1 \chi(\vartheta)d\vartheta - \frac{1}{\rho}\int_\rho^1 \frac{\vartheta\chi(\vartheta)}{\sqrt{\vartheta^2-\rho^2}}d\vartheta. \tag{A-3.4}$$

By substituting Eq. (A-3.4) into (A-3.3), the pressure distribution within the contact area is given by

$$\bar{\sigma}_{zz}(r) = \frac{\mu}{a\rho(1-\nu)}\frac{d}{d\rho}\int_\rho^1 \frac{\vartheta\chi(\vartheta)}{\sqrt{\vartheta^2-\rho^2}}d\vartheta. \tag{A-3.5}$$

The indentation depth is obtained by using Eq. (A-3.5) to obtain the value of $\chi(1)$. Applying integration by parts, Eq. (A-3.5) is alternatively expressed by

$$\bar{\sigma}_{zz}(r) = \frac{\mu}{a(1-\nu)}\left\{\frac{\chi(1)}{\sqrt{1-\rho^2}} - \frac{d}{d\rho}\left[\int_\rho^1 \sqrt{\vartheta^2-\rho^2}\,\frac{d\chi(\vartheta)}{d\vartheta}d\vartheta\right]\right\}. \tag{A-3.6}$$

By taking $r = a(1+\Delta)$ where Δ is small and positive, changing the variable ϑ to $u = 1-\vartheta$, and neglecting the second order of Δ, Eq. (A-3.6) is expressed as

$$\bar{\sigma}_{zz}(a-a\Delta) = -\frac{\mu}{(1-\nu)}\left\{\frac{\chi(1)}{\sqrt{2\Delta}} - \frac{d}{du}\left[\int_0^{\Delta}\sqrt{2(\Delta-u)}\,\frac{d\chi(1-u)}{du}du\right]\right\}. \tag{A-3.7}$$

If $\chi(\vartheta)$ is differentiable around $t = 1$, the integral in Eq. (A-3.7) is a finite value, V_f. Thus,

$$\bar{\sigma}_{zz}(a-a\Delta) = -\frac{\mu}{(1-\nu)}\frac{\chi(1)}{\sqrt{2\Delta}} + V_f. \tag{A-3.8}$$

If $\bar{\sigma}_{zz}(a-a\Delta)$ tends to a finite limit as $\Delta \to 0^+$,

$$\chi(1) = 0. \tag{A-3.9}$$

Applying integration by parts to Eq. (A-2.43) yields

$$\frac{\pi}{2}\chi(\vartheta) = \delta - \vartheta\left[\int_0^{\vartheta}\frac{1}{\sqrt{\vartheta^2-\rho^2}}\frac{df(\rho)}{d\rho}d\rho\right]. \tag{A-3.10}$$

By assigning $\vartheta = 1$ to Eq. (A-3.10) and rearranging the equation, the indentation depth is given by

$$\delta = \int_0^{1}\frac{1}{\sqrt{1-\rho^2}}\frac{df(\rho)}{d\rho}d\rho. \tag{A-3.11}$$

The contact load F_c is given by integrating the contact pressure over the contact area. Thus,

$$F_c = -2\pi \int_0^a r\bar{\sigma}_{zz} dr$$

$$= \frac{2\pi\mu a}{1-\nu} \int_0^\infty \zeta\psi(\zeta)d\zeta \int_0^a \rho J_0(\rho\zeta/a)d\rho . \qquad \text{(A-3.12)}$$

By using the property of the derivative of Bessel function, Eq. (A-3.12) is given by

$$F_c = \frac{2\pi\mu a}{1-\nu} \int_0^\infty \psi(\zeta)J_1(\zeta)d\zeta . \qquad \text{(A-3.13)}$$

By using Eq. (A-2.37) and the integral

$$\int_0^\infty \chi(\zeta)\cos(\zeta\vartheta)d\zeta = 1, \qquad 0 \le \vartheta < 1 \quad \text{(A-3.14)}$$

the contact load is given by

$$F_c = \frac{2\pi\mu a}{1-\nu} \int_0^1 \chi(\vartheta)d\vartheta . \qquad \text{(A-3.15)}$$

Combining Eq. (A-2.43) and Eq. (A-3.11) yields

$$\chi(t) = \frac{2}{\pi}\left\{ \int_0^1 \frac{1}{\sqrt{1-\rho^2}} \frac{df(\rho)}{d\rho} - \vartheta \int_0^\vartheta \frac{1}{\sqrt{\vartheta^2-\rho^2}} \frac{df(\rho)}{d\rho} d\rho \right\}. \qquad \text{(A-3.16)}$$

By substituting Eq. (A-3.16) into Eq. (A-3.15), the contact load is given by

$$F_c = \frac{4\mu a}{1-\nu} \int_0^1 \frac{\rho^2}{\sqrt{1-\rho^2}} \frac{df(\rho)}{d\rho} d\rho . \qquad \text{(A-3.17)}$$

Finally, the displacements within/outside the contact area are obtained. From Eq. (A-2.42), the displacement within the contact area is given by

$$\bar{u}_z(\rho) = \int_0^{\rho} \frac{\chi(\vartheta)}{\sqrt{\rho^2 - \vartheta^2}} d\vartheta. \qquad 0 \le \rho < 1 \quad \text{(A-3.18)}$$

From Eq. (A-2.35), the displacement outside the contact area is given by

$$\bar{u}_z(\rho) = \int_0^{\infty} \psi(\zeta) J_0(\rho\zeta) d\zeta. \qquad \text{(A-3.19)}$$

By using the integration, i.e.,

$$\int_0^{\infty} J_0(\zeta\rho)\cos(\zeta\vartheta) d\zeta = (\rho^2 - \vartheta^2)^{-1/2} H(\rho - \vartheta) \qquad \text{(A-3.20)}$$

where H is the Heaviside step function, the displacement outside the contact area, i.e., $\rho > 1$, is given by

$$\bar{u}_z(\rho) = \int_0^{1} \frac{\chi(\vartheta)}{\sqrt{\rho^2 - \vartheta^2}} d\vartheta. \qquad \rho > 1 \quad \text{(A-3.21)}$$